

**COMPUTATIONAL STUDIES OF GLYCOLIPIDS AND THEIR
INTERACTIONS WITH CARBON NANOTUBES**

ZAHRABATOUL MOSAPOUR KOTENA

**FACULTY OF SCIENCE
UNIVERSITY OF MALAYA
KUALA LUMPUR**

2015

**COMPUTATIONAL STUDIES OF GLYCOLIPIDS AND THEIR
INTERACTIONS WITH CARBON NANOTUBES**

ZAHRABATOUL MOSAPOUR KOTENA

**THESIS SUBMITTED IN FULFILMENT OF THE
REQUIREMENTS FOR THE DEGREE OF
DOCTOR OF PHILOSOPHY**

DEPARTMENT OF CHEMISTRY

FACULTY OF SCIENCE

UNIVERSITY OF MALAYA

2015

UNIVERSITY MALAYA

ORIGINAL LITERARY WORK DECLARATION

Name of Candidate: **ZHRABATOUL MOSAPOUR KOTENA** (I.C./Passport No.: **L95236932**)

Registration/Matrix No.: **SHC100022**

Name of Degree: **DOCTOR OF PHILOSOPHY**

Title of Project Paper/Research Report/Dissertation/Thesis ("this Work"):

"COMPUTATIONAL STUDIES OF GLYCOLIPIDS AND THEIR INTERACTIONS WITH CARBON NANOTUBES."

Field of Study: **PHYSICAL CHEMISTRY (COMPUTATIONAL CHEMISTRY)**

I do solemnly and sincerely declare that:

- (1) I am the sole author/writer of this Work;
- (2) This work is original;
- (3) Any use of any work in which copyright exists was done by way of fair dealing and for permitted purposes and any excerpt or extract from, or reference to or reproduction of any copyright work has been disclosed expressly and sufficiently and the title of the Work and its authorship have been acknowledged in this Work;
- (4) I do not have any actual knowledge nor do I ought reasonably to know that the making of this work constitutes an infringement of any copyright work;
- (5) I hereby assign all and every rights in the copyright to this Work to the University of Malaya ("UM"), who henceforth shall be owner of the copyright in this Work and that any reproduction or use in any form or by any means whatsoever is prohibited without the written consent of UM having been first had and obtained;
- (6) I am fully aware that if in the course of making this Work I have infringed any copyright whether intentionally or otherwise, I may be subjected to legal action or any other action as may be determined by UM.

Candidate's Signature

Date

Subscribed and solemnly declared before,

Witness's Signature

Date

Name: **RAUZAH HASHIM**

Designation: **PROFESSOR**

ABSTRACT

Carbon nanotubes (CNTs) have attracted the attention of many researchers due to their unique mechanical, structural, and electrical properties, and their apparent usefulness in nanotechnology, nanoelectronics, biosensors, biotechnology, biomedicine, and energy storage. Single-walled nanotubes (SWNTs) could be dispersed by surfactants, such as glycopyranoside, which is a family of non-ionic surfactants, from the more generic class of glycolipids found in nature, especially in biological membranes. Hydrogen bond is a dominant factor in different biological processes. This thesis focuses on the knowledge of the hydrogen bond formation in non-ionic surfactant such as glycolipids. Subsequently, we examined the effect of one of these surfactants on SWNTs via quantum chemical calculations.

Density functional theory calculations on two glycosides, namely, n-octyl- β -D-glucopyranoside (C_8O - β -Glc) and n-octyl- β -D-galactopyranoside (C_8O - β -Gal), were performed for geometry optimization at the B3LYP/6-31G level. Both molecules are stereoisomers i.e. both are epimers. They differ only in the orientation (axial vs equatorial) of the hydroxyl group at the C4 position. Thus, it is interesting to electronically investigate the effect of the direction of the hydroxyl group at the C4 position. The structure parameters of X-H...Y intra-molecular hydrogen bonds were analyzed and the nature of these bonds and the intra-molecular interactions were considered using the atoms in the molecules approach. Natural bond orbital analysis was used to determine the effective non-bonding interactions. These results showed that, while C_8O - β -Glc possess only one hydrogen bond, C_8O - β -Gal has two intra-molecular hydrogen bonds, which further confirms the anomalous stability of the latter in self-assembly phenomena.

In addition, density functional theory calculations on α/β -D-mannose (α/β -Man) and the corresponding glycosides of n-octyl- α/β -D-mannopyranoside (C_8O - α/β -Man) were carried out for geometrical optimization and stability predictions at the B3LYP/6-31G level of theory. These compounds are anomerically related, since they differ by only the orientation of the hydroxyl group at the C1 position. The aim of this study is to investigate the effect of the hydroxyl group's orientations at the C1 position on the intra-molecular interactions and the conformational stability of these isomers. The structural parameters of X-H...Y intra-molecular hydrogen bonds were analyzed, while the nature of these bonds was taken into account using the atoms in molecules approach. Natural bond orbital analysis was used to determine the effective non-bonding interactions. The results showed that while α -anomers possess only one intra-molecular hydrogen bond, β -anomers possess two intra-molecular hydrogen bonds, which further confirms the anomalous stability of the latter in the self-assembly phenomena.

In order to study the interaction between CNTs and surfactants, we report on a density functional theory calculation at the B3LYP/6-31G level of theory performed for the purpose of predicting the reactivity governing the nucleophilic and electrophilic attacks on the external surface of a SWNTs. The computational results predicted that glycolipid could induce in a strong interaction on the surface of the SWNT in both gas and aqueous phases. Therefore, surfactants disperse SWNTs in aqueous solutions, mainly via hydrophobic/hydrophilic interactions, where the hydrophobic tail of the surfactant molecule adsorbs on the surface of SWNT, while the hydrophilic head associates with water for the purpose of dissolution.

ABSTRAK

Tiub nano karbon (CNT) telah menarik perhatian ramai penyelidik kerana keunikan mekanikal, struktur, ciri-ciri elektrik, dan kegunaan mereka dalam teknologi nano, elektronik nano, pengesanan bio, bioteknologi, dan penyimpanan tenaga. Tiub nano berdinding tunggal (SWNT) boleh tersebar dengan surfaktan, contohnya, glikopiranosida, yang ditemui dalam alam semula jadi, terutamanya dalam membran biologi. Hidrogen adalah faktor dominan dalam pelbagai proses biologi. Tesis ini memberi tumpuan kepada jenis pembentukan ikatan hidrogen dalam surfaktan bukan ionic seperti glikolipid. Seterusnya, kita mengkaji kesan salah satu surfaktan pada tiub nano karbon penyebaran pengiraan kimia kuantum.

Pengiraan teori berfungsi ketumpatan terhadap dua glikosida, iaitu n-oktil- β -D-glukopiranosida ($C_8O-\beta$ -GLC) dan n-oktil- β -D-galaktopiranosida ($C_8O-\beta$ -Gal) telah dijalankan pada tahap B3LYP / 6-31G untuk mengoptimumkan geometri. Kedua-dua molekul adalah stereoisomer atau epimers. Mereka hanya berbeza dalam orientasi kumpulan hidroksil pada kedudukan C4. Oleh itu, adalah menarik untuk menyiasat secara elektronik kesan arah (paksi / khatulistiwa) kumpulan hidroksil pada kedudukan C4. Parameter struktur X-H...Y ikatan hydrogen intramolekul dianalisis, manakala sifat ikatan dan interaksi intramolekul dianggarkan menggunakan pendekatan atom dalam molekul. Analisis orbit ikatan asli telah digunakan untuk menentukan arahan ikatan dan interaksi bukan ikatan efektif. Keputusan ini menunjukkan bahawa, $C_8O-\beta$ -GLC memiliki hanya satu ikatan hidrogen, manakala $C_8O-\beta$ -Gal mempunyai dua ikatan hidrogen intramolekul, yang mengesahkan lagi kestabilan ganjil $C_8O-\beta$ -Gal dalam fenomena pemasangan diri.

Di samping itu, pengiraan teori berfungsi ketumpatan pada α/β -D-mannose (α/β -Man) dan glikosida sepadan n-oktil- α/β -D-mannopiranosida (C_8O - α/β -Man) telah dijalankan untuk pengoptimuman dan kestabilan geometri ramalan di peringkat B3LYP / 6-31G secara teori. Sebatian-sebatian ini berkaitan secara anomerik, kerana mereka berbeza hanya pada orientasi kumpulan hidroksil di kedudukan C1.

Tujuan kajian ini adalah untuk mengkaji kesan orientasi kumpulan hidroksil ini di kedudukan C1 terhadap interaksi antara molekul dan kestabilan isomer konformasi ini. Parameter struktur X-H ... Y ikatan hidrogen antara molekul dianalisis, manakala sifat ikatan ini dianggap menggunakan molekul-molekul atom dalam pendekatan. Analisis orbit ikatan asli (NBO) telah digunakan untuk menentukan arahan ikatan dan kesan interaksi bukan ikatan. Keputusan ini menunjukkan bahawa α -anomers mempunyai hanya satu ikatan antara molekul hidrogen, β -anomers mempunyai dua ikatan hidrogen antara molekul, yang lagi mengesahkan kestabilan ganjil yang kemudian pada fenomena pemasangan diri.

Untuk mengkaji interaksi antara tiub nano karbon dan surfaktan, seterusnya di sini kita melaporkan pada teori fungsional ketumpatan Pengiraan di peringkat yang B3LYP/6-31G teori dilakukan untuk tujuan meramalkan kereaktifan yang mengawal serangan nukleofilik dan elektrofilik pada permukaan luar sebuah SWNTs. Keputusan pengiraan meramalkan bahawa glikolipid, boleh mengakibatkan interaksi yang kuat pada permukaan SWNT di kedua-dua gas dan fasa akueus. Oleh itu, surfaktan menyebarkan tiub nano karbon di dalam larutan akueus melalui interaksi hidrofobik / hidrofilik, di mana ekor hidrofobik molekul surfaktan yang menjerap di permukaan SWNT, manakala kepala hidrofilik bersatu dengan air bagi tujuan pelarutan.

ACKNOWLEDGMENTS

During my research work I have been accompanied and supported by many people directly or indirectly. Today, I am very pleased to express my gratitude to all of them. First and foremost, I would like to express my sincere gratitude and thanks to my supervisor Prof. Dr. Rauzah Hashim for her valuable advice, guidance and given me insights on the workings of scientific research in general. Moreover, I thanked her for supporting me as a research assistant most of time in the past four years. I really appreciate you.

Special thanks are due to Associate Prof. Dr. Reza Behjatmanesh-Ardakani from Payame Noor University, Yaz, Iran-who has guided me step by step in the research process that I can imagine both personal and professional lives.

In addition, I would also like to give my thanks to head of chemistry department, Prof. Dr. Sharifuddin Bin Md Zain, very kind and knowledgeable person for the guidance and support during my stay in University Malaya.

I would like to appreciate High Impact Research (HIR) for providing generous support and the opportunity to attend seminars, conference and workshop especial for allowing me to attend training in KITPC, Beijing, China. I am grateful to UM.C/625/1/HIR/MOHE/05 for financial support and the Center of Information Technology (PTM) University of Malaya.

I would like to thank Mohamad Safwan Bin Jusof for his support regarding running Gaussian jobs and Gromacs in the computing center.

I got a lot of help from my nice classmate. I am grateful that our kind research group Dr. Noraini, Dr. Idayu, Dr. Hock Seng, Dr. Malinda, Dr. Fadhilah, Dr. Sara, Dr. Matiur,

Mirzade, Vijay, Liew, Amani, Najwa, and Nor Azilawati. I had many useful discussions with them and all others I special with Dr.Hock Seng and Dr.Idayu, really thanks.

I would like to extend my deepest gratitude to my beloved parents for encouraging and inspiring me all my life especially during these years. I would like to express my deepest love and appreciation to my beloved brother, sister, aunt and my best cousin for their caring support, encouragement and for always being there for me whenever I was in need and also to my best friends in Malaysia and my country as my inspiration throughout this research.

DEDICATION

This Thesis is Dedicated
to all
Physically, Visually, Mentally Disable Peoples
in the World.

TABLES OF CONTENTS

ORIGINAL LITERARY WORK DECLARATION	ii
ABSTRACT.....	iii
ABSTRAK	v
ACKNOWLEDGMENTS	vii
DEDICATION	ix
TABLES OF CONTENTS.....	x
LIST OF FIGURES	xiv
LIST OF TABLES	xvii
LIST OF SYMBOLS AND ABBREVIATIONS	xix
LIST OF APPENDICES	xxii

CHAPTER 1

INTRODUCTION	
--------------------	--

Part (I): Materials (Carbon nanotubes and glycolipids)

1. 1 Carbon nanotubes	4
1.1.1 Structure of carbon nanotubes.....	5
1.1.2 The physical properties of carbon nanotubes.....	7
1.1.3 Modification methods	8
1.1.4 Application of carbon nanotubes	10
1.2 Carbohydrate liquid crystals	11
1.2.1 Thermotropic liquid crystal phases	12
1.2.2 Lyotropic liquid crystal phases	13
1.3 Glycolipids (GLS)	15

1.3.1 Non-ionic surfactant.....	17
1.3.2 Glucose, galactose and mannose base glycolipids: a study of epimeric relationship	18
1.4 Hydrogen bonding	20
Part II :Theoretical Chemistry	
1.5 Computational chemistry methods.....	24
1.5.1 The many-body problem in quantum mechanics	25
1.5.2 The Born-Oppenheimer approximation	27
1.6 Quantum mechanics (QM).....	29
1.6.1 Ab initio, and semi empirical methods	29
1.6.2 Hartree-Fock (HF) theory	30
1.6.3 Thomas-Fermi (TF) theory	31
1.6.4 Density functional theory and methods.....	32
1.7 Basis sets.....	38
1.8 Atoms in molecules (AIM)	40
1.9 Natural bond orbital (NBO)	40
1.10 Software	43
1.11 Objective and outline of the chapters in this thesis	44
CHAPTER 2	
LITERATURE REVIEW.....	
2.1 The rule of surfactants in dispersion of carbon nanotubes	46
2.2 Dispersions of carbon nanotubes in water soluble	47
2.3 Organic solvents dispersions of carbon nanotubes	50
2.4 Carbon nanomaterial in biological systems	51
2.5 Hydrogen bonding in glycolipid surfactants	52
CHAPTER 3	
METHODOLOGY	
3.1 Gauss View (GV) software:.....	56
3.2 Gaussian software	57
3.3 AIM 2000 software.....	58
3.4 Calculated properties	59

3.4.1 Polarizable continuum (PCM) model.....	59
3.4.2 HOMO and LUMO.....	60
3.4.3 The topology of the electron density.....	61
3.4.4 The Laplacian of the electron density at the BCP $[\nabla^2 \rho(r)]$	64
3.4.5 The bond ellipticity.....	65
3.4.6 Energy densities at BCP.....	65
3.4.7 Chemical hardness (η), chemical potential (μ).....	66
3.4.8 Stabilization energy.....	67
3.4.9 Fukui function.....	68
3.5 Computational details.....	70

CHAPTER 4

HYDROGEN BOND IN GLUCO AND GALACTO PYRANOSIDE SURFACTANTS

.....	
4.1 The geometry parameters.....	76
4.2 The electronic energy.....	79
4.3 Dipole moment.....	80
4.4 The electronic properties.....	80
4.5 Atoms in molecules (AIM) analysis.....	82
4.6 Natural bond orbital (NBO) analysis.....	88

CHAPTER 5

HYDROGEN BOND IN MANNOSE AND MANNONSEPYRANOSIDE SURFACTANTS

.....	
5.1 The geometry parameters.....	92
5.2 The thermodynamic properties.....	93
5.3 The electronic properties.....	94
5.4 Atoms in molecules (AIM) analysis.....	98
5.5 Natural bond orbital (NBO) analysis.....	101

CHAPTER 6

INTERACTION BETWEEN CARBON NANO TUBES AND GLYCOLIPIDS

6.1 Fukui calculations	104
6.2 Energy calculations	106
CHAPTER 7	
CONCLUSIONS.....	104
7.1 Future works.....	117
REFERENCES	119
APPENDIX (A)	
Gaussian 09	132
A.1 Setting up and Running a typical Gaussian Job.....	132
A.2 Preparation of the input file in Gaussian 09 in Windows and Linux environment.....	132
"Input file for beta-mannose"	132
APPENDIX (B)	
AIM SOFTWARE	134
"Input file for beta-mannose"	134
APPENDIX (C)	
NBO ANALYSIS	136
"Output file for beta-mannose"	136
APPENDIX (D)	
PH.D PUBLICATIONS.....	143
D.1 Journal Articles	143
D.2 Manuscripts in preparation.....	144
APPENDIX (E)	
ATTANDANCE TO CONFERENCE/ SEMINAR/ WORKSHOP	145

LIST OF FIGURES

Figure 1.1: Possible application of nanotechnology (adopted from http://vtu.ac.in/nano-technology/).....	3
Figure 1.2: Schematic of single-walled carbon nanotubes consist of a single graphite sheet seamlessly wrapped in a cylindrical tube (adopted from http://cnanotubes.blogspot.com/2006/06/classifications.htm).	4
Figure 1.3: Carbon nanotube configurations with the chiral vector C and unit vectors a and b . (adopted from [16]).	6
Figure 1.4: Configuration of (armchair, zigzag and chiral) carbon nanotubes (adopted from http://theor.jinr.ru/disorder/carbon.html).	6
Figure 1.5: 3-D illustration of single-walled (left) and multi-walled (right) carbon nanotubes (adopted from http://education.mrsec.wisc.edu/nanoquest/carbon/.htm	7
Figure 1.6: Functionalization possibilities for SWNTs: (a) defect-group functionalization, (b) covalent sidewall functionalization, (c) non-covalent exohedral functionalization with surfactants, (d) non-covalent exohedral functionalization with polymers, and (e) endohedral functionalization. (Hirsch 2002).	9
Figure 1.7: Schematic illustration of phase transition behavior and the molecular order of liquid crystal (adopted from [49]).....	11
Figure 1.8: The examples of liquid crystal phases.....	12
Figure 1.9: Common molecular organizations in thermotropic liquid crystals. (a) Nematic, (b) Smectic, (c) Columnar and (d) Chiral nematic (cholesteric).(adopted from www.medicinescomplete.com).	14
Figure 1.10: Common molecular organizations in lyotropic liquid crystals.(adopted from www.hydrissolutions.com , and http://pubs.rsc.org/en/content/articlelanding/2006/nj/b610045g#!divAbstract).	14

Figure 1.11: Generic structure of a typical glycolipid. Y= alkyl chain (lipid)	16
Figure 1.12: Typical cell membrane with glycolipid (adopted from http://classroom.sdmesa.edu/eschmid/f3-7_plasma_membrane_st.jpg).	17
Figure 1.13: Surfactant classification according to the composition of their head : (a) non-ionic (b) antionic (c) cationic (d) zweitterionic.	17
Figure 1.14: Chemical structure for n-octyl- β -D-glycopyranoside ($C_8O-\beta$ -Glc) and n-octyl- β -D-galactopyranoside ($C_8O-\beta$ -Gal).	19
Figure 1.15: Chemical Structure for α -D-mannose (α -Man) and β -mannose (β -Man).	21
Figure 1.16: Chemical Structure for n-octyl- α -D-mannopyranoside ($C_8O-\alpha$ -Man) and n-octyl- β -D-mannopyranoside ($C_8O-\beta$ -Man).	21
Figure 2.1: schematic examples of surface functionalization of CNTs. (illustration adapted from [124]).	47
Figure 3.1: Visualizing molecules and reactions with Gauss view (adopted from http://www.gaussian.com/g_prod/gv5b.htm).	56
Figure 3.2: Numbering of (3,0) zigzag SWNT (a) front-view and (b) side-view. Carbon atoms are in grey and Hydrogen atoms are in white.	72
Figure 3.3: The structure of non-ionic surfactant n-octyl- β -D-glucopyranoside. C atoms are in grey and H atoms are in white and O atoms are in red.	73
Figure 4.1: Definition of HB geometry where the angle of hydrogen bonding of X-H...Y, θ , and hydrogen bond distance, d, [211, 212].	77
Figure 4.2: Schematic drawing of molecular structures for $C_8O-\beta$ -Glc and $C_8O-\beta$ -Gal.	77
Figure 4.3: The atomic orbital composition of the frontier molecular orbital for $C_8O-\beta$ -Glc and $C_8O-\beta$ -Gal.	84
Figure 4.4: Molecular graph in the $C_8O-\beta$ -Glc and $C_8O-\beta$ -Gal. Small red spheres and lines correspond to the bond critical points (BCP) and the bond paths, respectively.	85

Figure 5.1: The NBO composition of the frontier orbitals (HOMO) for α/β -Man.	96
Figure 5.2: The NBO composition of the frontier orbitals (LUMO) for α/β -Man.	96
Figure 5.3: The NBO composition of the frontier orbitals (HOMO) for C_8O - α/β -Man.	97
Figure 5.4: The NBO composition of the frontier orbitals (LUMO) for C_8O - α/β -Man.	97
Figure 5.5: Molecular graph in the α/β -Man. Small red spheres and lines correspond to the bond critical points (BCP) and the bond paths, respectively.	100
Figure 5.6: Molecular graph in the C_8O - α/β -Man. Small red spheres and lines correspond to the bond critical points (BCP) and the bond paths, respectively.	100
Figure 6.1: Variation of reactivity descriptors derived from MPA for different carbon atoms on the surface of (3,0) zigzag SWNTs computed at B3LYP/6-31G level, for (a) $f^+(k)$, $s^+(k)$, $f^-(k)$ and $s^-(k)$, and (b) for $s^+(k)/s^-(k)$, $s^-(k)/s^+(k)$, and $f^2(k)$	106
Figure 6.2: Various configurations of C_8O - β -Glc residing on the external surface of (3, 0) SWNTs at the B3LYP/6-31G level in the gas phase are depicted here before and after optimization. A configuration where CNT interact directly with the surfactant head group, at low concentration, B1H is shown in (a) before optimization and (b) after optimization, where the arrow indicate oxygen of the surfactant in B1H is bonded to the carbon of C6 of the carbon nanotube at low concentration.	111
Figure 6.3: Various configurations of C_8O - β -Glc residing on the external surface of (3, 0) SWNTs at the B3LYP/6-31G level in the gas phase is depicted here before and after optimization. A configuration where CNT interact directly with the surfactant head group (c) B1T configuration (CNT1–Surfactant tail group) after optimization at low concentration. The high concentration configurations after optimization are (d) B2H (CNT2–Surfactant head group) and (e) B2T (CNT2–Surfactant tail group).	112
Figure 7.1: schematic representation of surface functionalization of CNTs with other molecules including glycolipid. (illustration adapted from [124]).	117

LIST OF TABLES

Table 1.1: The dependence of SWNTs electrical conductivity on the (n, m) values.....	8
Table 1.2: Various computational methods with different strengths and relative computational costs.....	25
Table 3.1: Some properties of HOMO and LUMO.	60
Table 3.2: The four kinds of critical point (CP) are identified with an element of chemical structure (<i>r</i> :rank and <i>s</i> :signature).....	64
Table 4.1: General characteristic of the three major types of hydrogen bonding and important structural parameters [211, 212].....	78
Table 4.2: The geometrical parameters for C ₈ O-β-Glc and C ₈ O-β-Gal (the bonds in and the angles in degree), at the B3LYP/6-31 G by DFT method. The atom labels we used Mamony et al [215] and IUPAC [216].	79
Table 4.3: Electronic energy $E_{(a.u.)}$, and dipole moment $\mu(D)$, of studied compounds at B3LYP/6-31G level of theory in the gas and solution phases.	80
Table 4.4: Calculated the highest occupied molecular orbital energy $\varepsilon_{(HOMO)}$, and the lowest unoccupied molecular orbital energy $\varepsilon_{(LUMO)}$, ionization energy(<i>I</i>), electron affinity (<i>A</i>), chemical hardness (η), electronic chemical potential (μ), electrophilicity index (ω), and softness (<i>S</i>) in C ₈ O-β-Glc and C ₈ O-β-Gal at the B3LYP/6-31G level.All units are (e.V.).....	81
Table 4.5: Topological parameters (in a.u.) E, the electron densities, $\rho(r)$ at O...H BCPs, their Laplacians $\nabla^2\rho(r)$ and energetic parameters, <i>V</i> (<i>r</i>), <i>G</i> (<i>r</i>) and <i>H</i> (<i>r</i>) (in kcal/mol) in the C ₈ O-β-Glc and C ₈ O-β-Gal at the B3LYP/6-31G.....	85
Table 4.6: The second-order perturbation energies, $E^{(2)}$ (kcal/mol), corresponding to the most important charge transfer interaction (donor→acceptor) in the C ₈ O-β-Glc and C ₈ O-β-Gal at the B3LYP/6-31G.	90

Table 5.1: The geometrical parameters for α/β -Man and C ₈ O- α/β -Man (the bond lengths in Å and the bond angles in degree), at the B3LYP/6-31 G by DFT method. ...	93
Table 5.2: The properties for α/β -Man and C ₈ O- α/β -Man at the B3LYP/6-31 G level of theory in the gas phase.	94
Table 5.3: Calculated the highest occupied molecular orbital energy $\varepsilon_{(HOMO)}$, and the lowest unoccupied molecular orbital energy $\varepsilon_{(LUMO)}$, ionization energy (I), electron affinity (A), chemical hardness (η), electronic chemical potential (μ), electrophilicity index (ω), and softness (S) of studied compounds at the B3LYP/6-31G level.....	95
Table 5.4: Topological parameters E (in a.u.), the electron densities $\rho(r)$, at O...H BCPs, their Laplacians $\nabla^2\rho(r)$ and energetic parameters $V(r)$, $G(r)$, and $H(r)$ (in kcal/mol) in the α/β -Man and C ₈ O- α/β -Man at the B3LYP/6-31G.	99
Table 5.5: The second-order perturbation energies, $E^{(2)}$ (kcal/mol), corresponding to the most important charge transfer interaction (donor→acceptor) in the α/β -Man and C ₈ O- α/β -Man at the B3LYP/6-31G.	102
Table 6.1: The values of $f^+(k)$, $s^+(k)$, $s^+(k)/s^-(k)$, $s^-(k)/s^+(k)$, $f^-(k)$, $s^-(k)$ and $f^2(k)$ derived from MPA schemes at the B3LYP/6-31G level for various carbon atoms of (3,0) zigzag SWNT.	105
Table 6.2: Calculated structural parameters of C ₈ O- β -Glc and (3, 0) zigzag SWNTs at the B3LYP/6-31 G level in gas and solution phases.....	107
Table 6.3: Calculated binding energies of (3, 0) zigzag SWNTs in low concentration (one-surfactant) and high concentration (two-surfactants) in two configuration (head and tail) in gas and solution phases at the B3LYP/6-31G leve.....	108
Table 6.4: Calculated Gibbs free energy and enthalpy of complexes of (3,0) zigzag SWNTs at the B3LYP/6-31G level.....	109
Table 6.5: Calculated highest occupied molecular orbital (HOMO), lowest unoccupied molecular orbital (LUMO), energy gap for (3,0) zigzag SWNT with their complexes and chemical potential (μ) at the B3LYP/6-31G level.....	111

LIST OF SYMBOLS AND ABBREVIATIONS

CNTs	Carbon nanotubes
SWNTs	Single-walled carbon nanotubes
MWNTs	Multi-walled carbon nanotubes
(n , n)	Armchair
(n , 0)	Zigzag
(n , m)	Chiral
OH	Hydroxyl group
QM	Quantum mechanics
QC	Quantum chemistry
GV	Gaussview
BO	Born- Oppenheimer
TF	Thomas-Fermi
HF	Hartree-Fock
DFT	Density functional theory
B3LYP	Becke 3-Parameter (Exchange), Lee, Yang and Parr (correlation; density functional theory)
\hat{H}	Hamiltonian operator
ψ	Wavefunction
STO	Slater type orbital
GTO	Gaussian type orbital
PCM	Polarizable continuum model
AIM	Atoms in molecules
QTAIM	Quantum theory of atoms in molecules
NBO	Natural bond orbital

MPA	Mulliken population analysis
NAO	Natural atomic orbital
MO	Molecular orbital
CP	Critical point
BCP	Bond critical point
NCP	Nuclear critical point
RCP	Ring critical point
CCP	Cage critical point
$E^{(2)}$	Stabilization energy
∇^2	Laplacian operator
$\rho(r)$	Electron density
$\nabla^2 \rho(r)$	Laplacian of the electron density at the BCP
$G(r)$	Electronic kinetic energy density
$V(r)$	Electronic potential energy density
$H(r)$	Total energy density
ε	Ellipticity
HOMO	Highest occupied molecular orbital
LUMO	Lowest unoccupied molecular orbital
ε_{HOMO}	HOMO energies
ε_{LUMO}	LUMO energies
μ	Electronic chemical potential
η	Chemical hardness
ω	Electrophilicity index
$\Delta\varepsilon_{(L-M)}$	Band gap
$f(r)$	Fukui function
EA	Electron affinity

IP	Ionization energy
T _c	Clearing temperature
T _m	Melting temperature
LC	Liquid crystal
GLs	Glycolipids
Glc	Glycopyranoside
Gal	Galactopyranoside
Man	Mannopyranoside
C ₈ O- α/β -Glc	n-octyl- α/β -D-Glucopyranoside
C ₈ O- α/β -Gal	n-octyl- α/β -D-Galactopyranoside
C ₈ O- α/β -Man	n-octyl- α/β -D-Mannopyranoside
α/β -Man	α/β -D-Mannoside

LIST OF APPENDICES

APPENDIX (A) : Gaussian 09

A.1 Setting up and Running Gaussian Jobs

A.2 Preparation input file in Gaussian 09 W under Linux cluster

APPENDIX (B) : AIM software

APPENDIX (C) : NBO analysis

APPENDIX (D) : Published papers

APPENDIX (E) : Attandance to Conference/Seminar/Workshop

CHAPTER 1

INTRODUCTION

Part (I)

Materials (Carbon nanotubes and Glycolipids)

Nanotechnology is the study of matter manipulation at atomic and molecular scales [1]. Nanotechnology involves structures that are within 1–100 nm in one dimension. Nanotechnology also encompasses the development of materials or devices within the aforementioned size range, where the effects of mechanical quantum would be profound [2]. Some possible applications of nanotechnology are detailed in Figure 1.1.

Carbon nanotubes (CNTs) represent one of the most unique inventions in the field of nanotechnology. It remains one of the most researched materials in the 20th and 21st centuries. It can be conjugated non-covalently or covalently with nanoparticles, biomolecules, and drugs. This section will focus on the synthesis, properties, modification, and applications of CNTs.



Figure 1.1: Possible application of nanotechnology (adopted from <http://vtu.ac.in/nano-technology/>).

1. 1 Carbon nanotubes

Carbon nanotubes have diameters that falls within the nanometer range, while its corresponding lengths are micrometer. In 1970, Morinobu Endo synthesized carbon filaments that are about 7 nm in diameter via the vapor-growth technique. This materials was also synthesized by Iijima from the NEC Laboratory in 1991 [3], which he later christened single-walled carbon nanotubes in 1993. Carbon nanotubes (CNTs) are allotropes of carbon possessing cylindrical nanostructure, resulting in exceptional mechanical, thermal, and electrical properties, higher moduli, are stronger than steel, and are thermally stable to as much as 2800°C in vacuum, have a thermal conductivity that is double of diamond, and the electric-current-carrying capacity is 1000 times greater than that of a copper wire. An idealized nanotube is a hexagonal network of carbon atoms rolled up to form a cylinder with diameters that are in nanometers and lengths are micrometers with aspect ratio of 1000 or higher. Single-walled carbon nanotubes have a surface area of $\approx 1600 \text{ m}^2/\text{g}$. The next section will discuss some background information of carbon nanotubes, which will cover the synthesis methods, structure, physics properties, modification methods, and corresponding applications. Figure 1.2 shows schematic of SWNTs consisting of a single sheet seamlessly wrapped around a cylindrical tube.

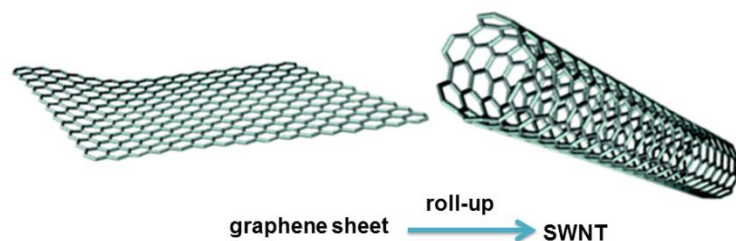


Figure 1.2: Schematic of single-walled carbon nanotubes consist of a single graphite sheet seamlessly wrapped in a cylindrical tube (adopted from <http://cnanotubes.blogspot.com/2006/06/classifications.htm>).

1.1.1 Structure of carbon nanotubes

Carbon nanotubes can be synthesized via several methods, such as laser ablation [4, 5], arc-discharge [6, 7], as well as chemical vapor deposition [8, 9, 10, 11, 12]. Each nanotube is a single molecule composed of millions of atoms [13]. The length of carbon nanotubes vary from several micrometers to hundreds of micrometers, with diameters of about 1.0–1.5 nm [12]. For MWNTs, their inner and outer diameters are around 5 and 100 nm, respectively. The distance between two walls of MWNTs is about 3.41 Å, which is comparable to the interlayer distance in graphite [14]. SWNTs exhibit unique electronic properties that can be significantly altered sing the chiral vector, $C = (n, m)$, which is the parameter indicating how the graphene sheet is rolled to form a carbon nanotube.

Therefore, SWNTs are characterized by the chirality indices (n, m) , where n and m are integers, with $n \geq m$. Its corresponding structure determines whether it is metallic or semiconducting, which in turn depends on the chirality. Chirality is a measure of the twist of the nanotube. Furthermore, chirality determines the size of the electronic band gap for semiconducting nanotubes. Carbon nanotube configurations with the chiral vector C and unit vectors \mathbf{a} and \mathbf{b} , is shown in Figure 1.3. Structurally, SWNTs are divided into three distinct types, which are armchair (n, n) tubes, zigzag $(n, 0)$ tubes, and chiral (n, m) tubes [15]. Figure 1.4 show examples of these structures (armchair, zigzag and chiral).

As shown in Figure 1.5, carbon nanotubes are divided into two configurations; single-walled carbon nanotubes (SWNTs) and multi-walled carbon nanotubes (MWNTs). SWNTs can be defined as a single graphite layer rolled up into a hollow

cylinder [12], while MWNTs consist of multiple rolled layers (concentric tubes) of graphite forming unordered columns [3].

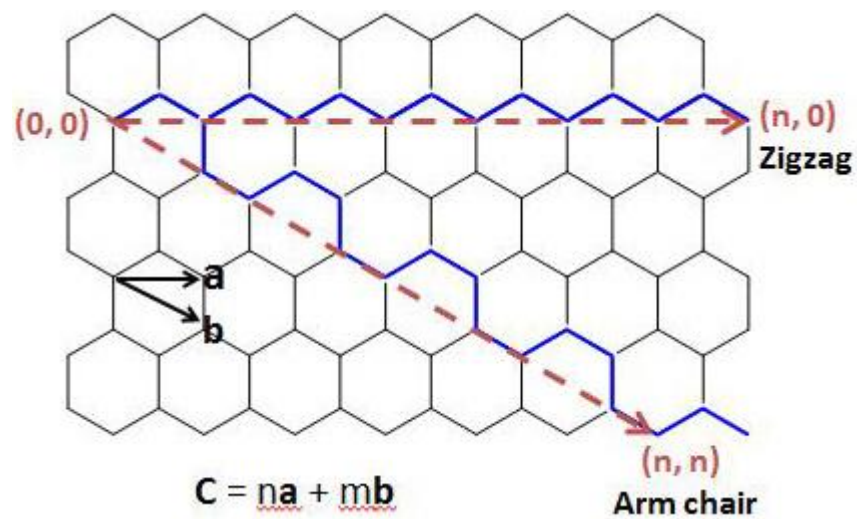


Figure 1.3: Carbon nanotube configurations with the chiral vector C and unit vectors a and b . (adopted from [16]).

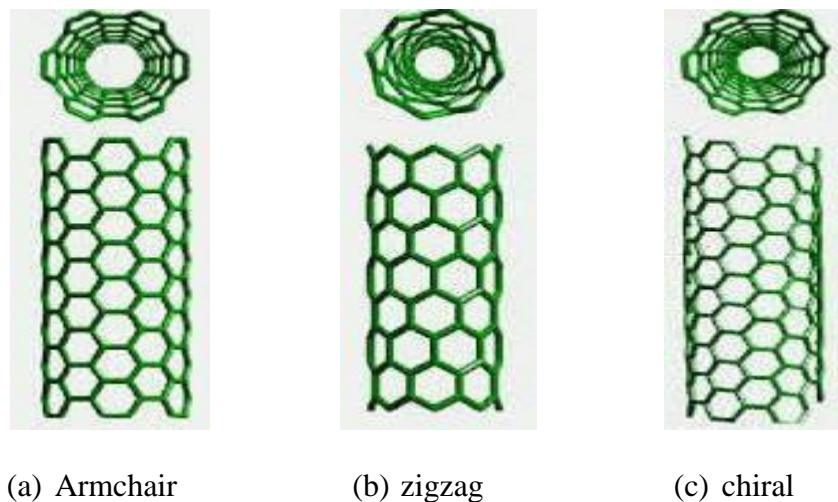


Figure 1.4: Configuration of (armchair, zigzag and chiral) carbon nanotubes (adopted from <http://theor.jinr.ru/disorder/carbon.html>).

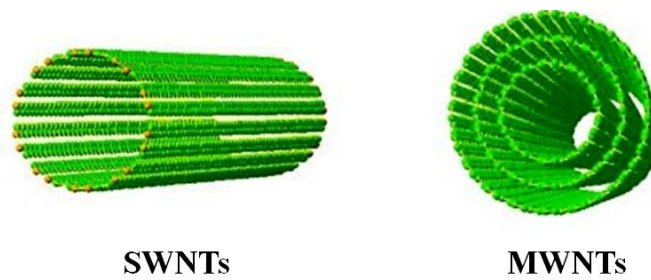


Figure 1.5: 3-D illustration of single-walled (left) and multi-walled (right) carbon nanotubes (adopted from <http://education.mrsec.wisc.edu/nanoquest/carbon/.htm>)

1.1.2 The physical properties of carbon nanotubes

The electronic properties of CNTs are extraordinary. Carbon nanotubes are characterized by two bonds: σ and π bonds. These materials possess sp^2 hybridization and four valence orbitals. The orbitals (s , p_x , p_y) combine to form the in-plane σ and σ^* (bonding or occupied and anti-bonding or unoccupied) while, lateral interaction with neighboring p_z orbitals creates the delocalized π and π^* (bonding and anti-bonding) orbitals. The π bonds are perpendicular to the surface of the nanotubes, and are responsible for the weak interaction between SWNTs in a bundle, similar to the weak interaction between carbon layers in pure graphite. Moreover, the σ in the nanotube form a hexagonal network that strongly connects the carbon atoms in the cylindrical wall of the tube. The σ bonds are most significant for the electronic properties of carbon nanotubes or graphite. The energy levels associated with the in-plane σ bonds are far from the Fermi energy in graphite, making them irrelevant to the electronic properties. On the other hand, the bonding and anti-bonding π -bands crosses the Fermi level at high-symmetry points in the Brillouin zone of graphene. Therefore, these properties render graphene and some carbon nanotubes metallic or quasi-metallic [14].

Depending on the roll orientation of the grapheme sheet (n,m) , SWNTs' band gap can vary from 0–2 eV. The band gaps of semiconductor nanotubes have an inverse relationship with diameter; for small tubes, the band gap is approximately 1.8 eV, while, for the widest, it is approximately 0.18 eV in stable SWNTs [17]. Thus, it demonstrates electrical conductivity that exceeds copper, while others demonstrate behaviors that are closer to silicon. The dependence of SWNTs electrical conductivity on the (n, m) values is shown in Table 1.1.

Carbon nanotubes possess amazing mechanical properties that are comparable to other materials, such as steel, resulting in sp^2 carbon-carbon bonds. For example, their densities can be as low as 1.3 g/cm^3 , which are one-sixth that of stainless steel. CNTs Young's moduli (measure of material stiffness) are larger than steel, with a typical value of 1 TPa, which is around 5 times higher than the latter [18]. The highest measured tensile strength or breaking strain for a carbon nanotube is 63 GPa, which is approximately 50 times higher than steel [18]. In addition, CNTs have good chemical and environmental stability, and high thermal conductivity ($\approx 3000 \text{ W/m.K}$, comparable to diamond).

Table 1.1: The dependence of SWNTs electrical conductivity on the (n, m) values.

(n , m)	Types of SWNTs	Electrical conductivity
(n, 0)	Zigzag	Metallic when n is the multiple of 3, otherwise, semiconducting
(n , n)	Armchair	Metallic
(n , m)	Chiral	Metallic when $(2n+m)/3$ is an integer, otherwise, semiconducting

1.1.3 Modification methods

Pristine CNTs are intrinsically hydrophobic, highly toxic, and are incapable of being dispersed uniformly in most solvents or biological media. The toxicity of CNTs is

mainly attributed to impurities, its length, surface chemistry, dispersion, and tendency to aggregate, or any combination of these factors [19]. Surface modification of CNTs is performed to introduce new properties to carbon nanotubes for highly specific applications. Thus, the functionalization of CNTs must be developed to improve their biocompatibility, solubility, dispersion, while lowering of its toxicity.

There are several functionalization methods [20], such as , (a) defect functionalization at the opens tips and sidewalls of CNT, (b) covalent functionalization outside CNT on their sidewalls, (c) non-covalent functionalization outside or external walls of CNT with surfactant (d) encapsulation of bioactive molecules or drugs inside CNT, and (e) endohedral functionalization (See Figure 1.6).

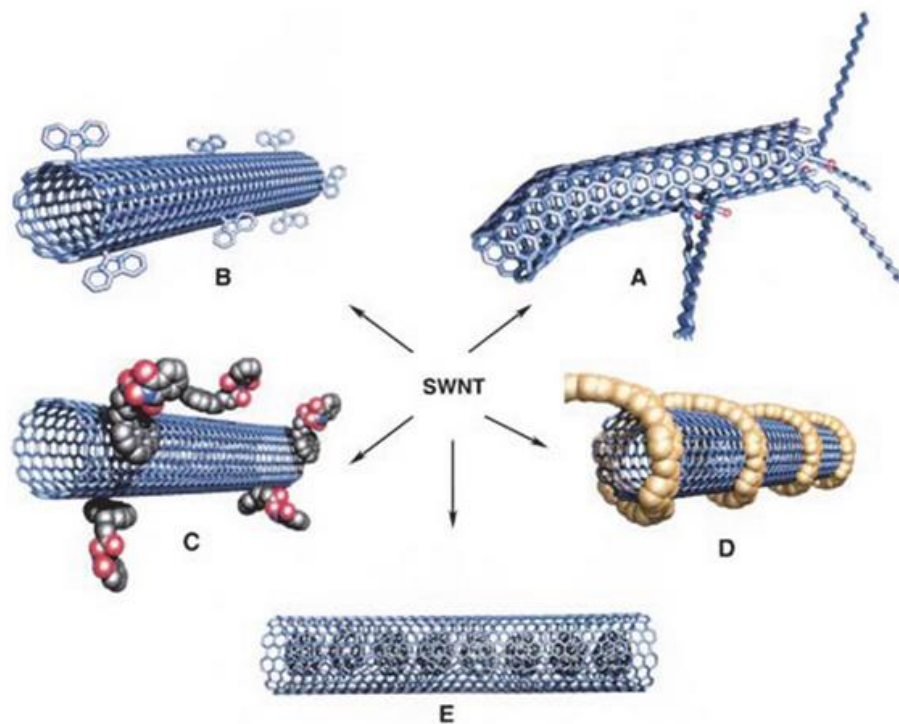


Figure 1.6: Functionalization possibilities for SWNTs: (a) defect-group functionalization, (b) covalent sidewall functionalization, (c) non-covalent exohedral functionalization with surfactants, (d) non-covalent exohedral functionalization with polymers, and (e) endohedral functionalization. (Hirsch 2002).

The dissolution of CNTs has been facilitated by covalently attaching functional moieties containing aromatic groups onto the external walls of CNT through π - π interactions [21]. However, this might alter the inherent properties of the nanotubes. Thus, non-covalent adsorption of lipids and detergents, polymers, and other biomolecules onto the surface of CNTs are prioritized, thereby preserving the extended π -networks of the tubes. Therefore, this thesis focuses on non-covalent functionalization by the sugar group onto the surface of single-walled carbon nanotubes for increasing dispersion and decreasing toxicity.

1.1.4 Application of carbon nanotubes

Due to their small dimensions, strength, and also remarkable properties [22], carbon nanotubes have been employed in many promising applications. Recently, CNTs are applied into many fields, such as a hydrogen storage [23, 24, 25] or filling media [26, 27], nanoscale electronic devices [28], nanoscale mechanical devices [29], field emitters [11, 30, 31], sensor materials and biosensor [32], aerospace, automobiles, telecommunications, biological, biomedical [33], vaccines [34], drug delivery [35], gene therapy, cancer therapy and textiles and with human cells [20].

CNTs may penetrate and travel to various parts of the body, causing tissue injury or be deposited into undesirable and highly protected human systems. Additionally, they could pollute the environment by increasing the concentration of nanoparticles in the air. Nanoparticles can also cause allergic reactions or enter the food chain cycle. Moreover, these nanomaterials, including carbon nanotubes, upon prolonged exposure, can also cause asbestosis types of diseases in humans [36, 37, 38].

1.2 Carbohydrate liquid crystals

Scientists are aware of liquid crystals since the end of the 19th century. In 1888, Friedrich Reinitzer [39] was the first to observe the liquid crystal, phase, and Lehman [40] identified this phase as a new state of matter. Liquid crystal is an intermediate phase, which exists between a solid crystal and an isotropic liquid [41]. They possess certain properties of liquids, such as fluidity, and some of solid crystals, such as optical birefringence properties, demonstrating unique anisotropic behaviors [42]. Figure 1.7 shows the phase transition behavior and the molecular order of liquid crystal. Liquid crystals are applicable in multiple fields, such as in detergent and the cosmetics industries [43, 44], biology for membrane function, vesicles, and the extraction of protein and peptides [45], the food industry [46], and emulsion technology as stabilizers [47, 48].

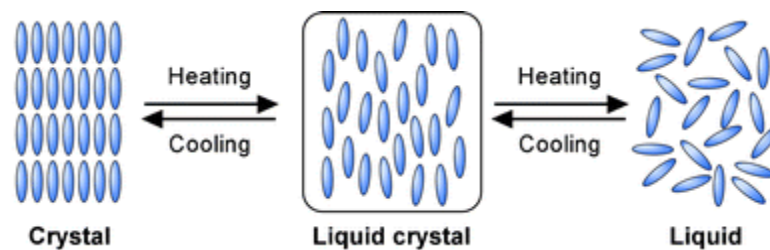


Figure 1.7: Schematic illustration of phase transition behavior and the molecular order of liquid crystal (adopted from [49]).

There are two types of liquid crystals phases; thermotropic liquid crystals and lyotropic liquid crystals [50]. A thermotropic liquid crystal is sensitive to temperature and pressure changes, while a lyotropic phase relies on concentration (of solvent) as well as temperature. Examples of liquid crystal phases are presented in Figure 1.8.

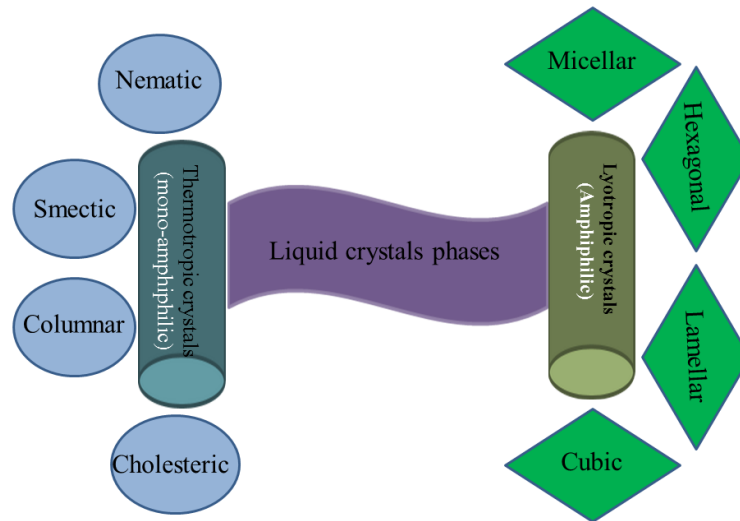


Figure 1.8: The examples of liquid crystal phases.

1.2.1 Thermotropic liquid crystal phases

Thermotropic liquid crystalline phases can be identified using several techniques, such as optical polarizing microscopy, miscibility studies, light scattering, X-ray, neutron diffractions, differential scanning calorimetry and spectroscopic techniques [51, 52]. Thermotropic liquid crystals can generally be formed by prolate (calamitic) or oblate (discotic) molecules. Liquid crystal phases formed by calamitic molecules (thermotropic phases) are also sub-divided into nematic, cholesteric (chiral nematic), smectic and columnar [41, 42, 53]. (See Figure 1.8 for the complete breakdown of these structures).

In terms of organization (hence ordering), the nematic phase is the simplest liquid crystal phase. It is characterized by a high degree of long range orientation order, but no translational order, while cholesteric phases shows nematic ordering, but the “preferred direction”, also called the director, rotates throughout the sample. Another phase is smectic, which possess further degrees of translational ordering (hence the layered structure) compared to the nematic phase. The columnar phases form columns, and they

are the discotic equivalent of the smectic phase. Figure 1.9 illustrates the common molecular organizations in thermotropic liquid crystals.

1.2.2 Lyotropic liquid crystal phases

Lyotropic liquid crystal structures can be identified by an optical polarizing microscope and X-ray diffraction techniques. The lyotropic liquid crystals are generally made up of amphiphilic molecules [54]. These often consist of a polar head group attached to one or more non-polar chains, and are often known as surfactants (surface active agents). When these are dissolved in an appropriate solvent, they proceed to self-assemble, so that the polar (hydrophilic) heads avoid the non-polar (hydrophobic) tails. The most commonly observed lyotropic phases are micelles, the fluid lamellar, hexagonal and cubic phases [55]. (See Figure 1.8 for the organization). This means that at low surfactant concentrations, they are roughly spherical. Additionally, as the surfactant concentration increases, other phases such as the hexagonal phase are formed, where the amphiphiles form cylinders that are packed in a hexagonal array, while the amphiphiles in the lamellar phase form a bilayer structure. Figure 1.10 illustrates the common molecular organizations in lyotropic liquid crystals.

Many surfactants, such as non-ionic surfactants, could self-assemble into ordered lyotropic liquid crystal phases at high concentrations. Recently, sugar-based surfactants have been the source of much attention due to their non-ionic, less toxic and bio-surfactant properties. Glycolipids exhibit amphiphilic behavior, and is found in biological systems [56].

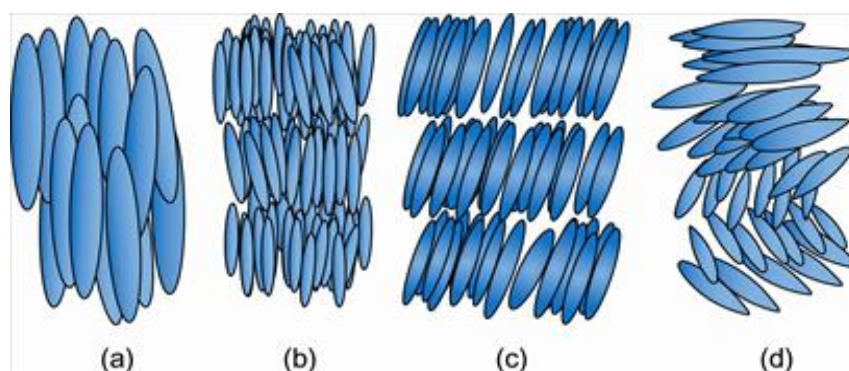
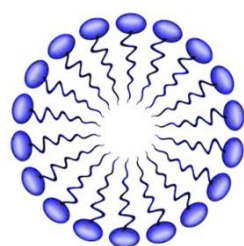
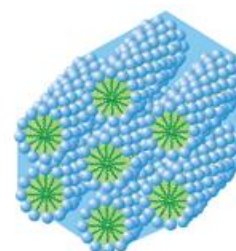


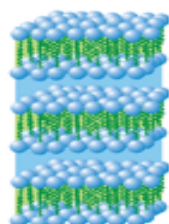
Figure 1.9: Common molecular organizations in thermotropic liquid crystals. (a) Nematic, (b) Smectic, (c) Columnar, and (d) Chiral nematic (cholesteric). (adopted from www.medicinescomplete.com).



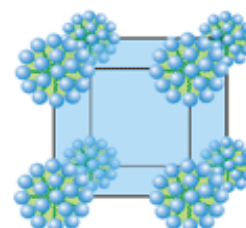
Micellar



Hexagonal



Lamellar



Cubic

Figure 1.10: Common molecular organizations in lyotropic liquid crystals. (adopted from www.hydrationsolutions.com, and <http://pubs.rsc.org/en/content/articlelanding/2006/nj/b610045g#!divAbstract>).

1.3 Glycolipids (GLs)

Carbohydrate liquid crystals are a special type of liquid crystals. They are commonly known as glycolipids, and have different rules pertaining to their self-assemblies. Glycolipids are an amphiphilic molecule, which includes hydrophilic (head) and hydrophobic (tail) groups. Therefore, their potential applications are quite different from the normal thermotropic liquid crystals that are commonly used in display devices. Attaching a lipid to a sugar moiety results in a glycolipid molecule, whose solubility and physical properties undergo substantial changes. A glycolipid molecule possesses a water-loving polar head group, linked to a water-hating hydrophobic alkyl tail. Some generic structure of a typical glycolipid is shown in Figure 1.11.

This dichotomy within the glycolipid molecule is an enabling feature, which drives the molecules to form many interesting self-assembly structures, hence resulting in liquid crystalline properties, both via thermal and solvent effects. The ability of these materials to form a diverse range of self-assembly structures thermotropically, as well as lyotropically, paves the way for many potential applications in nano-and biotechnology [57]. Compared to many conventional ionic surfactants, glycolipids are biodegradable and biocompatible [58], non-toxic, and may be derived from many common and cheap natural resources [59]. Glycolipids are commonly found in nature, especially in cell's membranes (See Figure 1.12), and are known to be involved in cellular functions [60], suggesting that they are particularly attractive as a new type of lipid for targeted liposomal drug delivery systems [61, 62].

Natural glycolipids can be classified as glycolycerolipids, glycosphingolipids, and glycosyl phosphopolyrenols. They exist in nature, but can be synthesized either chemically or enzymatically [63]. Moreover, they can be produced at a relatively low

cost from locally available raw materials, such as palm oil and sugar [64]. A great deal of attention has been paid to many of bio-surfactants, such as glycolipids in the last decade, particularly for their self-aggregation properties and characterization. These compounds are stabilized by the hydrogen bonding interaction between the sugar moieties [65]. The chirality of the sugar moieties also plays an important role in their thermotropic and lyotropic phase behaviors [66].

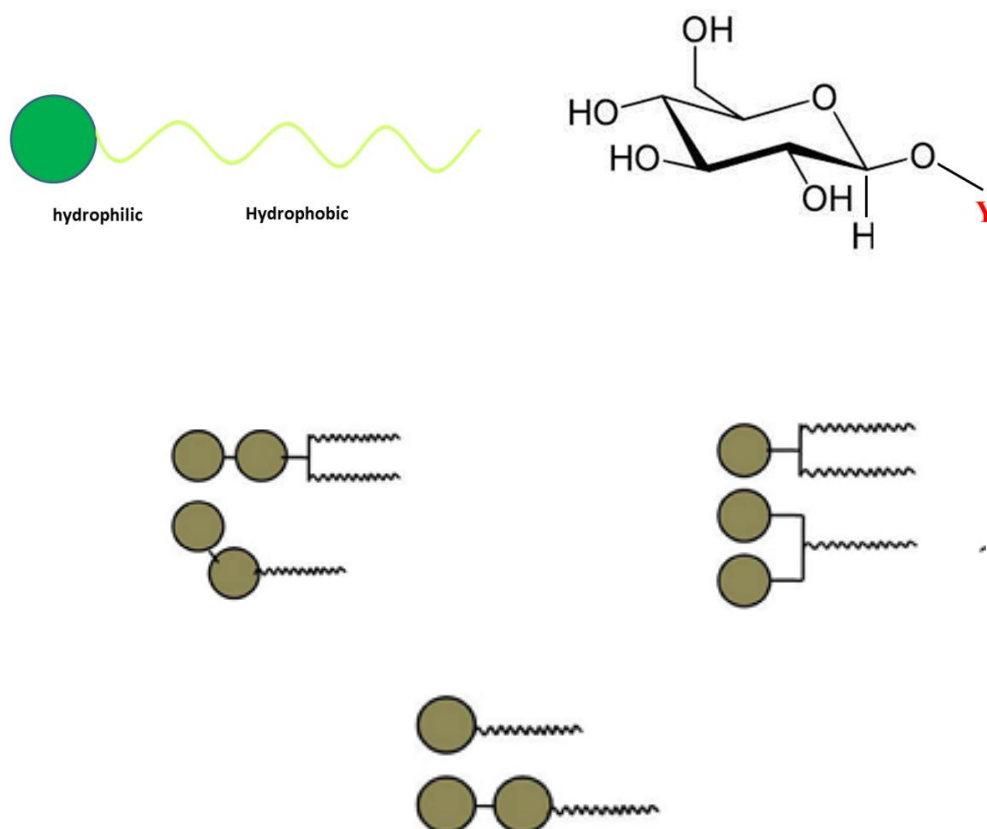


Figure 1.11: Generic structure of a typical glycolipid. Y= alkyl chain (lipid)

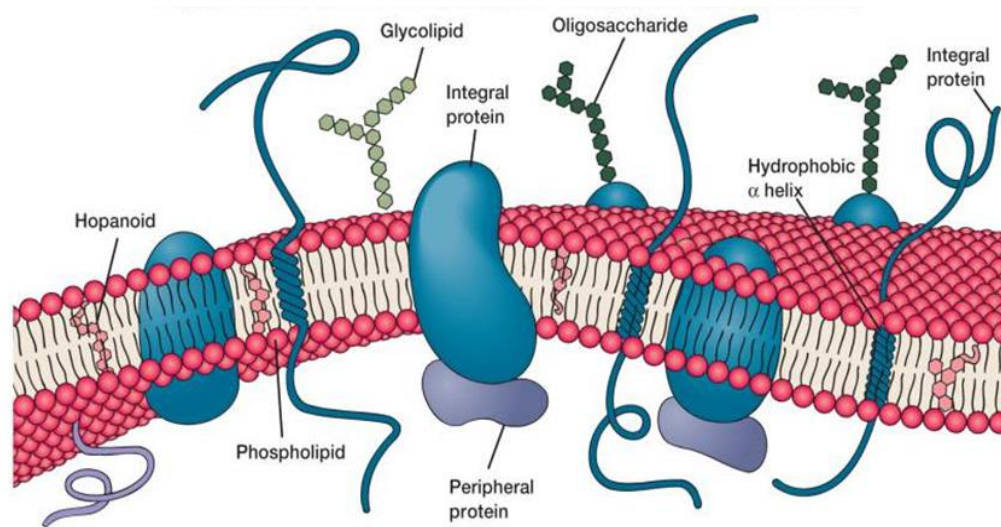


Figure 1.12: Typical cell membrane with glycolipid (adopted from http://classroom.sdmesa.edu/eschmid/f3-7_plasma_membrane_st.jpg).

1.3.1 Non-ionic surfactant

Surfactants are classified by the charge of their polar head group, such as cationic, anionic, zwitterionic, and non-ionic [67, 68]. Surfactant classifications according to the composition of head groups, is detailed in Figure 1. 13.

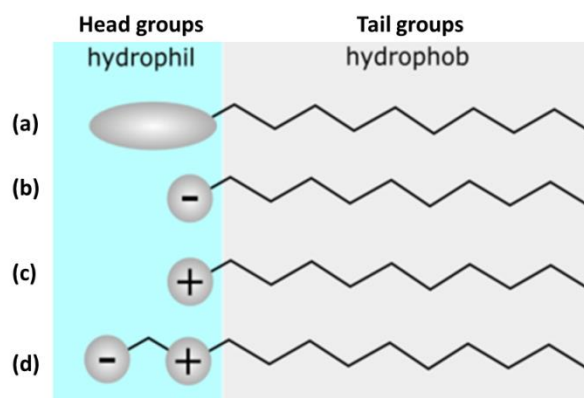


Figure 1.13: Surfactant classification according to the composition of their head : (a) non-ionic (b) antionic (c) cationic (d) zweitterionic.

Non-ionic surfactants are solubilized in water due to the presence of polar groups, but are incapable of disassociating into ions. They are compounds with a general formula of $R(\text{OCH}_2\text{CH}_2)_n\text{OH}$, obtained by condensing an alcohol or a phenol with ethylene oxide [69]. The R group is hydrophobic, whereas the hydroxyl group and the -O- links in the polyethoxyl moiety are water-seeking. In the present study, our non-ionic surfactants possess hydroxyl groups within the head region. The polar head group of non-ionic compounds does not carry any overall charge. This thesis employs the following sugar-based non-ionic surfactants:

n-octyl- α/β -D-Glucopyranoside = $\text{C}_8\text{O-}\alpha/\beta\text{-Glc}$

n-octyl- α/β -D-Galactopyranoside = $\text{C}_8\text{O-}\alpha/\beta\text{-Gal}$

n-octyl- α/β -D-Mannopyranoside = $\text{C}_8\text{O-}\alpha/\beta\text{-Man}$

α/β -D-Mannose = $\alpha/\beta\text{-Man}$

1.3.2 Glucose, galactose and mannose base glycolipids: a study of epimeric relationship

In membrane science, the subtle difference between a glucolipid and its C4 epimer is a galactolipid, which has demonstrated a profound impact on the cell functions, galactolipid is pervasively found in plant cells, while its epimer is usually found in bacteria [70]. The former is thought to be involved in photosynthesis. One widely studied sugar-based surfactant is n-octyl- α/β -D-glucopyranoside ($\text{C}_8\text{O-}\alpha/\beta\text{-Glc}$) [71, 72]. It has been used for a variety of applications, from being a stabilizer, reconstituting, purifying, and crystallizing membrane proteins and membrane-associated protein complexes without denaturation [73, 74], to being used for molecular recognition and cell signaling [75]. Both molecules are stereoisomers (epimers), differing only in the orientation of the hydroxyl group at the C4 position. The OH in C4 position for n-octyl- β -D-glucopyranoside is equatorial, while it is axial

for *n*-octyl- β -D-galactopyranoside. The conformers of *n*-octyl- β -D-glucopyranoside and *n*-octyl- β -D-galactopyranoside are shown in Figure 1.14.

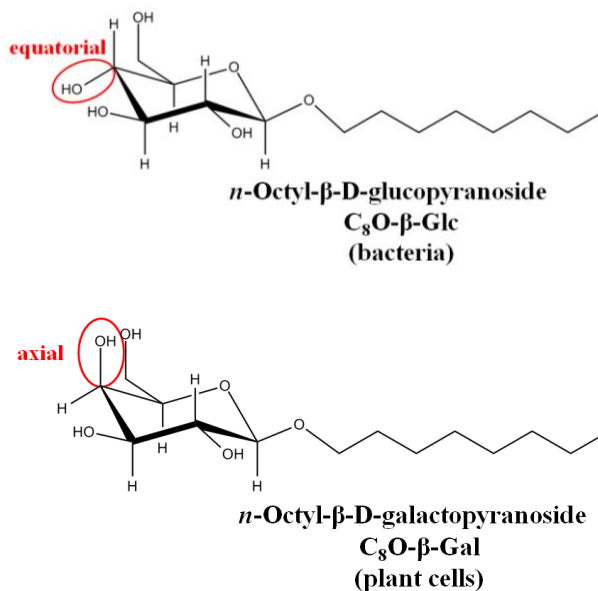


Figure 1.14: Chemical structure for *n*-octyl- β -D-glycopyranoside (C_8O - β -Glc) and *n*-octyl- β -D-galactopyranoside (C_8O - β -Gal).

In addition to the C2 epimer of glucose, mannose is classified as a simple sugar from the aldohexose series of the carbohydrate family [76]. Mannose are generally found in a number of fruits (including cranberries) [77], and dextro mannose (D-mannose) is thought to keep bacteria from remaining on the walls of the urinary tract, which is why it is used to prevent and treat urinary tract infections [78]. The only difference between mannose and glucose are the fact that its epimers are at the C2 position, but surprisingly, many of their physical behaviors differ by a wide margin [79].

Moreover, there are two possible stereoisomers at the C1 position and, two possible orientations (axial/equatorial) of the hydroxyl group, resulting in two anomers, α -D-mannose and β -D-mannose. Mannose is chiral in the ring form, but achiral in the linear form. Physically, α -D-mannose is a sweet-tasting sugar, while β -D-mannose, on

the other hand, tastes bitter. A pure solution of α -D-mannose, however, loses its sweetness over time. When monosaccharides are dissolved in water, they undergo reversible ring-opening reactions, so the ring forms exist in equilibrium with the linear forms. The C1 is then free to rotate (mutarotation), allowing for the formation of β -D-mannose when it changes back into the ring form. When equilibrium is reached, there are more β -isomer than the α -isomer, because in the β -isomer, the hydroxyl on the C1 is in a more stable (equatorial) position [80].

Like its sugar component, the axial at C2 gives n-octyl-D-mannopyranoside an epimer of n-octyl-D- glycopyranoside, while the axial or equatorial position at the OH group at C1 defines whether the molecule is α - or β - isomer, respectively. The role of polar interaction of monosaccharide head group is important, as it stabilizes self-assembly. The axial/equatorial orientation of C1-O1 (α/β) is a key factor related to the number of hydrogen bonding, which may exist to stabilize self-assembly, and in turn influence the melting (T_m) and clearing points (T_c) of n-octyl- α/β -D-mannopyranoside surfactants. The conformers of α/β -D-mannose are shown in Figure 1.15, while n-octyl- α/β -D-mannopyranoside is shown in Figure 1.16. The physical and chemical properties of these monosaccharides depend upon the molecular shape and the extent of hydrogen bonding interactions.

1.4 Hydrogen bonding

Given the central role played by the hydrogen bond in the chemistry and biochemistry of glycolipids it is useful at this point to discuss what a hydrogen bond is, how it arises, and why it is significant. In order to discuss the nature of the hydrogen bonding present in molecular crystals, it is necessary that its common structural features are characterized. A general hydrogen bond comprises of a donor group X-H and an acceptor A, and is referred to as X-H...A. Perhaps a more useful refinement is given by

Steiner and Saenger [81], where a hydrogen bond is defined as: “any cohesive interaction X-H...A where H carries a positive and A a negative (partial or full charge) and the charge on X is more negative than on H”. This definition, although focusing only upon the electrostatic aspects of the hydrogen bond, and hence restrictive with respect to weak hydrogen bonds, is sufficient for the types of hydrogen bonds that will be encountered in this work.

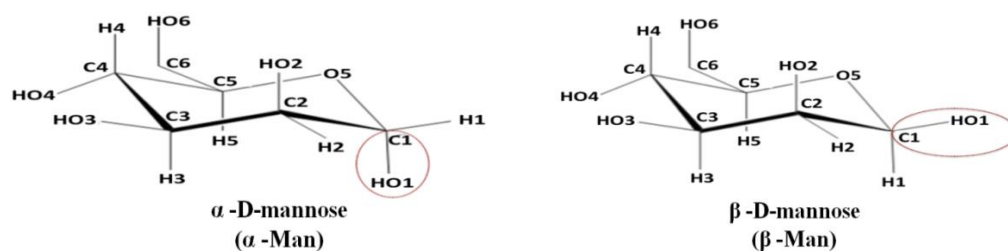


Figure 1.15: Chemical Structure for *α* -D-mannose (*α* -Man) and *β* -mannose (*β* -Man).

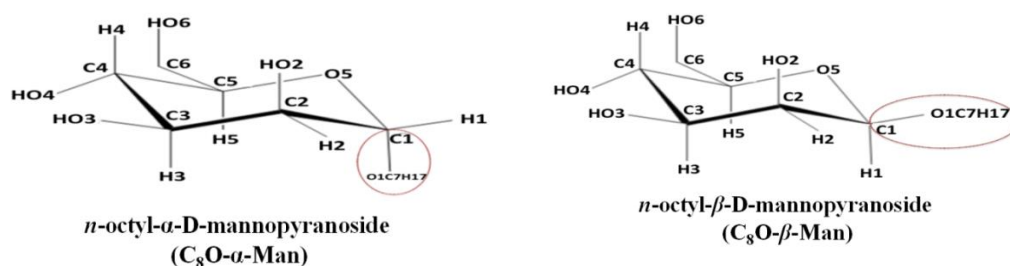


Figure 1.16: Chemical Structure for *n*-octyl- *α* -D-mannopyranoside (*C*₈O- *α* -Man) and *n*-octyl- *β* -D-mannopyranoside (*C*₈O- *β* -Man).

A hydrogen bond is defined as an interaction between two electronegative atoms: donor and acceptor, via an intermediate atom that is covalently connected to the donor [82]. It has been categorized as a middle range interaction, falling between the weak van der Waals interaction and the strong covalent or ionic interactions.

In many chemical and biochemical systems, one of the most important interactions is hydrogen bond, which is responsible for the formation and function of

cell membranes [83, 84]. Glycolipids systems have the ability to participate in hydrogen bonds both as donors and acceptors, unlike phosphatidcholines, which can only fulfill the role of an acceptor [85]. The thermal stability and different phase behavior of these compounds are believed to be related to intermolecular interactions within the assembly, due to the presence of strong hydrogen bonds in the head group region [86]. For example; the clearing point of alkyl glycosides increases with a large number of hydrogen bonds between the carbohydrates moieties.

Therefore, understanding its interactions among the constituent molecules is of special interest. In principle, molecular interactions are a major contributor in the course of determining the formation of mesophases. Most notably, the hydrophobic region is mainly governed by non-bonded van der Waals force, whereas within the hydrophilic region, the long- range electrostatic interaction from the hydroxyl group plays a vital role. Additionally, distance- and direction-orientated hydrogen bonding interaction within the hydrophilic domain determines the thermodynamic stability of the self-assembled structure [87, 88]. The directionally oriented hydrogen bond primarily affects the physico-chemical properties of sugars, such as melting and clearing temperatures. In this thesis, we use the definition suggested by Bader, since the atom in molecule (AIM) theory [89] was applied to understand, in greater detail, the nature of HBs. Excellent reviews have been published [90, 91] regarding the applications of AIM for such calculations. Within AIM, the analysis of the bond critical points (BCP) on the electronic density distribution has been proven useful to the study of different chemical features, such as the structure, nature, and geometry of hydrogen-bonded systems [92, 93, 94].

Part II

Theoretical Chemistry

This part will focus on the theoretical background of computational chemistry methods, such as *ab initio*, semi or empirical methods, and density functional theory, the Hartree-Fock, and the Thomas-Fermi theory to solve the many-electron problems. Also, some of the practicalities that are necessary to consider in performing these calculations, such as basis sets, will help solve chemical problems as well. We will also describe atoms in molecules (AIM) and natural bond orbital (NBO) methods that are used to investigate hydrogen bond compounds.

1.5 Computational chemistry methods

Computational chemistry methods range from highly accurate techniques, for example configuration interaction (CI), to very approximate techniques, such as molecular dynamics (MD). While the highly accurate methods are typically feasible only for small systems, large molecules can be studied by semi-empirical approximate methods. For larger molecules such as proteins, they are assumed to adhere to classical mechanics methods that employ what are called molecular mechanics. These days, in QM/MM methods, small portions of large complexes are treated quantum mechanically (QM), and the remainder is treated approximately by molecular mechanics (MM). All constants appearing in the equations of molecular mechanics (MM) must be obtained beforehand from experimental data or *ab initio* calculations. Molecular dynamics (MD) utilize quantum mechanics, Newton's laws of motion or a mixed model to examine the time-dependent behavior of systems, including vibrations or Brownian motion and reactions. MD combined with density functional theory, leads to hybrid models. For that reason, these computational methods are widely used to design new drugs and materials. Table 1.2 illustrates the wide range of computational methods with different strengths and its relative computational costs.

Table 1.2: Various computational methods with different strengths and relative computational costs.		
	Quantum mechanics (QC)	
Molecular mechanics (MM)	Semi-empirical	<i>ab initio</i>
100,000 atoms	1000 atoms	100 atoms
Use empirically derived potential function	Schrödinger's equation solve	
	Approximate	Exact
Empirical parameters needed	computationally demanding	

1.5.1 The many-body problem in quantum mechanics

The behavior of electrons may be predicted by a quantum mechanical model [95]. In 1926, physicist Erwin Schrödinger proposed an equation [96], that fundamentally solve the wave functions of fundamental particles, such as electrons, protons, and atoms, called the Schrödinger's equation.

There are two types of Schrödinger's equations; time-independent and time-dependent. The non-relativistic time-independent Schrödinger's equation is used when dealing with stationary states, as they do not change over time, while in the time-dependent Schrödinger's equation; the wave function is a function of position and time. In chemistry, we mostly deal with stationary states. Generally, time-independent Schrödinger's equation can be written as:

$$\hat{H}\psi = E\psi \quad (1.1)$$

where \hat{H} is the Hamiltonian operator, ψ is the wavefunction and E is the total energy of the system. ψ is a function of the positions of all the fundamental particles (electrons and nuclei) in the system, and \hat{H} is the operator associated with the observable energy.

E is the total energy of the system, which is independent of time and it's a scalar (number). Therefore, the Hamiltonian \hat{H} in classical mechanics is defined as:

$$\hat{H} = \hat{T} + \hat{V} \quad (1.2)$$

The Hamiltonian operator consists of the kinetic energy and the potential energy. The energy is derived from the eigenvalues for the corresponding wave, also known as the eigenfunctions. The kinetic and potential energies are transformed into the Hamiltonian, which acts upon the wavefunction to generate the evolution of the wavefunction in time and space. The Schrodinger's equation provides the quantized energies of the system and the form of the wavefunction so that other properties may be calculated. For a single electron system such as a hydrogen atom, the kinetic and the potential energy operators can be written as:

$$\hat{T} = \frac{-\hbar^2}{8\pi^2m} \nabla^2 \quad (1.3)$$

and

$$\hat{V} = \frac{-Ze^2}{r} \quad (1.4)$$

where, m is the mass electron, r is the distance between the electron and the nucleus,

Z is the atomic number, e is the unit of electron charge, and $(\nabla^2 = \frac{\partial^2}{\partial x^2} + \frac{\partial^2}{\partial y^2} + \frac{\partial^2}{\partial z^2})$

is the Laplacian operator in the Cartesian coordinate system. To solve the Schrödinger's equation for a system with more than one atom (many-body atoms) in atomic units (energy in Hartree and length in Bohr), \hat{H} can be expanded as [97]:

$$\begin{aligned} \hat{H} = & -\frac{1}{2} \sum_{i=1}^{electrons} \nabla_i^2 - \frac{1}{2} \sum_{A=1}^{nuclei} \frac{1}{M_A} \nabla_A^2 - \sum_{i=1}^{electrons} \sum_{A=1}^{nuclei} \frac{Z_A}{r_{iA}} + \sum_{i=1}^{electrons} \sum_{j>i}^{nuclei} \frac{1}{r_{ij}} \\ & + \sum_{A=1}^{electrons} \sum_{B>A}^{nuclei} \frac{Z_A Z_B}{R_{AB}} \end{aligned} \quad (1.5)$$

In the aforementioned equation, M_A is the ratio of the mass of nucleus A to the mass of an electron, Z_A is the atomic number of A, the distance between i -th and j -th electron is $r_{ij} = |r_i - r_j|$, the distance between A-th and B-th nucleus is $R_{AB} = |R_A - R_B|$. The ∇_i^2 and ∇_A^2 are the Laplacian operators. The first two terms in Equation 1.5 represent the kinetic energy of electrons and nuclei, respectively. The third term is the Coulomb's attraction between electrons and nuclei, and the fourth and fifth terms are the repulsions between electrons and between nuclei, respectively.

1.5.2 The Born-Oppenheimer approximation

There are different approximations that help solve some coupling terms that appear in this Hamiltonian. One of the most reliable approximation that is vital to electronic structure calculations is Born-Oppenheimer (BO) approximation [97]. By applying the Born-Oppenheimer approximation, (the electrons are moving in a field produced by the fixed nuclei), the second term in Equation 1.5 was neglected, and the final term, which represents the repulsion between nuclei, could be treated as a constant for a fixed configuration of nuclei. Therefore, with the BO approximation, full many-body Hamiltonian becomes simpler to that of an electronic Hamiltonian:

$$\hat{H}^{elec} = -\frac{1}{2} \sum_{i=1}^{electrons} \nabla_i^2 - \sum_{i=1}^{electrons} \sum_{A=1}^{nuclei} \frac{Z_A}{r_{iA}} + \sum_{i=1}^{electrons} \sum_{j>i}^{nuclei} \frac{1}{r_{ij}} \quad (1.6)$$

The solution to a Schrödinger's equation involving the electronic Hamiltonian,

$$\hat{H}^{elec} \psi^{elec} = E^{elec} \psi^{elec} \quad (1.7)$$

is the electronic wavefunction,

$$\psi^{elec} = \psi^{elec}(r_i, R_A) \quad (1.8)$$

which describes the motion of the electrons and explicitly depends on the electronic coordinates (r_i), but parametrically on the nuclear coordinates (R_A). Furthermore, to completely specify an electron, it is necessary to assign the corresponding spin (ω), so together with the spatial coordinates, we denote these four coordinates collectively by x ,

$$x = \{r, \omega\} \quad (1.9)$$

and the wave function for an N-electron system is written as $\psi(x_1, x_2, \dots, x_N)$. The total energy of fixed nuclei will also include the constant nuclear repulsion term, leading to,

$$\hat{H} = E^{elec} + \sum_{A=1}^{nuclei} \sum_{B>A}^{nuclei} \frac{Z_A Z_B}{R_{AB}} \quad (1.10)$$

Several different ways have been introduced to approximately solve Schrödinger's equation (Equation 1.10), such as the Hartree-Fock method, MØller-Plesset perturbation theory, and coupled cluster methods. These methods rely on the many body wave functions as a central quantity. Another more commonly used technique is the density functional theory (DFT), where the energy of a molecule can be determined from the electron density instead of a wave function. The advantage of using the electron density is that the integrals for Coulomb repulsion only solve the electron density, which is a three-dimensional function, thus scaling as N^3 . This means that

using electron density over the wave functions results in much reduced dimensionality. Regardless of how many electrons one has in the system, the density is always 3 dimensional.

1.6 Quantum mechanics (QM)

The theoretical prediction of molecular structures and properties can be very valuable to (a) obtain an idea about stable molecular structures, (b) explore whether reactions are exothermic or endothermic, and (c) predict molecular properties such as spectroscopic transitions or thermodynamic constants. We shall briefly illustrate some of the first principle theoretical methods including; *ab initio* and semi-empirical or empirical quantum chemistry. The following sections will review *ab initio*, density functional theory, and semi or empirical methods, Thomas-Fermi, Hartree-Fock theory, followed by a more detailed discussion on DFT.

1.6.1 *Ab initio*, and semi empirical methods

ab initio or the first principal method, is based entirely on quantum mechanics and basic physical constants such as Planck's constant over $2\pi/\hbar$, mass and charge of electron: m_e , e , etc. It eschew experimental parameters in the computations [98]. The method is particularly useful for predicting the properties of unique materials and the trends for a wide range of materials that cannot be accomplished with empirical or semi empirical methods. The use of empirical parameters in semi empirical calculations was to decrease the number of electron-electron repulsion integrals that needs to be computed. Comparing the *ab initio* with the semi empirical or empirical method, it is noted that the level of sophistication for the former is higher, but applies to smaller systems, and fast processes only due to the fact that computationally, it is more expensive. In addition, almost all *ab-initio* methods rely on specific approximations,

such as the Born-Oppenheimer and Schrödinger's equations. The nuclear and electronic motions are decoupled and treated separately by the Born-Oppenheimer approximation. The Schrödinger's equation cannot be solved exactly, with the notable exception of very simple systems such as hydrogen atom. Semi empirical methods do not use exact solutions of the Schrödinger's equation, but include empirical parameters instead [99].

The density functional theory method is often considered to be an *ab initio* method for determining the molecular electronic structure, despite the fact that many of the most common functionals use parameters derived from empirical data, or from more complex calculations. In DFT, the total energy is expressed in terms of the total one-electron density rather than the wave function. In this thesis we will focus on the density functional theory of *ab initio* quantum chemistry method to calculate electronic energy of some glycolipids and the interaction energy between carbon nanotubes and glycolipids.

1.6.2 Hartree-Fock (HF) theory

The simplest form of *ab initio* electronic structure calculation is the Hartree-Fock (HF) model to solve the time-independent Schrödinger's equation for a multi-electron atom or molecule, (See Equation 1.7). It relies on the Born-Oppenheimer (BO), the independent electron, and the linear combination of atomic orbitals approximation. The Hartree-Fock theory has a prominent status, as it often paves the way towards more accurate calculations in modern quantum chemistry. The HF equations can be solved numerically (exact Hartree-Fock), or they can be solved in the space spanned by set of basis functions (Hartree-Fock-Roothan equation).

1.6.3 Thomas-Fermi (TF) theory

One of the tractable scheme for solving the many-electron problems is by introducing the electron density $\rho(r)$ as the central variable and the total energy of the system as a functional of the density, as proposed by Thomas and Fermi (TF) [100, 101]. The electron density $\rho(r)$ determines the probability of finding any of the N electrons within the volume (r) with an arbitrary spin, while the other $N-1$ electrons have an arbitrary positions and spins in the state represented by (ψ). The electron density is defined as:

$$\rho(r) = N \int \dots \int |\psi(x_1, x_2, \dots, x_N)|^2 dx_1 dx_2 \dots dx_N \quad (1.11)$$

This is a nonnegative simple function of three variables; x , y , and z , integrated to the total number of electrons,

$$\int \rho(r) dr = N \quad (1.12)$$

The kinetic energy of electrons in the TF theory are derived from the quantum statistical theory based on the uniform electron gas, but the interaction between electron-nucleus and electron-electron are treated in the classical manner.

The kinetic energy of the electrons within this model, is defined as;

$$T[\rho] = C_F \int \rho^{\frac{5}{3}}(r) dr \quad (1.13)$$

with

$$C_F = \frac{3}{10} (3\pi^2)^{\frac{2}{3}} = 2.871 \quad (1.14)$$

From the equation, the approximation results in the kinetic energy of the electron depend exclusively on the electron density. By adding the interaction between electron-nucleus and electron-electron into Equation (1.14), the total energy of the Thomas-Fermi of electron density is composed of three terms,

$$E[\rho] = C_F \int \rho^{\frac{5}{3}}(r) dr - Z \int \frac{\rho(r)}{r} dr + \frac{1}{2} \iint \frac{\rho(r_1)\rho(r_2)}{|r_1 - r_2|} dr_1 dr_2 \quad (1.15)$$

The first term is the kinetic energy, while the second and third terms represent the electron-nucleus and electron-electron interactions of the system, respectively.

The Thomas-Fermi scheme is exactly at the limit where the nuclear charge is infinite. However, there are severe deficiencies in the model. The charge density is infinite at the nucleus, and it does not decay exponentially far from the nucleus of an atom, but as a function of r^{-6} . Furthermore, the TF theory does not predict atoms binding to form molecules or solids [102]. The main source of error for this model comes from the approximation of the kinetic energy. Another problem is the over-simplified description of the electron-electron interactions, which are treated classically, and hence do not take into account of quantum phenomena such as the exchange interaction [103]. The importance of this simple Thomas-Fermi model is not how well it performs in computing the ground state energy and density, but as a description the energy that can be determined purely using electron density.

1.6.4 Density functional theory and methods

Density functional theory (DFT) is used to study the physical properties and reaction energies of compounds containing up to 100 or more heavy atoms with the perturbation theory [104]. This theory involves electronic ground state based on the electronic density distribution. This method considers the many-electron problems as a

single electron problem, by using the exchange-correlation potential, which gathers all the many-body quantum phenomena such as the electron correlation and Pauli's exclusion principle. The exchange-correlation potential is a function of the charge density $\rho(r)$. A range of excellent review articles [105, 106], and textbooks [107, 108] provide a fairly detailed overview of DFT, as well as descriptions of exchange-correlations function and approaches to solving numerical issues.

Density functional theory-based methods are derived from quantum mechanics research from the 1920's using the Thomas-Fermi-Dirac model, and Hartree-Fock-Slater's methods work in quantum chemistry in the 1950's. DFT method is regarded as being more accurate than Hartree-Fock (HF) method, with a slight increase in computational times [98]. Although these theories are approximate, modern density functional theory is, in principle, exact for the ground state. In addition, these approach had several failings, such as the instability in binding atoms to form molecules [102]. The most important modern density functional method were developed by Kohn and Sham [109], who had a great deal of success in detailing the quantum mechanical ground state of electronics in systems of interest in quantum chemistry and solid-state physics.

Walter Kohn was awarded the Nobel Prize in Chemistry in 1998. The Kohn-Sham equations are similar in form to the time-independent Schrödinger's equation. The next section will detail the Hohenberg-Kohn theorems.

1.6.4.1 Hohenberg-Kohn theorem

Modern density functional theory originated in 1964, described in a paper authored by Hohenberg and Kohn [110]. It is based on two theorems related to the systems consisting of moving the influence of an external potential. The two key results of this paper are:

Theorem 1: The external potential and hence the total energy, is a unique functional of the electron density.

Theorem 2: The ground state energy can be found variationally; the density that minimizes the total energy is the exact ground state density.

The first part was proven simply via many elegant methods using the principle of reduction absurdum, derived for a non-degenerate system [111]. Let's assume that there is a collection of electrons enclosed into a box influenced by an external potential $v(r)$. Assuming we know the electron density of this system, it will allow us to determine $v(r)$, and all other properties. If there is another external potential $v'(r)$ that differs from $v(r)$ by more than a constant that can also provide the same electron density $\rho(r)$ for the ground state, we will then have two different Hamiltonians; \hat{H} and \hat{H}' ; whose the ground state electron densities are similar with different normalized wave functions ϕ and ϕ' . This will result in:

$$\begin{aligned} E_0 &< \langle \phi' | \hat{H} | \phi' \rangle = \langle \phi' | \hat{H}' | \phi' \rangle + \langle \phi' | \hat{H} - \hat{H}' | \phi' \rangle \\ &= E'_0 + \int \rho(r) [v(r) - v'(r)] dr \end{aligned} \quad (1.16)$$

where E_0 and E'_0 are the ground-state energies for \hat{H} and \hat{H}' , respectively. Similarly, we can get:

$$\begin{aligned} E'_0 &< \langle \phi | \hat{H} | \phi \rangle = \langle \phi | \hat{H}' | \phi \rangle + \langle \phi | \hat{H} - \hat{H}' | \phi \rangle \\ &= E_0 - \int \rho(r) [v(r) - v'(r)] dr, \end{aligned} \quad (1.17)$$

Adding Equations (1.16) and (1.17), we obtain:

$$E_0 + E'_0 < E'_0 + E_0 \quad (1.18)$$

This represents a clear contradiction. So, there are no two different external potentials that can provide the same $\rho(r)$. Thus, $\rho(r)$ uniquely determines $v(r)$ and all ground-state properties. Now, we can write the energy E explicitly as a function of $\rho(r)$:

$$\begin{aligned}
 E[\rho] &= T[\rho] + T_{ne}[\rho] + V_{ee}[\rho] \\
 T_{ne}[\rho] &= \int \rho(r)v(r)dr \\
 &= \int \rho(r)v(r)dr + F_{HK}[\rho]
 \end{aligned} \tag{1.19}$$

where $T[\rho]$ represents kinetic energy, $T_{ne}[\rho]$ represents electron-nucleus attractions. Also, $v(r)$ represents the electric potential field of the nuclei as experienced by the electrons.

$$F_{HK}[\rho] = T[\rho] + V_{ee}[\rho] \tag{1.20}$$

Here, note that $F_{HK}[\rho]$ is only dependent on ρ and independent from any external potential $v(r)$. Thus, $F_{HK}[\rho]$ is a universal function of ρ .

The second Hohenberg-Kohn theorem describes that the ground state energy can be obtained variationally, with the density that minimizes the total energy being the exact ground state density. This is expressed as:

$$E_0[\rho_0] \leq E_v[\rho] \tag{1.21}$$

where $E_v[\rho]$ is the energy functional of Equation (1.19). Following the first part of the theorem, let's assume that the ground state wave function is ϕ and its related electron density is ρ . Thus, the ρ uniquely defines the external potential $v(r)$. If there is another wave function ϕ' with an arbitrary variation from ϕ , and its electron density is ρ' , then we can obtain:

$$\langle \phi' | \hat{H} | \phi' \rangle = \int \rho'(r) v[r] + F_{HK}[\rho'] = E[\rho'] \geq E[\rho] \quad (1.22)$$

So, the energy will be minimized only when the electron density is the ground state electron density.

1.6.4.2 The Kohn-Sham (KS) formulation

From the Hohenberg-Kohn theorem, we can obtain the ground-state energy by minimizing the energy function,

$$E[\rho] = \int \rho(r) v(r) dr + F_{HK}[\rho(r)] \quad (1.23)$$

Although the Hohenberg-Kohn theorem proved that on principle, the total energy could be obtained from the ground state density, it was not yet known how to get the $\rho(r)$, or $F_{HK}[\rho(r)]$.

In 1965, Kohn and Sham [109] published a paper that transformed density functional theory into practical electronic structure theory. Kohn and Sham recognized that the failure of Thomas-Fermi theory mainly results from the bad description of kinetic energy. To address this problem, they decided to re-introduce the idea of one electron orbitals and approximate the kinetic energy of the system using the kinetic energy of non-interacting electrons. This led to the central equation in Kohn-Sham DFT, which is the one-electron Schrödinger-like equation expressed as:

$$\left(-\frac{1}{2}\nabla^2 + v(r) + \int \frac{\rho(r')}{|r-r'|} dr' + v_{xc}(r)\right)\phi_i = \epsilon\phi_i \quad (1.24)$$

Here, ϕ_i are the Kohn-Sham orbitals and the electron density is expressed by,

$$\rho[r] = \sum_i^N |\phi_i(r)|^2 \quad (1.25)$$

The terms on the left side of Equation (1.24) are the kinetic energy of the non-interacting reference system, the external potential, the Hartree potential, and exchange-correlation potential, respectively. ε is the energy of the Kohn-Sham orbital. In addition, the exchange-correlation potential is given by,

$$v_{xc} = \frac{\delta E_{xc}[\rho(r)]}{\delta \rho(r)} \quad (1.26)$$

and $E_{xc}[\rho(r)]$ is the exchange-correlation functional. Moreover, we can define an effective potential (v_{eff}) which is,

$$v_{eff} = v(r) + \int \frac{\rho(r')}{|r-r'|} dr' + v_{xc}(r) \quad (1.27)$$

This allows Equation (1.24) to be rewritten in a more compact form of,

$$\left(-\frac{1}{2}\nabla^2 + v_{eff}\right)\phi_i = \varepsilon\phi_i \quad (1.28)$$

Clearly, this is a Hartree-Fock like single particle equation, which needs to be solved iteratively. Finally, the total energy can be determined from the resulting density through:

$$E = \sum_i^N \varepsilon_i - \frac{1}{2} \iint \frac{\rho(r)\rho(r')}{|r-r'|} dr dr' + E_{xc}[\rho] - \int v_{xc}(r)\rho(r) dr \quad (1.29)$$

Equations (1.25), (1.26), and (1.28) are the celebrated Kohn-Sham equations. Note that, (v_{eff}) depends on $\rho(r)$ through Equation (1.27). So, the Kohn-Sham equation must be solved self-consistently. The general procedure is to begin with an initial guess of the electron density, construct (v_{eff}) from Equation (1.27), and then obtain the Kohn-Sham orbitals. Based on these orbitals, a new density is obtained from Equation (1.25),

and the process is repeated until convergence is achieved. Finally, the total energy will be calculated from Equation (1.29) with the final electron density. If each term in the Kohn-Sham energy functional was known, we would be able to obtain the exact ground state density and total energy.

Unfortunately, there is one unknown term; the exchange-correlation (xc) functional (E_{xc}). E_{xc} includes the non-classical aspects of the electron-electron interaction, along with the component of the kinetic energy of the real system different from the fictitious non-interacting system. Since E_{xc} is not exactly known, it needs to be estimated.

1.7 Basis sets

A basis set is a set of wave functions that are made up of atomic orbitals (AOs). The linear combination of atomic orbital to form a molecular orbital is generally used in quantum chemical calculation for solving theoretical and computational chemistry problems. It will be helpful to take some issues [112] into account when considering a basis function: (a) the basis function should allow for the wave function/density to be accurately described with a computational cost as low as possible, (b) the basis function should have a behavior, which capture some of the physics of the problem. This means that in bond atomic or molecular systems, the function should go to zero when the distance between the nucleus and the electron becomes large.

There are two types of basis function that are generally used in electronic structure calculations. Early in quantum chemistry (QC), Slater-type orbital (STO) was used as a basis function due to their similarity to the solutions of the hydrogen atom. The STO possess this configuration in spherical coordinates:

$$\phi_i(\xi, n, l, m, r, \theta, \varphi) = Nr^{(n-1)}e^{(-\xi r)}Y_{(i,m)}(\theta, \phi) \quad (1.30)$$

where N is the normalization constant, ξ is called the exponent, and Y is the spherical harmonic function. n , l , and m are the quantum numbers: principal, angular momentum, magnetic, respectively. In QC calculations, Slater orbitals are restricted to atomic and diatomic systems, because the calculation involving three and four center two electron integrals is extremely slow and has no analytical form. It is used when high accuracy is required [113].

In contrast, numerous quantum chemistry codes employ Gaussian-type orbital (GTO), which gives less accurate results, but it utilizes a simple calculation process, making it faster and more favorable. Thus, GTO has become the most popular basis functions in QC [113]. The Gaussian function type orbital has the following form in Cartesian coordinates:

$$g(\xi, l_x, l_y, l_z, x, y, z) = N e^{-\xi r^2} x^{l_x} y^{l_y} z^{l_z} \quad (1.31)$$

where the sum of l_x , l_y , and l_z determine the types of orbital. Therefore, their sum ($L = l_x + l_y + l_z$) is analogous to the angular momentum for atoms, and to mark functions as the s-type ($L = 0$), p-type ($L = 1$), d-type ($L = 2$), and f-type ($L = 3$), etc.

The most important factor for using Gaussian functions (STO or GTO) and determining location (nuclei) of basis set is to decide what set/number of functions that are to be used. The minimum basis set that must be used corresponds to the number of possible functions, such as the number of atomic orbitals in the system. For example, the minimum basis set for hydrogen is only a single-type function, while they differ for the first or second row elements in the periodic table. Some common basis set, generally called Pople style basis set are mentioned by Jensen, including; STO-nG basis set, 3-

21G, 6-31G and 6-311G. In Pople style basis sets, polarization or diffuse functions can be added for further improvements. The purpose of adding diffuse functions (normally s- and p- function is denoted by + or ++) before G is to improve the description at large distances from the nuclei. In addition, an asterisk (*) is added after G to represent the polarization function for heavy and hydrogen atoms. The largest standard Pople style basis set is 6-311++G, which is derived for hydrogen and first row elements. The 6-31G* basis is identical to 6-31G (d), while 6-31G** basis is identical to 6-31G (d, p) [113].

1.8 Atoms in molecules (AIM)

The quantum theory of atoms in molecules (QTAIM) uses physics to define an atom and its contribution to observable properties in a given system. QTAIM was developed by Professor Richard Bader at McMaster University in the early 1960s.

Atoms in molecules (AIM) is a powerful and novel theory for understanding chemistry, acting as a bridge between fundamental chemical concepts such as, the atom, the bond, the molecular structure, and quantum mechanics. It is widely used in both theoretical and crystallographic research, including interpreting experimental charge densities. The theory is also applied to hydrogen-hydrogen bonds as they occur in molecules [114].

1.9 Natural bond orbital (NBO)

In 1952, the concept of natural orbitals was first introduced by Per-Olov Löwdin, to describe the unique set of orthonormal 1-electron functions that are intrinsic to the N-electron wavefunctions [115]. The natural bond orbitals analysis is a powerful tool in population analysis calculations, which is more robust than the traditional Mulliken approach. Furthermore, it is almost insensitive to the change of basis set,

while Mulliken's Population analysis (MPA) is highly sensitive to any basis set change. Another advantage of the NBO analysis is that it provides a localized description of electron density over a molecule, rendering it intuitive for chemists.

A complete description of the distribution of electrons in molecules is provided by the electron density function, but it could be difficult to operate. It can be simplified by somehow dividing the charge cloud among the atoms, generating a partial charge assigned to each atom.

The Milliken population analysis (MPA) is one way to achieve this, which divides the so-called overlap population equally among the basis functions. A better procedure to generate partial charges is based on the eigenvalue equation of the first order reduced density operator, which is called the natural bond orbital analysis [116, 117].

$$\Gamma \psi_i = P_k \psi_i \quad (1.32)$$

where the P_k eigenvalues represent the population of the ψ_i eigenorbitals. In fact, the density operator (Γ) is the one-electron projection of the N-electron density distribution defined by the probability $[\phi^2]$ (Γ is a Hermitian operator, a one dimensional projector), hence it is very suitable for characterizing the one-electron properties of the wavefunctions. The natural bond orbital analysis includes a series of transformations that generate localized (NAO), hybrid (NHO), bonding (NBO) or natural localized molecular orbitals (NLMO) from the initial functions of the selected basis set.

$$\chi_\mu \rightarrow \text{NAO} \rightarrow \text{NHO} \rightarrow \text{NBO, NLMO}$$

Moreover, the basis functions can be transformed to delocalized natural orbitals (NO) or to the canonical molecular orbitals (MO). Orbitals obtained in each step form

an orthonormal set, i.e. they span the same dimensionality as the original basis set, which means that they can be used to generate the wavefunction to calculate the properties of the whole system alike. The natural atomic orbitals (NAO) are one-centered localized orbitals that represent the "effective" natural orbitals of atom A in the molecules. The shape of NAOs is optimized for their effective atomic charge in the molecular environment, therefore, if an atom A has a more cationic character, then the NAOs are more contracted; and if it is more anionic, the NAOs are more extended. In addition, NAOs incorporate the proper nodal features due to steric (Pauli) confinement in the molecular environment.

Neglecting the mutual orthogonality between two atoms, the pre-orthogonal NAOs (PNAOs) can be obtained, which overlaps with the PNAOs of other atoms. This feature enables us to estimate the strength of different interactions by calculating the stabilization energy coming from the overlap. The natural bond orbitals (NBOs) are multiple-centered localized orbitals that provide a Lewis-type description of the chemical bond. The NBOs are composed of natural hybrid orbitals:

$$\Omega_{AB} = a_A h_A + a_B h_B, h_A = \sum_k a_k \psi_k^{(A)} \quad (1.33)$$

where $a_A^2 + a_B^2 = 1$. Depending on the values of these coefficients the character of the NBO can range between covalent ($a_A^2 = a_B^2$) or ionic ($a_A^2 \gg a_B^2$) shapes. The pre-orthogonal hybrid orbitals (PNHOs) can be derived from PNAOs using similar coefficients.

They also form a complete basis set, which spans the dimensionality of the original basis set. NBO analysis can also provide a description standing close to the valence bond theory namely; it calculates the composition of the aforementioned hybrid

orbitals by using the conventional sp^λ notation, where λ expresses the p-character (percentage of-p) or s-character (percentage of-s) of the hybrid; characterized in this manner to correspond to the NBOs. Not surprisingly, the core NBOs exhibited an almost total NAO character, whereas the non-bonding NBOs (a lone pair of electrons localized on one center) are identical to normalized NHOs ($h_A = h_B$). All NBOs are made up of valence NHOs that must be orthogonal to the anti-bonding NBOs, which are defined as follows:

$$\Omega_{AB}^* = a_B h_A - a_A h_B \quad (1.34)$$

The $\Omega_{AB}^* - s$ is typically the most important non-Lewis type acceptor orbitals, playing an important role in supermolecular donor-acceptor interactions, such as hydrogen bonds. Knowledge of these properties is essential to understand the number of non-covalent and delocalization-related phenomena, which are beyond the concepts of Lewis-structures. Neglecting Rydberg-type NBOs, the NBO set can also be reduced to the size of the NMB in accordance with the chemical perspective. From NBOs, one can create the pre-orthogonal orbitals (as PNAOs are created from NAOs), which are the PNBOs that are able to overlap with each other. These overlaps can explain donor-acceptor interactions, such as the formation of Hydrogen bonds, which is usually regarded as an overlap between an anti-bonding orbital of an X-N bond (acceptor) and a lone pair of electrons of an atom with high electronegativity, such as F, O or N atoms.

1.10 Software

Today, computational chemistry method calculations using software such as Gaussian are popular in chemistry and biochemistry. It is a powerful tool that predicts the types of interaction and helps determine the electronic properties.

In the current investigation, we have used Gaussian 09 in Windows and Linux OS. Molecular orbitals and imaginary frequencies have been viewed using Gauss view 5.0. AIM 2000 is software that displays paths, followed by the electron density between atoms within a molecule. In addition, it allows the study of the bonding properties of the system to be studied, with changes in bonding being observed to check whether the bonds are covalent, ionic, etc. NBO3.1 is software that can be used to investigate intramolecular interactions in a molecule. This utility program within Gaussian is used to evaluate the energies of orbitals, stability and other important properties, and to study the changes in bonding and electron density during the reaction.

1.11 Objective and outline of the chapters in this thesis

This thesis is divided into seven chapters. The first chapter includes a general introduction on carbon nanotubes and glycolipids, hydrogen bonding and a brief overview of the principles of quantum mechanics. The second chapter describes literature review on carbon nanotubes and the formation hydrogen bonds in multiple biological systems. The methodology and technical parts of computational research, namely; the density functional theory (DFT) calculation and atoms in molecules (AIM) analysis and natural bond orbital analysis will be provided in Chapter 3. Chapters 4 and 5 details the investigation of the rule of hydrogen bonds in sugar-based surfactants, such as galactopyranoside, glucopyranoside, mannose, and mannopyranoside using the density functional theory, atoms in molecules approach, and natural bond orbital analyses. The interaction and mechanism between glucopyranoside and carbon nanotubes based on density functional theory are presented in Chapter 6. Finally, the overall conclusion of the work and some future possible research plans are discussed in Chapter 7.

CHAPTER 2

LITERATURE REVIEW

For the past decades, the unique nature of nanomaterials and its corresponding excellent mechanical, thermal, and electronic properties are responsible for the exponential progress of fields such as nanoelectronics, molecular assemblies, nanocomposites, tissue engineering and biomedicine.

2.1 The rule of surfactants in dispersion of carbon nanotubes

The discovery of carbon nanotubes offers exciting opportunities for the development of novel functional materials such as drug delivery systems. In these cases a variety of surfactants have been used as dispersing agents to SWNTs, for examples those possessing the aryl-thiols and alkylthiol with various end groups (e.g. 4-methylbenzene, 4-nitrobenzene, 4-aminebenzene, 4-bromobenzene, 4-hydroxybenzene, 4-fluorobenzene, 4-methoxybenzene, H-benzene, 4 nitrilebenzene) and (e.g. OH, perfluoro, SH, CH=CH₂, CH₃, NH₂) respectively [118]. Generally, ionic surfactants are preferable as emulsifiers for carbon nanotubes/water soluble solutions. On the other hand, non-ionic surfactants are proposed when organic solvents have to be used.

To decrease agglomerations of nanotubes, several techniques, namely ultrasonication and high shear mixing, have been used to alter the surface chemistry of the tubes either covalently (functionalization), or non-covalently (adsorption) [119]. Common functionalized CNTs, such as MWNT-COOH, are obtained via oxidation using different acids, ozone or plasma, which creates other oxygen functional groups (e.g., -OH, -C=O). COOH groups on carbon nanotube surfaces are useful sites for further modification. Various molecules, such as synthetic and natural polymers can be grafted through the creation of amide and ester bonds [120].

Figure 1 illustrates many routes to chemically modify (covalently functionalization) the surface of CNTs. In this section, we review the recent progress and advances of carbon

nanotubes dispersions in aqueous and organic media by covalent and non-covalent adsorption of surfactants and polymers.

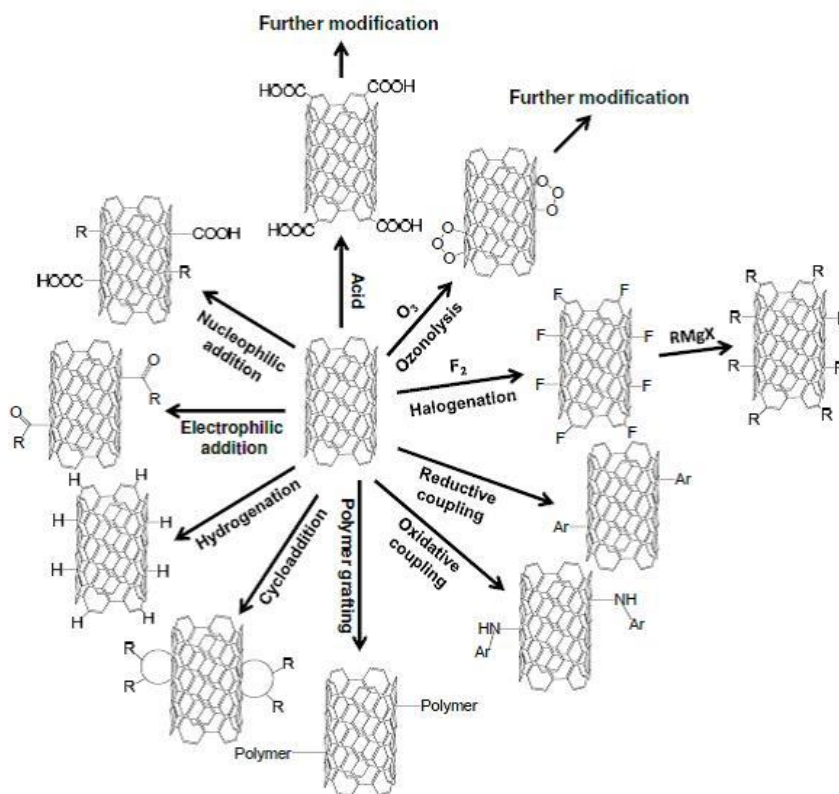


Figure 2.1: schematic examples of surface functionalization of CNTs. (illustration adapted from [121]).

2.2 Dispersions of carbon nanotubes in water soluble

Carbon nanotubes can be dispersed in water when they are coated by adsorbed surfactants that have relatively high HLB (hydrophilic-lyphophic balance). This non-covalent method is classically employed for dispersing both organic and inorganic particles in aqueous solutions.

The concentration and the nature of the surfactant and type of interaction are known to play a crucial role in the phase behavior of classical colloids [122], as well as carbon nanotubes [123, 124, 125].

The interaction (adsorption) mechanism with ionic surfactants, and the colloidal stability of CNT suspensions can be understood from the knowledge of the surface charge of carbon nanotubes in different media. Multi walled-carbon nanotubes were found to be negatively charged in water from the zeta-potential analysis of the tube [126]. However, some groups have shown insufficient debundling power of the anionic surfactant SDS being due to charge repulsions.

The effect of head-group charge was investigated for various systems [127, 128], revealing no clear conclusion on the superiority of either cationic or anionic surfactants in dispersing the tubes. Adsorption mechanism of ionic surfactants, which is promoted by electrostatic interactions with the CNTs surface, is heavily controlled by the purification process and wall-functionalization of the tube, which in turn determine its surface charge. Ionic surfactants such as SDS [123, 129, 130] and dodecyl-benzene sodium sulfonate (NaDDBS) [131, 132, 133] were commonly used to decrease CNT aggregative tendency in water. The benzene ring along the surfactant was assumed to be one of the main reasons for high dispersive efficiency of NaDDBS [131] and even better efficiency of anionic alkyldiphenyl-oxide disulfonate such as Dowfax surfactant. Dowfax surfactant have twice the charge of NaDDBS and a di-benzene group [134]. π -stacking interactions of the benzene rings onto the carbon nanotube surface are believed to increase the adsorption ratio of surfactants [131] as well as of other highly aromatic molecules [135] and rigid conjugated polymers [136].

In addition, it was shown that not only aromatic groups but also naphthenic (saturated rings) group provides good surfactant-tube affinity. Therefore, Ultraviolet-visible (UV-Vis) spectroscopy analysis confirm that aerosol OS surfactant (sodium diisopropyl-naphthalene sulfonate) showed higher fractions of individual tubes compared to the results obtained with NaDDBS and Dowfax surfactants [134].

In non-ionic surfactants such as Tween-60 and Tween-80 (polyethylene oxide (20) sorbitan monostearate, and monooleate, the advantage of a dispersant containing a carbon double bond, and with similar head group and tail length, was confirmed by particle size analysis [127]. Tween-80 have a higher surface activity compared to Tween-60, since the former has unsaturated carbon in its tail structures. These results are confirmed by SEM images of highly dispersed MWNT in polyethylene glycol (PEG) matrix. Triton X-100 wetted SWNT was further treated with PEG to prevent the adsorption of streptavidin proteins on the side walls of the tubes [137]. The addition of a weakly bond semi flexible polymer to the NaDDBS/SWNT system helped to increase the dispersion and generated highly oriented nanotubes in the polymer solution when sufficient shear stresses were provided [132].

The utilization of surfactant-coated CNT has become a standard procedure for various applications. Thus, chemical functionalization of SDS-coated nanotubes by aryldiazonium salts was reported [138, 139]. Surfactants such as cetyltrimethylammonium bromide (CTAB) [140] and π -10 (polyethylene oxide (10) nonylphenyl ether) [141], were successfully used during in-situ polymerization of CNT-polymer composites. Polystyrene (PS) and poly (methyl methacrylate (PMMA) microspheres were dropped into aqueous solution of MWNT and CTAB (or NaDDBS) to produce carbon nanotube adsorbed polymeric microspheres [142]. Re-condensation of SDS-dispersed SWNT in polymer solution stream enabled the creation of rigid fibers and ribbons of preferentially oriented nanotubes [143, 144].

According to unzipping mechanism [145], a surfactant has to get into the small spaces between the bundle and the isolated tube, and to prevent them from re-aggregating. As a result, surfactants with bulky hydrophobic groups will be prevented from penetrating into the inter-tube region, and exhibit reduced debundling efficiency.

However, bulky hydrophilic groups were reported to be advantageous in the case of nanotubes suspended with non-ionic surfactants, probably due to the enhanced steric stabilization provided by longer polymeric groups [146]. There are three commonly used models for adsorption; CNT encapsulation within a cylindrical detergent micelle [147], hemispherical absorption of detergent onto CNTs [131], and random adsorption of detergent onto the tube-surfactant [123].

2.3 Organic solvents dispersions of carbon nanotubes

Compared to water-soluble systems, thus far only limited research work has been carried out with surfactant-assisted dispersions in organic solvents. Carbon nanotubes have been shown to exhibit a sufficient solubility only in a limited number of solvents, such as dimethyl formamide (DMF), dimethyl acetamide (DMAc) and dimethyl pyrrolidone (NMP) [148]. When SWNT was immersed in DMF, the CNT structure was damaged [149]. In order to improving the thermo-mechanical properties of the nanocomposite, a non-ionic surfactant to carbon nanotube has to be added. For example, by adding non-ionic surfactant such as polyoxyethylene 8 laury to produce MWNT-epoxy composites, the dispersion of the filler in acetone was increased [150].

On the other hand, the addition of carbon nanotubes without the surfactant had only moderate effects on the polymer glass transition temperature and its corresponding elastic modulus. Tergitol NP-7 (polyethylene oxide (7) nonylphenyl ether) is non-ionic surfactant in the processing of CNT-epoxy composite was also investigated [151]. The thermo-mechanical response of PMEMA was reported to be significantly improved by only 1 wt.% of MWNT dispersed in tetrahydrofuren (THF), with the aid of Triton X-100 surfactant [152].

2.4 Carbon nanomaterial in biological systems

Carbon nanotubes (CNTs) could be one of the most advanced nanovectors for the highly efficient system for the delivery of drugs and biomolecules owing to their large surface areas with unique optical and electrical properties. They can be conjugated non-covalently with drugs, proteins, biopolymers, and synthetic polymers, namely; DNA, RNA, polyvinyl pyrrolidone, polystyrene sulfonate and surfactants (sodium dodecyl sulfate or SDS, etc) to form supermolecular assemblies. In addition, they can be modified covalently, for example, the esterification or amidation of acid-oxidized nanotubes and sidewall covalent attachment of functional groups [153].

Polymer wrapping was proposed by *Smalley et al.* as a non-covalent scheme to soluble tubular carbon nanostructures [147]. In this scheme, polyvinyl pyrrolidone (PVP), polystyrene sulfonate (PSS), or SDS binds to SWNT surfaces in double helix, triple helix, multiple parallel wrapping.

The helical wrapping was described by *Zheng et al.* as the binding of single-stranded DNA (ssDNA), specifically poly (T), to an SWNT [154]. In this model, ssDNA was treated as a flexible molecule with bond torsions within the sugar phosphate backbone.

Georgakilas et al. showed the covalent binding of SWNTs with amino acids, the building blocks of protein [155]. *Huang et al.* attached the protein BSA to SWNTs via diimide-activated amidation under ambient conditions [156]. Moreover, larger proteins such as fibrinogen (Mw 340 kDa) exhibit poorer binding abilities to SWNTs than smaller proteins such as streptavidin (MW 60 kDa) [137].

Amphiphiles such as SDS, Triton X-100, Pluronic F108, and phospholipids are often more advantageous than macromolecules such as linear polymers, protein, and

nucleic acids in rendering SWNTs water soluble, due to the large curvature and small diameter (0.8–2 nm) of an SWNTs. The use of zwitterionic lysophosphatidylcholine (LPC) was demonstrated recently for solubilizing SWNTs in aqueous solutions [157].

The negative charged surfactant such as SDS was introduced by *Smalley et al.* was found in many applications in photoluminescence of SWNTs and in the optical detection of SWNT translocation [129, 158]. There have been numerous computational studies of carbon nano tubes interaction with surfactants. *B. Shirvani et al.* [159] reported that the adsorption is dependent on the tube's diameters via using density functional theory. The results indicated that with the increase of the diameter of zigzag and armchair tubes, the binding energy molecule decreases.

Wang et al. [160] investigated the effect of different substituent group on single walled-carbon nanotube by the ONIOM (B3LYP:UAM1) method and explained the theoretical evidence for a two-step mechanism in the functionalization CNTs by aryl diazonium salts. *Wallace et al.* [161] also showed this using coarse-grained (CG) molecular dynamics to study the self-assembly of CNTs with various amphiphile for CNT solubilization whilst minimizing perturbation of cell's membrane integrity.

2.5 Hydrogen bonding in glycolipid surfactants

The properties of hydrogen bonds have been widely investigated, both theoretically and experimentally [162, 163, 164]. The axial/equatorial orientation of C1-O1 (α/β) is a key factor related to the number of hydrogen bonding, which may exist to stabilize the self-assembly, and in turn influence the melting (T_m) and clearing points (T_c) values of surfactants. Therefore, the role of polar interaction of monosaccharide head group is important, as it stabilizes self-assembly. Generally, this bond has an energy value ranging from as low as 0.24–0.28 kcal/mol (for weak hydrogen bond), and

this value could reach up to a maximum value of 38 kcal/ mol. On average, most HB ranges between 1.2–7.2 kcal/mol [165, 166, 167]. In the context of the sugar groups, the water carbohydrate bond energies are in the range of approximately 3.34–6.45 kcal/mol [168].

For a system such as maltose with eight hydroxyl groups (OHs), the intra- and intermolecular hydrogen bonds between the sugar groups and the solvent play a crucial role in determining the behavior of the conformations [169, 170, 171]. The strength of these hydrogen bonds allows for strong resistance to thermal distortion of the structure at room temperature, which is about a magnitude higher than kT . Thus, the conformation of sugar and their solvation properties is influenced by the presence of HB [170].

Generally, for carbohydrate monomers, the ring puckering and the multiple bonding sites for primary and secondary hydroxyl groups contribute many conformational preference observables, which in turn helps in stable structure predictions [172]. To understand the complex conformational spaces, a systematic study at the rotors, specifically at glycosidic bonds between monomers and linkage at hydroxymethyl groups provides meaningful expositions for the flexibility shown by a monomer. The hydroxymethyl group (primary alcohol) has three staggered rotamers about the O5-C5-C6-O6 dihedral angle namely, gauche-gauche (gg), gauche-trans (gt) and trans-gauche (tg) [173]. A recent computational study has shown that gauche effect in sugar monomers determines the conformation of gg, gt and tg population in both vacuum and explicit water environments. In glucose moiety, gg conformer is preferred in vacuum compared to gt and tg conformers. But in the presence of water, the preference changes in the order of $gt > gg > tg$. A similar trend is shown by galactose is observed, where the order of hydroxymethyl population changes from $gt > gg > tg$ in

vacuum to $gt > tg > gg$ in water environment. This can be explained by the existence of intra-molecular hydrogen bonding among the hydroxyl groups and bridging hydrogen bonds with water molecules due to the change in conformer populations [173].

Interestingly, an *ab initio* study by *Grabowski* [174] provides an inverse proportional relationship between the distances of (OH...O) and (O-H) bond strength. When HB is stronger, the length of O-H bond becomes greater, but the H...O and O...O distances are shorter, and these results do agree with those from previous studies [175]. Cook et al. [176, 177] have investigated the role of hydrogen bond in stabilizing the liquid crystal phase behavior of methyl-6-O-(n-dodecanoyl)- α -D-glucopyranoside using variable temperature FTIR spectroscopy and X-ray diffraction. From this study, they proposed a model where a combination of hydrogen bonding and conformational arrangements (enthalpy versus entropic effects) leads to the formation of smectic-like domains in the isotropic phase, subsequently stabilizing the smectic A phase [177].

In the molecular dynamic simulation study of these systems by *Chong et al.*[171], it was found that the thermal stability of the self-assembly structure was related to the intra layer instead of the interlayer hydrogen bonds. These results were far from being conclusive and a more detailed calculation is necessary to establish a relationship.

In the next chapter, we will describe the methodology, including quantum calculation of compound studies with GAUSSIAN 09 and atoms in molecules (AIM) and natural bond orbitals (NBO) analysis.

CHAPTER 3

METHODOLOGY

In this chapter, quantum chemistry (QC) software was used to study the interaction between glycolipid and a single-walled carbon nanotube is briefly reviewed. In addition, the computation of the intra-hydrogen bond formation in glycolipid is described.

3.1 Gauss View (GV) software:

One of the most advanced and powerful graphical software available in the Gaussian package is Gaussview (GV). Gaussview can import several formats, such as pdb, ml2, mols, cif, sdf, and rxn or build molecular structures. It can also set up, launch, monitor, and control Gaussian calculations, retrieve, and view the results, all without ever leaving the application. This software can also display molecule orbitals calculated by the Gaussian program and natural bond orbital program in Gaussian. The version used by this work is GaussView 5.0, which includes many new features designed to make working with large systems of chemical interest convenient and straightforward. It also provides full support for all of the new modeling methods and features in Gaussian 09. GaussView 5.0 also presents predicted spectra and other numeric results as plots or graphs. Figure 3.1 illustrates the brief application of Gauss View.

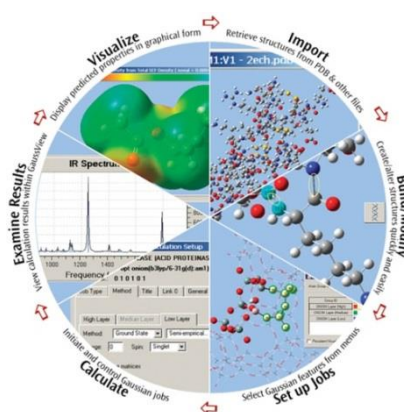


Figure 3.1: Visualizing molecules and reactions with Gauss view (adopted from http://www.gaussian.com/g_prod/gv5b.htm).

3.2 Gaussian software

These are many programs such as Materials Studio CASTEP, General Atomic and Molecular Electronic Structure System (GAMESS), etc, to calculate electronic structure. Gaussian is the most popular computer program for computational chemistry to solve *ab initio* and semi empirical problems. It was initially released in 1970 by John Pople and his research group at Carnegie-Mellon University, bearing the name Gaussian 70 [178]. The major release history is Gaussian (70, 76, 77, 80, 82, 83, 85, 86, 88, 90, 92, 93, 94, 95, 96, 98, 03). The name originated from the Pople's use of the Gaussian orbitals to speed up calculations compared to those using the Slater-type orbitals, which is a choice made to improve the performance on the limited computing capacities of the then-current computer hardware for Hartree-Fock calculations. Originally, the software was available through the quantum chemistry program exchange (QCPE), and it was later licensed out of Carnegie Mellon University, and since 1987 has been developed and licensed by Gaussian, Inc.

The latest version in the Gaussian series of programs is Gaussian 09. It is a cross-platform, running on Windows (G09W), power-pc-based Mac (G09M), and Linux/UNIX systems. The research presented in this thesis operated using Windows and Linux environment (G09W Cluster/Network Parallel versions). The calculation on Windows system is easy, but the multiprocessor version of G09W is limited to 4 processors (or cores). Similarly, any individual node within a cluster/network parallel job can take advantage of at most, 4 processors/cores. Additionally, the path file (.chk) under two systems is different. In a Linux system, the file is saved as a read-write file (.rwf) or integral file (.int) to create a folder in root or user.

Gaussian 09 predicts the energies, molecular structures, vibrational frequencies, and molecular properties and reactions in a wide variety of chemical environments. It can be applied to both stable species and compounds that are difficult or impossible to experimentally observe (short-lived intermediates and transition structures). The setting up and running of a typical Gaussian Job in Windows and Linux is described in the Appendix A.

3.3 AIM 2000 software

Quantum theory of atoms in molecules (QTAIM) was initially developed by Professor Richard Bader and his research group at McMaster University. QTAIM is applied to molecular and condensed matter electronic systems (such as crystals) with unusually short distances between neighboring molecules as observed by the X-ray diffraction technique. It defines chemical bonding and structure of a chemical system based on the topology of the electron density. An electron density distribution of a molecule is an average probability distribution of the electronic charge throughout the real space in the attractive field exerted by the nuclei. According to QTAIM, molecular structure is revealed by the stationary points of the electron density together with the gradient paths of the electron density that originate and terminate at these points. AIM 2000 is a software package for performing quantitative and visual quantum theory of atoms in molecules analyses of molecular systems, which starting from molecular wavefunction data. This program is designed by Friedrich Biegler-König and Jens Schönbohm.

The (*.wfn) is an input file for AIM 2000 program. There are two types output files. The first is (*.aim) to view the structure at critical point (molecule graph), and (*.txt) is to obtain some properties such as:

$\rho(r)$ or $\rho(r)$: electron density

$\nabla^2 \rho(r)$: corresponding Laplacian

$G(r)$: electronic kinetic energy density

$V(r)$: electronic potential energy density

$G(r)+V(r)=H(r)$: electronic energy density

More detail descriptions are given in Appendix B.

3.4 Calculated properties

3.4.1 Polarizable continuum (PCM) model

The polarizable continuum model (PCM) is a computational method to model solvation effects. It was originally developed 30 years ago by *Miertus et al* [179]. PCM model predicts the possible chemical reaction in the solution phase using *ab initio* calculations. Therefore, modeling the solvent as a polarizable continuum, rather than individual water molecules, makes the *ab initio* computation feasible.

Solute-solvent interactions can have dramatic effects on molecular energies, structures, and properties and in many cases such effects can be computed very effectively in the framework of continuum solvation models. In these models the bulk of the solvent is represented as a structureless polarizable medium characterized mainly by its dielectric constant. Even when specific interactions require the introduction of some explicit solvent molecules, which strongly bound to the solute, the continuum picture is still very useful (and often necessary) to account for long range interaction.

The PCM framework is based on one of the most effective continuum approaches, due to two main characteristics, namely; the use of a molecular cavity and use of a surface charge distribution. These two characteristics in fact make the PCM an extremely versatile method in terms of possible applications to solutes of any shape and charge distribution and to properties and processes, which strongly depend on solvent-induced deformations of both the shape and the charge. More recently, PCMs are popularly used; D-PCM (D stands for dielectric) which deals the continuum as a polarizable dielectrics and C-PCM (C stands for conductor-like PCM) which deals the continuum as a conductor-like picture [180, 181]. The PCM model is available to calculate energies and gradients at the Hartree-Fock and the density functional theory levels in various quantum chemical computational packages such as Gaussian, GAMESS, etc.

3.4.2 HOMO and LUMO

The bonding and anti-bonding molecular orbitals that are a linear combination of molecular atomic orbitals are based on the molecular orbitals (MO) theory. Due to the bonding orbital being lower energy than the anti-bonding orbitals, the bonding orbital is the first to be occupied, while the anti-bonding are unoccupied. HOMO is the highest occupied molecular orbital, while the LUMO is the lowest unoccupied molecular orbital. Some properties of HOMO and LUMO are given in Table 3.1.

Table 3.1: Some properties of HOMO and LUMO.	
HOMO	LUMO
donated electrons	receives electrons
characteristic for nucleophilic component	characteristic for electrophilic component
most available for bonding	lowest energy orbital available
most weakly held electrons	-

One of the key parameter for understanding the electronic structures is the energy difference between LUMO and HOMO. The energy gap [182] is defined as:

$$\Delta\mathcal{E}_{(L-M)} = \mathcal{E}_{LUMO} - \mathcal{E}_{HOMO} \quad (3.1)$$

The softness (S) and chemical hardness (η) of molecules are determined by the energy gap, where a high energy gap means lower softness and vice versa.

3.4.3 The topology of the electron density

Atoms in molecules theory [183] relies on quantum observables such as the electron density $\rho(r)$ (r is the spatial coordinate) and the energy density at the critical points (CP). A display of $\rho(r)$ for a molecule will make visible to the eye, without further mathematical analysis, and the definitions of its atoms with a particular set of lines linking certain pairs of nuclei within the molecular graph. A critical point (CP) in the electron density is a point in space where the first derivatives of density vanish, i.e., $\nabla\rho(r)=0$. This means that the gradient of a scalar function, such as $\rho(r)$ at CP is equal to zero. Therefore, they determine the positions of extrema in the charge density; maxima, minima, or saddles. One can discriminate between a local minimum, a local maximum, or a saddle point by considering the second derivations, and the elements of the tensor $\nabla\nabla\rho$. There are nine second derivatives of $\rho(r)$ that can be arranged in the so-called “Hessian matrix”, which when evaluated at a CP located at $\rho(r)$, is written as:

$$A(r_c) = \begin{bmatrix} \frac{\partial^2 \rho}{(\partial x^2)} & \frac{\partial^2 \rho}{(\partial x)(\partial y)} & \frac{\partial^2 \rho}{(\partial x)(\partial z)} \\ \frac{\partial^2 \rho}{(\partial x)(\partial y)} & \frac{\partial^2 \rho}{(\partial y^2)} & \frac{\partial^2 \rho}{(\partial y)(\partial z)} \\ \frac{\partial^2 \rho}{(\partial z)(\partial x)} & \frac{\partial^2 \rho}{(\partial z)(\partial y)} & \frac{\partial^2 \rho}{(\partial z^2)} \end{bmatrix}_{r=r_c} \quad (3.2)$$

The Hessian matrix can be diagonalized because it is real and symmetric. The diagonalization of $A(r_c)$, is equivalent to a rotation of the coordinate system $r(x, y, z) \rightarrow r(x', y', z')$ superimposing the new axes x', y', z' with the principal curvature axes of the critical point. The rotation of the coordinate system is accomplished via a unitary transformation, $r' = rU$, where U is a unitary matrix constructed from a set of three eigenvalue equations $Au_i = \lambda_i u_i (i=1,2,3)$ where u_i is the i^{th} column vector (eigenvector) in U . A similar transformation $U^{-1}AU = (\Lambda)$ transforms the Hessian into its diagonal form, which is written explicitly as:

$$\Lambda = \left[\begin{array}{ccc} \frac{\partial^2 \rho}{(\partial x'^2)} & 0 & 0 \\ 0 & \frac{\partial^2 \rho}{(\partial y'^2)} & 0 \\ 0 & 0 & \frac{\partial^2 \rho}{(\partial z'^2)} \end{array} \right]_{r'=r_c} = \left[\begin{array}{ccc} \lambda_1 & 0 & 0 \\ 0 & \lambda_2 & 0 \\ 0 & 0 & \lambda_3 \end{array} \right] \quad (3.3)$$

where λ_1 , λ_2 and λ_3 are the curvatures of the density with respect to the three principal axes x', y', z' .

An important property of the Hessian is that its trace is invariant to rotations of the coordinate system. The trace of the Hessian of the density is known as the Laplacian of the density $\nabla^2 \rho(r)$ and, when $x = x'$, $y = y'$ and $z = z'$, it is given by:

$$\nabla^2 \rho(r) = \nabla \nabla \rho(r) = \frac{\partial^2 \rho(r)}{(\partial x^2)} + \frac{\partial^2 \rho(r)}{(\partial y^2)} + \frac{\partial^2 \rho(r)}{(\partial z^2)} \quad (3.4)$$

$$\frac{\partial^2 \rho(r)}{(\partial x^2)} = \lambda_1, \frac{\partial^2 \rho(r)}{(\partial y^2)} = \lambda_2, \frac{\partial^2 \rho(r)}{(\partial z^2)} = \lambda_3 \quad (3.5)$$

where the primes of the principal axes are dropped.

There are four possible kinds of stable critical points in $\rho(r)$ and each will be associated with a particular element of structure. We shall assume that atoms exist in

molecules and that they may be linked together to form structures consisting of chains, rings, and cages [184]. Critical points are classified according to their ranks (r) and signatures (s), and are symbolized as (r, s) . The rank is the number of non-zero curvatures of the critical point. A critical point that has $\omega < 3$ is mathematically unstable, and will vanish or bifurcate under small perturbations of the density caused by nuclear motions. They are generally not found in equilibrium charge distributions, and one nearly always finds $\omega = 3$. The signature is the algebraic sum of the signs of the curvatures, i.e. each of the three curvatures contributes ± 1 , depending on whether it is a positive or negative curvature.

There are four types of stable critical points having three non-zero eigenvalues:

$(3, -3)$ three negative curvatures: ρ is a local maximum,

$(3, -1)$ two negative curvatures: ρ is a maximum in the plane defined by the corresponding eigenvectors but is a minimum along the third axis, which is perpendicular to this plane,

$(3, +1)$ two positive curvatures: ρ is a minimum in the plane defined by the corresponding eigenvectors and a maximum along the third axis, which is perpendicular to this plane,

$(3, +3)$ three curvatures are positive: ρ is local minimum.

Each kind of CP described above is identified with an element of chemical structure: $(3, -3)$ nuclear critical point (NCP); $(3, -1)$ bond critical point (BCP); $(3, +1)$ ring critical point (RCP); $(3, +3)$ cage critical point (CCP) [116]. (See Table 3.2 for more details).

The bond path is a universal indicator of chemical bonding of all kinds; weak, strong, closed-shell, and open-shell interactions [185]. The point on the bond path with the lowest value of the electron density (minimum along the path) is the bond critical point (BCP). The collection of bond paths linking the nuclei of bonded atoms in equilibrium geometry, with the associated critical points, is known as the molecular graph. The molecular graph provides an unambiguous definition of the molecular structure, and is thus used to locate changes in the structure along a reaction path.

Table 3.2: The four kinds of critical point (CP) are identified with an element of chemical structure (r :rank and s :signature).

(r,s)	Symbol	Descriptions
(3, -3)	NCP	All curvatures are negative, a local maximum – a nuclear critical point.
(3, -1)	BCP	Two curvatures are negative and one is positive, ρ is a maximum in a plane and a minimum perpendicular to this plane – a bond critical point.
(3, +1)	RCP	Two curvatures are positive and one is negative, ρ is a minimum in a plane and a maximum perpendicular to this plane – a ring critical point.
(3, +3)	CCP	All curvatures are positive, a local minimum – a cage critical point.

3.4.4 The Laplacian of the electron density at the BCP $[\nabla^2 \rho(r)]$

Because the Laplacian is essentially a second derivative, its sign indicates regions of local electronic charge concentration or depletion with respect to the immediate neighborhood. Thus, where $\nabla^2 \rho(r) > 0$, the density is locally depleted and expanded relative to its average distribution; where $\nabla^2 \rho(r) < 0$ the density is locally concentrated, tightly bound, and compressed relative to its average distribution. A local charge concentration behaves as a Lewis base (electron donor), whereas the local charge depletion acts as a Lewis acid (electron acceptor).

The Laplacian at the BCP is the sum of the three curvatures of the density at the critical point, the two perpendicular to the bond path, λ_1 , and λ_2 , being negative (by convention, ($|\lambda_1| > |\lambda_2|$)), whereas the third, λ_3 , lying along the bond path, is positive. The negative curvatures measure the extent to which the density is concentrated along the bond path, while the positive curvature measures the extent to which it is depleted in the region of the interatomic surface and concentrated in the individual atomic basins. In covalent bonding, the two negative curvatures are dominant and $\nabla^2 \rho(r) < 0$. In contrast, in closed-shell bonding, for example ionic, hydrogen-bonding, or van der Waals interactions, the interaction is characterized by a depletion of density in the region of contact of the two atoms and $\nabla^2 \rho(r) > 0$.

3.4.5 The bond ellipticity

One of the interesting parameters to measure bond stability is the ellipticity (ε). It provides a quantitative measure of the π -bond character and delocalization of electronic charge. The ellipticity is defined as:

$$\varepsilon = \frac{\lambda_1}{\lambda_2} - 1 \quad (3.6)$$

where $|\lambda_1| \geq |\lambda_2|$.

If $\lambda_1 = \lambda_2$, then $\varepsilon=0$, and the bond is cylindrically symmetrical. High ellipticity values indicate the instability of the bond [89].

3.4.6 Energy densities at BCP

The Laplacian of the charge density plays a central role in the theory of atoms in molecules where it appears as an energy density, which is,

$$L = -\left(\frac{\hbar^2}{4m}\right)\nabla^2\rho(r) \quad (3.7)$$

The energy densities at the bond critical points including electronic potential energy density $V(r)$, electronic kinetic energy density $G(r)$, and total energy density $H(r)$ are used to summarize the mechanics of a bonding interaction. The electronic potential energy density $V(r)$, also known as the virial field, is negative everywhere, the energy kinetic energy density is positive everywhere. The local statement of the virial theorem expresses the relationship between the virial field, kinetic energy density, and the Laplacian, which when written for a stationary state, is:

$$\left(\frac{\hbar^2}{4m}\right)\nabla^2\rho(r) = 2G(r) + 2V(r) \quad (3.8)$$

Since we always have $G(r) > 0$, and, $V(r) < 0$, the local virial theorem when applied at a BCP, implies that interactions, for which $\nabla^2\rho(r) < 0$, are dominated by a local reduction of the potential energy. In contrast, interactions for which $\nabla^2\rho(r) > 0$, are dominated by local excess in the kinetic energy. In regions where the Laplacian is negative, the charge density is tightly bound and compressed above its average distribution, while, in regions where the Laplacian is positive, the charge density is expanded relative to its average distribution, the pressure is positive, and the kinetic energy of electrons is dominating [186].

3.4.7 Chemical hardness (η), chemical potential (μ)

Density functional theory (DFT) has provided the basis for rigorous mathematical definitions of reactivity descriptors such as chemical potential, electronegativity, chemical hardness, softness, etc.

Chemical hardness (η) is a useful concept for understanding the behavior of chemical systems. Essentially, it measures the resistance of a chemical species to change the electron distribution in a collection of nuclei and electrons (electronic configuration). The chemical potential (μ) is the negative of the atom's electronegativity. It defines the change in free energy per mole when electrons are added or removed from the system. Chemical potential and chemical hardness is related to ionization potential (IP) and electron affinity (EA) of the atom which are defined as follows:

$$\mu = -\frac{(IP + EA)}{2} = \frac{1}{2}(\varepsilon_L + \varepsilon_H) \quad (3.9)$$

$$\eta = \frac{(IP - EA)}{2} = \frac{1}{2}(\varepsilon_L - \varepsilon_H) \quad (3.10)$$

$$IP = -\varepsilon_{HOMO} \quad (3.11)$$

$$EA = -\varepsilon_{LUMO} \quad (3.12)$$

In which, ε_L and ε_H are the energies of the highest occupied molecular orbital (HOMO) and the lowest unoccupied molecular orbital (LUMO), respectively.

In addition, the inverse of global hardness defines the global softness (S):

$$S = \frac{1}{\eta} \quad (3.13)$$

3.4.8 Stabilization energy

In the NBO [187] analysis, the electronic wave functions are interpreted in terms of a set of occupied Lewis and a set of unoccupied non-Lewis localized orbitals. Delocalization effects can be identified from the presence of off-diagonal elements of the Fock matrix. The strengths of these delocalization interactions are estimated by the second order perturbation theory $E^{(2)}$. In addition, the stabilization energy $E^{(2)}$ is

associated with $i \rightarrow j$ delocalization, and is explicitly estimated by the following equation:

$$E^{(2)} = \Delta E_{ij} = q_i \frac{F(i, j)^2}{\varepsilon_j - \varepsilon_i} \quad (3.14)$$

where q_i is the i^{th} donor orbital occupancy, ε_j and ε_i are diagonal elements (orbital energies), and $F(i, j)$ is the off-diagonal element, respectively. Therefore, there is a direct relationship between $F(i, j)$ off-diagonal elements and the orbital overlap.

3.4.9 Fukui function

A wide variety of reactions can be described and understood using DFT-based reactivity descriptors [188, 189, 190, 191, 192]. The Fukui function is one of the ways used to explain local reactivity. These descriptors can be used to determine the places where the molecules are highly reactive. According to Parr and Yang, the Fukui function $f(\vec{r})$ [193] is defined as:

$$f(\vec{r}) = \left[\frac{(\partial\mu)}{(\partial v(r))} \right]_N = \left[\frac{(\partial\rho(r))}{(\partial N)} \right]_{v(\vec{r})} \quad (3.15)$$

where μ is the chemical potential for the system, $v(\vec{r})$ is the external potential of system, N is the total number of electrons in the system, and $\rho(\vec{r})$ is the electron density. The local softness [194] is another demanding local reactivity descriptor, which is written in the following form:

$$s(\vec{r}) = \left[\frac{(\partial\rho(r))}{(\partial\mu)} \right] = f(\vec{r})S \quad (3.16)$$

where S is the global softness [193], which is defined as:

$$S = \frac{1}{(IP - EA)} \quad (3.17)$$

Here, IP and EA represent the ionization potential and electron affinity of the system, respectively. These can be computed in terms of the energies of N and $N \pm 1$ electron systems. For an $N \pm 1$ -electron system with energy E_N , these may be expressed in the following forms:

$$IP = E_{(N-1)} - E_N \quad (3.18)$$

$$EA = E_{(N)} - E_{(N-1)} \quad (3.19)$$

Yang and Mortier [194] proposed a simple way to analyze the Fukui function. The condensed-to-atom Fukui functions are the Fukui indices (for atom k) which are defined as:

$$f^+(k) \cong p_{(N+1)}(k) - p_N(k) \quad (3.20)$$

$$f^-(k) \cong p_{(N)}(k) - p_{(N-1)}(k) \quad (3.21)$$

The Equation 3.20 is defined for nucleophilic attack, while Equation 3.21 is defined for electrophilic attack. $p_{(N-1)}(k)$, $p_{(N)}(k)$ and $p_{(N+1)}(k)$ are the electronic populations on atom (k) for $N - 1$, N , and $N + 1$ electron systems, respectively. There are different local softness for any particular atom (k) [193]. These can be written as:

$$s^+(k) \cong Sf^+(k) \quad (3.22)$$

$$s^-(k) \cong Sf^-(k) \quad (3.23)$$

The Equation 3.22 is defined for nucleophilic attack while Equation 3.23 is defined for electrophilic attack. However, in some compounds, the centers with high electrophilicity (i.e., having high $s^+(k)$ values) also show high nucleophilicity (i.e., having high $s^-(k)$

values). This indirectly suggests that for a reliable trend of reactivity (i.e., acidity and basicity), we need to consider both features. Therefore, the relative electrophilicity, $s^+(k)/s^-(k)$, and nucleophilicity, $s^-(k)/s^+(k)$, which are the ratio of local softness parameters, will help to locate the preferable site (or atom) in a molecule for nucleophilic and electrophilic attacks, respectively. In particular, $s^+(k)/s^-(k)$ and $s^-(k)/s^+(k)$ are equal to $f^+(k)/f^-(k)$ and $f^-(k)/f^+(k)$, respectively [195].

In addition, *Morell et al.* [196] proposed a new selectivity index, named dual reactivity descriptors, which is written as [197]:

$$f^2(k) = [f^+(k) - f^-(k)] \quad (3.24)$$

If $f^2(k) > 0$, the site or atom is favored for a nucleophilic attack, whereas the site or atom is susceptible to an electrophilic attack if $f^2(k) < 0$.

3.5 Computational details

Three methods were used to investigate intra-molecular hydrogen bond formation in octyl- α/β -D-glucopyranoside (C₈O- β -Glc), n-octyl- α/β -D-galactopyranoside (C₈O- β -Gal), α/β -D-mannose (α/β -Man) and n-octyl- α/β -D-mannopyranoside (C₈O- α/β -Man) in namely; density functional theory (DFT), atoms in molecules (AIM) approach and natural bond orbital (NBO) analysis.

The first and the second results obtained from our investigation are shown in the Chapter 4 and 5. An efficient and widely used technique to study a molecular structure, DFT, with B3LYP/6-31G level of calculation was applied to optimize the molecules under investigation, (C₈O- β -Glc and C₈O- β -Gal, α/β -Man, and C₈O- α/β -Man), both in gas and solution phases. The B3LYP (Becke-Lee-Yang-Parr) version of DFT is the combination of

Becke's three-parameter non-local hybrid functional of exchange terms [198] with the Lee, Yang and Parr correlation functional [199]. The basis set 6-31G contains a reasonable number of basis set functions that are able to reproduce experimental data [200, 201]. The solution phase was studied by polarizable continuum model (PCM), [179]. All calculations were performed using Gaussian 09 software package [202]. GaussView 5.0 [203] was used to prepare the input file and to visualize the optimized structures.

Using the DFT method, the best minimum energy conformations were achieved by full geometry optimization of each glycolipids. In order to prove that each of them is located at a stable minimum point of the potential energy surface, frequency calculations were carried out based on these optimized structures and subsequently obtain their vibration frequencies. Furthermore, using the results obtained from the calculation, the structural and electronic properties such as ionization potentials (I), HOMO energies, LUMO energies, bond length, electron affinity (A), chemical hardness (η), electronic chemical potential (μ), electrophilicity index (ω), were investigated. The topological parameters such as electron densities and their Laplacians, at BCP were obtained from the Bader theory [186, 204] by using AIM 2000 software [203]. The nature of intramolecular interactions of C₈O- β -Glc, C₈O- β -Gal, α/β -Man, and C₈O- α/β -Man were investigated using the NBO 3.1 package [205].

The last part of the present study is shown in Chapter 6. The (3,0) single-walled zigzag carbon nanotubes is considered, whose diameter is 2.41 Å, while an average C-C bond length is 1.43 Å. The (3,0) SWNTs, containing 36 carbon atoms and 6 hydrogen atoms, was selected for this purpose. The edges of (3,0) SWNTs are terminated by the presence of hydrogen atoms. Due to symmetry, we have selected only 6 different carbon atoms in these nanotubes. The positions of carbon atoms are depicted in Figure 3.2. The

C₈O- β -Glc molecule has a total of 48 atoms, with the sugar head group attached to a non-polar linear alkyl chain via an -O- glycoside linkage;(See Figure 3.3).

For calculating Fukui functions and local softness, we first performed geometrical optimization at N state of the SWNTs, followed by single-point calculations for $N + 1$ and $N - 1$ the states of the SWNTs, using the B3LYP/6-31G geometries. The electron population $p(k)$ adopted for computing Fukui functions and local softness in the present study are determined from the Mulliken population analysis (MPA) [206].

We have calculated the binding energies ΔE_b of different positions (head and tail groups) of the surfactants residing on the external surface of (3, 0) zigzag SWNTs. The head and tail groups of the surfactant are placed at a distance of approximately 2Å from the external surface of the carbon nanotubes. These structures are optimized using the hybrid density functional theory at the B3LYP/6-31G [198, 199] used in gas and solution phases by the Gaussian 09 software [202]. The optimized structures in the gas phase was re-optimized at B3LYP/6-31G level, employing the polarizable continuum model (PCM) [179] solvation model.

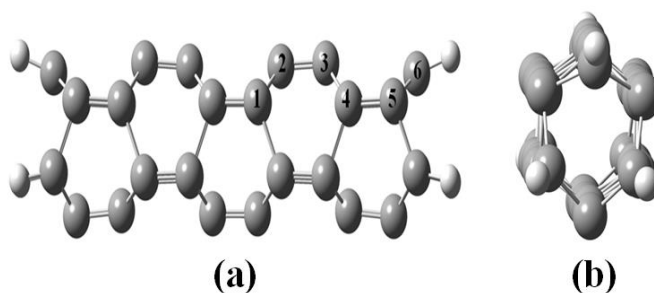


Figure 3.2: Numbering of (3,0) zigzag SWNT (a) front-view and (b) side-view. Carbon atoms are in grey and Hydrogen atoms are in white.

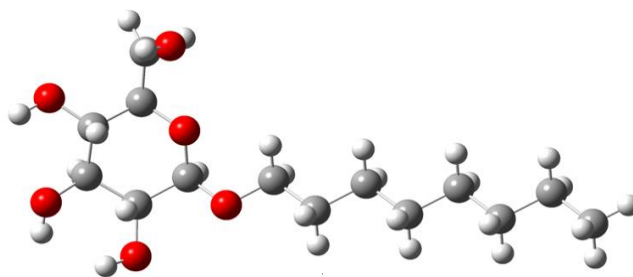


Figure 3.3: The structure of non-ionic surfactant n-octyl- β -D-glucopyranoside. C atoms are in grey and H atoms are in white and O atoms are in red.

The equilibrium geometries were confirmed by the subsequent calculation of force constants and vibration analysis. Each structure was found to be a minimum, with no negative values obtained in the frequency calculations. Therefore, the binding energies of complex and isolated forms in the fully optimized geometry are calculated from Equation. 3.1.

$$\Delta E_b = E_{(Complex)} - (E_{(SWNT)} + nE_{(surfactant)}) \quad (3.25)$$

where $E_{(Complex)}$ denotes the total energy of the optimized complex (carbon nanotube surfactant), n represents the number of surfactants, and $E_{(SWNT)}$ and $E_{(surfactant)}$ corresponds to the total energies of the optimized isolated systems. By this definition, $\Delta E_b < 0$ corresponds to an exothermic adsorption, which leads to a stable structure and strong adsorption between the surfactant and carbon nanotubes. Finally, using the results obtained from the calculation, the structural and electronic properties, such as HOMO energies (ϵ_{HOMO}), LUMO energies (ϵ_{LUMO}), and gap energies can be investigated. Then, we examine the usefulness of local reactivity descriptors in order to predict the reactivity of carbon atom sites on the external surface of (3, 0) zigzag single-walled carbon nanotubes (SWNTs). Then, the interactions between (3, 0) zigzag carbon nanotubes and

n-octyl- β -D-glucoopyranoside (C_8O - β -Glc) were analyzed in both gas and solution phases based on the density functional theory (DFT) methods. Our computational strategy was to obtain optimal structures at the B3LYP/6-31G level, and to use these structures for binding energy calculations at similar levels. Finally, the highest occupied molecular orbital-lowest unoccupied molecular orbital and energy gaps of complexes were also determined.

CHAPTER 4

HYDROGEN BOND IN GLUCO AND GALACTO PYRANOSIDE SURFACTANTS

(J Mol Model: .2013,19(2):589-599)

The aim of the present chapter is to analyze the intra-molecular OH...O hydrogen bonds for n-octyl- β -D-glucopyranoside (C₈O- β -Glc) and n-octyl- β -D-galactopyranoside (C₈O- β -Gal) for an insight into their detailed bonding nature. To achieve this aim, density functional theory (DFT) was used to calculate the equilibrated geometry of these structures, while AIM approach was used to characterize the nature of the intra-molecular hydrogen bonds. Useful parameters such as electronic density at the bond critical point and, its Laplacian, are used to estimate the strength of the hydrogen bonds [207]. The natural bond orbital (NBO) analyses [187, 208] of decomposition were applied to analyze the charge transfer effect on the OH...O interaction of the calculated data.

4.1 The geometry parameters

Figure 4.1 defines the hydrogen bonding geometry based on Jeffrey and Saenger [209], while other related properties to this definition are presented in Table 4.1 [162, 210]. Table 4.1 shows general characteristics of strong, moderate, and weak hydrogen bonds. Strong hydrogen bond interaction is partially covalent; moderate ones involves mostly electrostatic, while a weak hydrogen bond involves electrostatic or dispersed interaction. In addition, it should be noted that the normal covalent bond length is about 0.96 Å, while that of the intra-molecular hydrogen bond in the carbohydrate moiety is in the range of 1.8-2.6 Å [209]. The optimized geometries of both pyranosides at the B3LYP/6-31G level of theory are shown in Figure 4.2. The bond lengths and bond angles of C₈O- β -Glc and C₈O- β -Gal values are given in Table 4.2. The four normal bond lengths of hydroxyl groups (refer to Figure 4.2 for atom labels) are O2-HO2, O3-HO3, O4-HO4 and O6-HO6 having values of about 0.97 ± 0.01 Å.

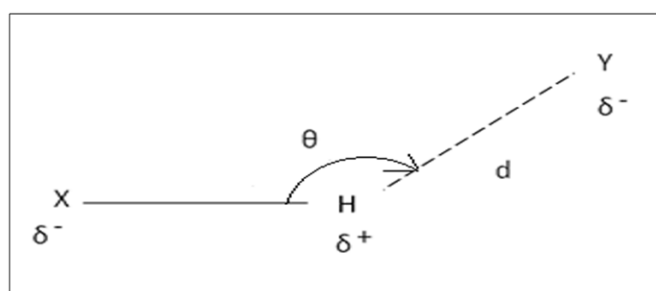


Figure 4.1: Definition of HB geometry where the angle of hydrogen bonding of X-H...Y, θ , and hydrogen bond distance, d, [209, 210].

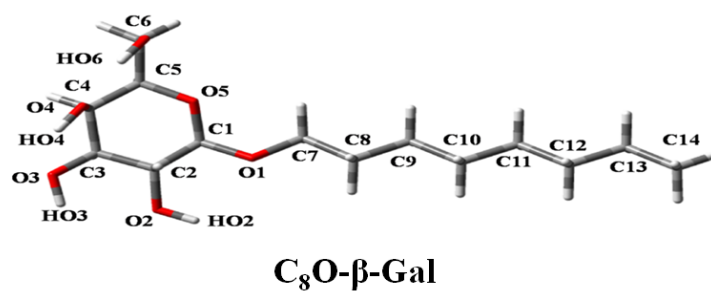
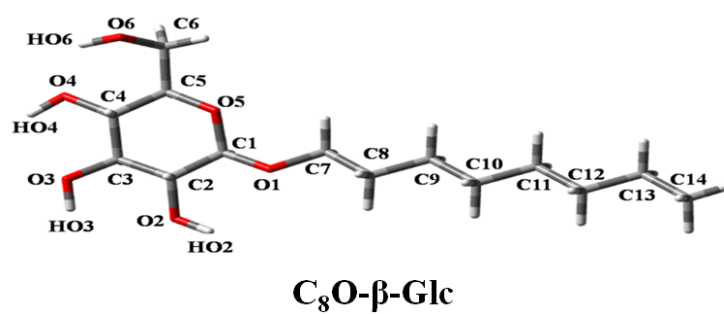


Figure 4.2: Schematic drawing of molecular structures for C₈O-β-Glc and C₈O-β-Gal.

From AIM (see later discussion), an extra intra-molecular hydrogen bond of HO6... O4 for C₈O- β -Glc is observed. On the other hand, for C₈O- β -Gal, two extra bonds are observed, corresponding to HO6...O4 and HO4...O3. These intra-molecular hydrogen bonds are expected to be weaker than the normal covalent O-H. The optimized HO6...O4 bond length in C₈O- β -Glc is about 2.11 Å. For C₈O- β -Gal, the values of the two optimized hydrogen bonds (HO6...O4 and HO4...O3) are 1.85 Å and 2.09 Å, respectively. These distances are similar to those found for other sugar intra-molecular hydrogen bonding. For example, the calculated values for pentahydrates of α - and β -D-glucopyranose [211], α - and β -D-mannopyranose [212], and α - and β -D-galactopyranose [213] range from 2-3 Å. The O6-HO6-O4 angle in both C₈O- β -Glc and C₈O- β -Gal are 127 ° and 140 °, respectively. However, the O4-HO4-O3 angle in the C₈O- β -Gal is 114 °. The results agree with experimental data [209].

Table 4.1: General characteristic of the three major types of hydrogen bonding and important structural parameters [209, 210].

Interaction type	Strong	Moderate	Weak
	Partially covalent	Mostly electrostatic	Electrostatic/ dispersed
Bond lengths H...Y (Å)	1.2-1.5	1.5-2.2	2.2-3.3
Lengthening of X-H (Å)	0.08-0.25	0.02-0.08	< 0.02
X-H vs H...Y	X-H \approx H...Y	X-H < H...Y	X-H \ll H...Y
X...Y (Å)	2.2-2.5	2.5-3.2	> 3.2
Directionality	Strong	moderate	Weak
Bond angles (°)	170-180	> 130	> 90
Bond energy (kcal/mol)	> 8	4-8	< 4

4.2 The electronic energy

The calculated electronic energies of C₈O- β -Glc and C₈O- β -Gal, both at the B3LYP/6-31G level of theory in the gas and solution phases (water solvent), are summarized in Table 4.3. The results show that C₈O- β -Gal is more stable than C₈O- β -Glc in both gas and solution phases. The differences in electronic energies between C₈O- β -Gal and C₈O- β -Glc in the gas and solution phases are -1.6 kcal/mol and -3.0 kcal/mol respectively, indicating that both C₈O- β -Gal and C₈O- β -Glc are more stable in the solution phase than in the gas phase. Additionally, the electronic energy difference for the C₈O- β -Glc in PCM and gas phases and that of C₈O- β -Gal are -10.3 kcal/mol and -11.7 kcal/mol respectively, implying that C₈O- β -Gal is more stable than C₈O- β -Glc.

Table 4.2: The geometrical parameters for C ₈ O- β -Glc and C ₈ O- β -Gal (the bonds in and the angles in degree), at the B3LYP/6-31 G by DFT method. The atom labels we used Mamony et al [213] and IUPAC [214].		
	C₈O-β-Glc	C₈O-β-Gal
Covalent bond lengths (Å)		
O2-HO2	0.97	0.97
O3-HO3	0.97	0.97
O4-HO4	0.98	0.98
O6-HO6	0.98	0.98
Hydrogen bond lengths (Å)		
HO4...O3	-	2.09
HO6...O4	2.11	1.85
Hydrogen bond angle (°)		
O4-HO4-O3	-	114
O6-HO6-O4	127	140

4.3 Dipole moment

The dipole moment analysis in the gas phase and PCM is given in Table 4.3. Dipole moment in the C₈O- β -Gal is higher than in C₈O- β -Glc in both gas and PCM phases. Differences in the dipole moment between the two compounds in the gas phase and PCM are 0.38 and 1.4 Debye, respectively, and the ratio for C₈O- β -Gal is three times that for C₈O- β -Glc. This ratio value is in accordance with the calculated results for water by Silvestrelli and Parrinello [215].

Table 4.3: Electronic energy $E_{(a.u.)}$, and dipole moment $\mu(D)$, of studied compounds at B3LYP/6-31G level of theory in the gas and solution phases.				
	$E_{(a.u.)}$		$\mu(D)$	
	Gas phase	PCM	Gas phase	PCM
C₈O-β-Glc	-1001.36598	-1001.38236	4.011	4.231
C₈O-β-Gal	-1001.36851	-1001.38709	4.390	5.609

4.4 The electronic properties

Table 4.4 lists the electronic properties of C₈O- β -Glc and C₈O- β -Gal, including the energy of the highest occupied molecular orbital ε_{HOMO} , and energy of the lowest unoccupied molecular orbital ε_{LUMO} , ionization energy (I), electron affinity (A), chemical hardness (η), electronic chemical potential (μ), electrophilicity index (ω), and softness (S).

Parr et al. [197] have defined electrophilicity index (ω), as a new descriptor to quantify the global electrophilic nature of a molecule within a relative scale. This index measures the stabilization energy when the system acquires an additional electronic

charge from the environment. The small value of electrophilicity index (ω), indicates that the molecule is stable. Chemical potential (μ), chemical hardness (η), and softness (S), are known as global reactivity descriptors [216, 217, 218]. Global hardness and softness are of interest, since resistance to change of the electron cloud of the chemical system can be understood from the values of hardness (η), and softness (S). The stability of chemical species can be associated with its hardness. Hard molecules have a large energy gap while, soft molecules have a small one [182, 219].

Table 4.4: Calculated the highest occupied molecular orbital energy $\epsilon_{(HOMO)}$, and the lowest unoccupied molecular orbital energy $\epsilon_{(LUMO)}$, ionization energy (I), electron affinity (A), chemical hardness η , electronic chemical potential (μ), electrophilicity index (ω), and softness (S) in $C_8O-\beta$ -Glc and $C_8O-\beta$ -Gal at the B3LYP/6-31G level. All units are (e.V.)

Electronic properties	Formula	$C_8O-\beta$ -Glc	$C_8O-\beta$ -Gal
Energy of LUMO	$\epsilon_{(LUMO)}$	0.22210	0.21689
Energy of HOMO	$\epsilon_{(HOMO)}$	-0.27449	-0.25821
Ionization energy	$I = -(\epsilon_{HOMO})$	0.27449	0.25821
Electron affinity	$A = -(\epsilon_{LUMO})$	-0.22210	0.21689-
Chemical hardness	$\eta = \frac{(I - A)}{2}$	0.24829	0.23755
Electronic chemical potential	$\mu = -\frac{(I + A)}{2}$	-0.02619	-0.02066
Electrophilicity	$\omega = \frac{\mu^2}{\eta}$	0.00138	0.00089
Softness	$S = \frac{1}{\eta}$	4.27467	4.2964

It can be readily seen from Figure 4.3, that the gap for C₈O- β -Glc is 0.49659 eV, which is higher than that for C₈O- β -Gal 0.47510 eV, indicates C₈O- β -Glc is hard specie, while, C₈O- β -Gal is soft specie. A comparison of reactivity descriptors in Table 4.4 also indicates that C₈O- β -Glc is harder than C₈O- β -Gal. Due to the inverse relationship between hardness and stability, C₈O- β -Gal is reactive specie compared to C₈O- β -Glc. As shown in Table 4.4, the electrophilicity values for C₈O- β -Glc and C₈O- β -Gal are 0.00138 and 0.00089, respectively. The smaller value of electrophilicity for C₈O- β -Gal indicates that C₈O- β -Gal is more stable than C₈O- β -Glc. This further implies that C₈O- β -Glc is less likely to associate itself with electrons from its surroundings compared to C₈O- β -Gal. After all, the latter has two intra-molecular hydrogen bonds, as seen from the AIM analysis.

4.5 Atoms in molecules (AIM) analysis

Bader's theory of atoms in molecules [186] is widely used as a theoretical tool to understand and analyse hydrogen bonds. The formation of HB is associated with the appearance of a BCP between the hydrogen atom of donor group and acceptor. This theory is based on the critical points (CPs) of the molecular electronic charge density $\rho(r)$. At these points, the density [220] gradient $\nabla\rho(r)$, vanishes, and these points are characterized by the three eigenvalues ($\lambda_i = 1, 2, 3$) of the Hessian matrix, (λ_1) and (λ_2), corresponding to the perpendicular curvatures, while (λ_3) provides a curvature along the internuclear axis. The CPs is labelled (r, s), according to their ranks r (number of non-zero eigenvalues), and signatures s , (the algebraic sum of the signs). Four types (r, s) of CPs are of interest in the molecules, which are (3,+3), (3,+1), (3,-3), (3,-1). In our case, a (3,-1) point or bond critical point is generally found between two neighboring nuclei, indicating the existence of a bond between them.

Popelier and Bader [220] employed the AIM analysis to address several important chemical issues [221] where he proposed a set of criteria for the existence of hydrogen bond within AIM formalism. Two of these criteria are related to electron density $\rho(r)$ and the Laplacian of the electron density $\nabla^2\rho(r)$ evaluated at the bond critical point (BCP) of two hydrogen-bonded atoms. In general, if hydrogen bond exists, the range of $\rho(r)$ and $\nabla^2\rho(r)$ are 0.002-0.035 and 0.024-0.139 a.u., respectively [220]. We have tabulated the $\nabla\rho$ topological parameters collected in Table 4.5. It is evident from this table that the values of $\rho(r)$ and $\nabla^2\rho(r)$ in the C₈O- β -Glc, in HO6...O4 interaction are 0.0209 and 0.0730 a.u, respectively. However, in the C₈O- β -Gal, HO6...O4 and HO4...O3 interaction, they were 0.0332, 0.0217 and 0.1217, 0.0839 a. u, respectively. These characteristic electron densities at BCP imply the presence of hydrogen bond interaction.

The Laplacian of charge density at the bond critical point, $\nabla^2\rho(r)$, is the sum of the curvatures in the charge density along any orthogonal coordinate axes at the BCP. The sign of $\nabla^2\rho(r)$ indicates whether the charge density is locally depleted $\nabla^2\rho(r) > 0$, or locally concentrated $\nabla^2\rho(r) < 0$. Thus, when the curvatures are negative i.e. (λ_1) and (λ_2) dominate at the BCP, the electronic charge is locally concentrated within the inter atomic regions leading to interaction such as covalent or polarized bonds and being characterized by large $\rho(r)$ values, $\nabla^2\rho(r) < 0$, and $|\lambda_2/\lambda_3| > 1$.

On the other hand, if the curvature is positive, i.e. λ_3 is dominant, the electronic density is locally concentrated in each of the atomic basins. The interaction is now referred to as a closed-shell and it is characteristic of highly ionic bonds, hydrogen

bonds, or van der Waals interactions. It is characterized by relatively low $\rho(r)$ values $\nabla^2\rho(r) > 0$, and $|\lambda_2/\lambda_3| < 1$ [186]. The molecular graphs (indicating critical points and bond paths) for these two molecules are shown in Figure 4.4. The position of the bond's critical point strongly depends on electronegativity.

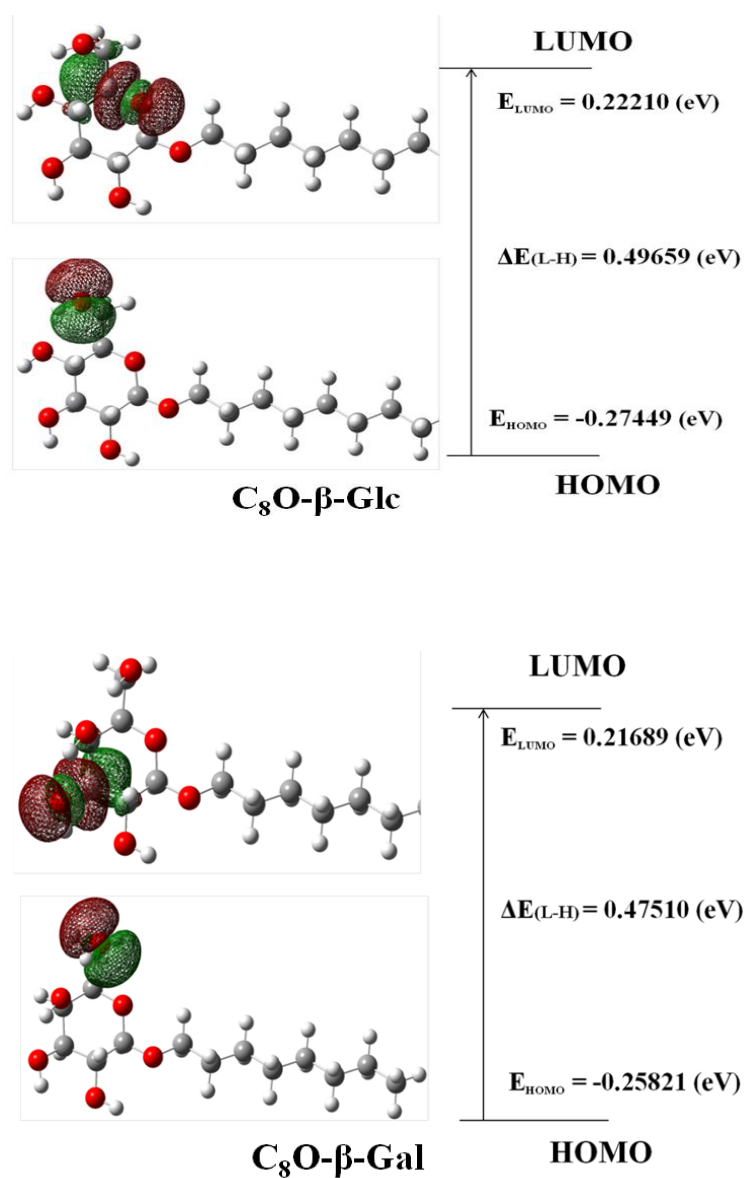


Figure 4.3: The atomic orbital composition of the frontier molecular orbital for C₈O- β -Glc and C₈O- β -Gal.

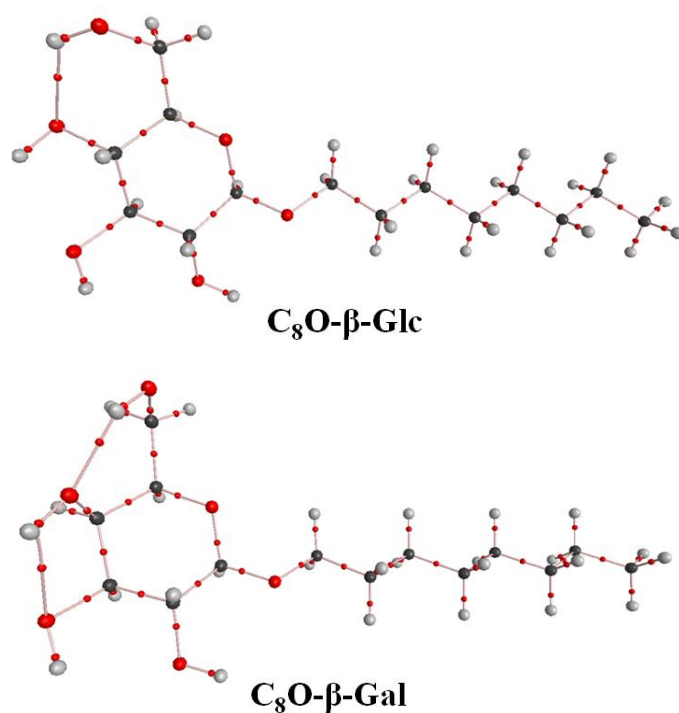


Figure 4.4: Molecular graph in the C₈O-β-Glc and C₈O-β-Gal. Small red spheres and lines correspond to the bond critical points (BCP) and the bond paths, respectively.

Table 4.5: Topological parameters (in a.u.) E , the electron densities, $\rho(r)$ at O...H BCPs, their Laplacians $\nabla^2\rho(r)$ and energetic parameters, $V(r)$, $G(r)$ and $H(r)$ (in kcal/mol) in the C₈O-β-Glc and C₈O-β-Gal at the B3LYP/6-31G.

Compound studied	HB-length	$\rho(r)$	$\nabla^2\rho(r)$	$V(r)$	$G(r)$	$H(r)$	Ellipticity
C ₈ O-β-Glc	HO6...O4=2.11	0.0209	0.0730	-0.0189	0.0186	-0.0003	0.1538
	HO6...O4=1.85	0.0332	0.1217	-0.0315	-0.0309	-0.0005	0.0338
C ₈ O-β-Gal	HO4...O3=2.89	0.0217	0.0839	-0.0206	0.0206	0.0004	0.3886

The values of the electron density $\rho(r)$, its Laplacian $\nabla^2\rho(r)$, total energy density $H(r)$, electronic kinetic energy density $G(r)$, and electronic potential energy density $V(r)$, at BCP, are given in Table 4.5. For $C_8O-\beta$ -Glc, the molecular graph represents one intra-molecular hydrogen bond, while for $C_8O-\beta$ -Gal, the molecular graph represents two intra-molecular hydrogen bonds. The signs of $\nabla^2\rho(r)$ and $H(r)$ in the $C_8O-\beta$ -Glc are positive and negative, respectively. Therefore, this bond is classified as partially covalent–partially electrostatic (Pc-Pe) [222].

In addition, the values of $\nabla^2\rho(r)$ and $H(r)$, in $C_8O-\beta$ -Gal for the HO6...O4 interaction are positive and negative, respectively, but in the HO4...O3 interaction, they are positive. Therefore, HO6...O4 interaction is partially covalent–partially electrostatic, while the HO4...O3 interaction is van der Waals. By comparing the values of $\nabla^2\rho(r)$, and $H(r)$, it can be concluded that the partially covalent–partially electrostatic of HO6...O4 in $C_8O-\beta$ -Gal is greater than in $C_8O-\beta$ -Glc, and in good agreement with the smaller HO6...O4 distance calculated in $C_8O-\beta$ -Gal. The density change is due to the charge transfer from the proton acceptor to the proton donor (X-H) bond. The process increases the O-H's bond length, and decreases the charge density in both $C_8O-\beta$ -Glc and $C_8O-\beta$ -Gal, causing the bond to be weaker. Consequently, the electrons are delocalized in the bond.

The total electron energy density $H(r)$, and the Laplacian $\nabla^2\rho(r)$, at BCP are two topological parameters often applied to classify and characterize hydrogen bonds. It should be mentioned that hydrogen bond is characterized by $H(r) < 0$ and $\nabla^2\rho(r) < 0$ for strong hydrogen bonds, while medium hydrogen bonds with $H(r) < 0$, and $\nabla^2\rho(r) > 0$, and $H(r) > 0$, and $\nabla^2\rho(r) > 0$ are established for the weaker ones [120].

From the current work, the HO6...O4 interaction in the C₈O-β-Glc [$\rho(r)=0.0209$, $\nabla^2\rho(r)=0.0730$, $H(r)=-0.0003$] and those of the C₈O-β-Gal [$\rho(r)=0.0332$, $\nabla^2\rho(r)=0.1217$, $H(r)=-0.0005$] are classified as medium hydrogen bonds. In addition, the HO4...O3 hydrogen bonds in the C₈O-β-Gal [$\rho(r)=0.0217$, $\nabla^2\rho(r)=0.0839$, $H(r)=+0.00040$] are placed in the weak hydrogen bonds category. The values of $\rho(r)$ and $\nabla^2\rho(r)$ at HO6...O4 bond critical points in the C₈O-β-Gal are greater than the corresponding values in the C₈O-β-Glc. On the other hand, for the HO6...O4 in the C₈O-β-Gal, the bond length is shorter than the corresponding value in the C₈O-β-Glc (see Table 4.2). Thus, the HO6...O4 hydrogen bond in the C₈O-β-Gal is stronger than that in C₈O-β-Glc. Furthermore, comparing two hydrogen bonds in C₈O-β-Gal, we can assume that the HO6...O4 hydrogen bond is stronger than HO4...O3.

Another interesting parameter is ellipticity (ε), defined as follows:

$$\varepsilon = \left[\frac{\lambda_1}{\lambda_2} - 1 \right] \quad (4.1)$$

where λ_1 and λ_2 are the curvatures of the density with respect to the two principal axes X and Y. It is indicative of the similarity between the perpendicular curvatures (λ_1 and λ_2) at the BCP. In terms of the orbital model of electronic structure, ellipticity provides a quantitative measure of the π -bond character and delocalization of the electronic charge. Also, ellipticity is a measure of bond stability, i.e. high ellipticity values indicate instability of the bond [89, 223]. As shown in Table 4.5, ellipticity (ε) in the C₈O-β-Glc is 0.1538 a.u for the HO6...O4, while in the C₈O-β-Gal, it is 0.0338 a.u. This means that hydrogen bond in the C₈O-β-Glc is unstable compared to C₈O-β-Gal. The ellipticity of two positions (HO6...O4, HO4...O3) in the C₈O-β-Gal is 0.0338 and

0.3886, respectively. These values show that hydrogen bonding in the HO6...O4 interaction is more stable than the bond in HO4...O3.

4.6 Natural bond orbital (NBO) analysis

In the NBO analysis [187], electronic wave functions are interpreted in terms of a set of occupied Lewis and a set of unoccupied non-Lewis localized orbitals. Delocalization effects can be identified from the presence of off-diagonal elements of the Fock matrix in the NBO basis. The strengths of these delocalization interactions $E^{(2)}$ are estimated by second order perturbation theory. In addition, the stabilization energy $E^{(2)}$ associated with $i \rightarrow j$ delocalization is explicitly estimated by the following equation:

$$E^{(2)} = \Delta E_{ij} = q_i \frac{F(i, j)^2}{\varepsilon_j - \varepsilon_i} \quad (4.2)$$

where q_i is the i^{th} donor orbital occupancy, ε_j and ε_i are diagonal elements (orbital energies) and $F(i, j)$ is the off-diagonal element, respectively, associated with the NBO Fock matrix. Therefore, there is a direct relationship between $F(i, j)$ off-diagonal elements and the orbital overlap. NBO analysis is a sufficient approach to investigate the effect of the stereoelectronic interactions on the reactivity and dynamic behaviors of chemical compounds. The larger the $E^{(2)}$ value, the more [187] intensive the interaction between electron donors and electron acceptors [205, 224]. The formation of hydrogen bonds in the C₈O- β -Glc and C₈O- β -Gal implies that certain amounts of electronic charge are transferred from the lone pair to the anti-bonding orbital.

Furthermore, some of the significant donor-acceptor interactions and their second order perturbation stabilization energies $E^{(2)}$, which are calculated at the B3LYP/6-31G level of theory for studied compounds, are given in Table 4.6. The orbital energies (ϵ), are reported in a.u., while the second order perturbation energies are reported in kcal/mol. As can be seen from Table 4.6, electronic charge is transferred from a lone pair orbital $n(O)$ atom in the donor fragment to $\sigma^*(O-H)$ anti-bonding orbital of the acceptor fragment. The lengthening of the O-H bond is a result of such $\sigma^*(O-H)$ character ($HO6...O4=2.11$ for $C_8O-\beta$ -Glc and $HO6...O4 = 1.85$, $HO4...O3=2.09$ for $C_8O-\beta$ -Gal).

The stabilization energies of $n(O) \rightarrow \sigma^*(O-H)$, are 4.85, 0.73 and 11.55, 3.49 kcal/mol) in the $C_8O-\beta$ -Glc and in the $C_8O-\beta$ -Gal, respectively. In the $C_8O-\beta$ -Glc, the charge transfer energy is smaller than that in the $C_8O-\beta$ -Gal. These must be higher than the mentioned threshold limit for the other positions. A comparison between the NBO analysis of $C_8O-\beta$ -Glc and $C_8O-\beta$ -Gal shows that the value of second-order perturbation energy for $(n2O4 \rightarrow \sigma^*(O6-HO6))$ is higher than the value of $(n2O3 \rightarrow \sigma^*(O4-HO4))$. Hence, the strength of hydrogen bond in the $C_8O-\beta$ -Gal is greater than that in the $C_8O-\beta$ -Glc.

On the other hand, we can see (Table 4.6) that the lowest value (0.73 kcal/mol) is observed for $C_8O-\beta$ -Glc in $(n2O3 \rightarrow \sigma^*(O4-HO4))$. This means that the hydrogen bond in $(n2O3 \rightarrow \sigma^*(O4-HO4))$ is weaker than that of $(n2O4 \rightarrow \sigma^*(O6-HO6))$. The data clearly indicates that the bonds ($HO6...O4$) and ($HO4...O3$) are favorably constructed in the $C_8O-\beta$ -Gal, but are almost impossible to be built in $HO4...O3$ in the $C_8O-\beta$ -Glc. Our calculation shows that the energy gaps between HOMO and LUMO in the $C_8O-\beta$ -Glc and $C_8O-\beta$ -Gal are 0.49659 and 0.47510 (a.u), respectively. The calculated data are shown in Figure 4.3.

In addition, the calculated wavelengths for the understudied compounds are 2497 and 2610 nm, respectively, thus falling in the short-wavelength infrared region (1400 - 3000) [224]. Therefore, as the results show, these materials absorb the infrared frequency, which may be exploited as an infrared sensor material, similar to that suggested for carbohydrates previously [225].

Table 4.6: The second-order perturbation energies, $E^{(2)}$ (kcal/mol), corresponding to the most important charge transfer interaction (donor→acceptor) in the $C_8O-\beta$ -Glc and $C_8O-\beta$ -Gal at the B3LYP/6-31G.

Compound studied	Donor NBO(<i>i</i>)	Acceptor NBO(<i>j</i>)	$E^{(2)}$ (kcal/mol)	$\varepsilon_j - \varepsilon_i$
	<i>n</i> (O)	σ^* (O-H)	(O)→ σ^* (O-H)	
$C_8O-\beta$-Glc	LP(2)O4	BD*(1)HO6-O6	4.85	0.79
	LP(2)O3	BD*(1)HO4-O4	0.73	0.74
$C_8O-\beta$-Gal	LP(2)O4	BD*(1)HO6-O6	11.55	1.04
	LP(2)O3	BD*(1)HO4-O4	3.49	0.78

CHAPTER 5

HYDROGEN BOND IN MANNOSE AND MANNONSEPYRANOSIDE SURFACTANTS

(Liq Cryst: 2014,41(6):784-792)

Chapter 5 has the objective to analyze the intra-molecular hydrogen bond for four compounds; α/β -D-mannose (α/β -Man) and the corresponding glycolipids, n-octyl- α/β -D-mannopyranoside (C_8O - α/β -Man) to get an insight into the nature of their bonding. Hence, the density functional theory was used to calculate the equilibrated geometry/electronic energy of these structures, while AIM was used to characterize the nature of the intra-molecular hydrogen bonds. Useful parameters, such as electronic density at the critical point and its Laplacian [207] are used to estimate the strength of the hydrogen bonds. The natural bond orbital [187, 208] analysis was applied to analyze the charge transfer effect on the OH...O interaction of the calculated data. From the detailed investigation on the energy and intra-molecular hydrogen bond at C1 position of these compounds, the implications to the biological systems at the structural and functional levels may be understood.

5.1 The geometry parameters

The bond lengths and bond angles of carbohydrates, such as α/β -Man and C_8O - α/β -Man at the B3LYP/6-31G level of theory are presented in Table 5.1. The bond lengths of hydroxyl groups of O1-HO1, O2-HO2, O3-HO3, O4-HO4 and O6-HO6 have normal values of about 0.97 ± 0.01 Å. From the AIM theory (see later discussion), in α -anomers (α -Man and C_8O - α -Man), an extra intra-molecular hydrogen bond is observed to correspond to O2...HO3. On the other hand, in the β -anomer (β -Man and C_8O - β -Man), two extra bonds are observed to correspond to O1...HO2 and O2...HO3. These intra-molecular hydrogen bonds are expected to be weaker than the normal covalent O-H. The optimized O2...HO3 bond length in α -Man and C_8O - α -Man is about 2.19 and 2.18 Å, respectively. For β -Man and C_8O - β -Man, the values of hydrogen bond lengths in (O2...HO3) position is 2.18 and 2.16 Å, respectively, while hydrogen bond lengths for β -Man and C_8O - β -Man in (O1...HO2) position are 2.17 and 2.17 Å, respectively. It

should be noted that the normal covalent bond length is 0.96 Å, while that of the intermolecular hydrogen bond in the carbohydrate moiety is in the range of 1.8-2.6 Å [209]. The calculated hydrogen bond distances for both of α/β -D of glucopyranose, galactopyranose, mannopyranose and allopyranose are in the range of 2-3 Å [212, 213, 226, 227].

Table 5.1: The geometrical parameters for α/β -Man and C ₈ O- α/β -Man (the bond lengths in Å and the bond angles in degree), at the B3LYP/6-31 G by DFT method.				
	α -Man	β -Man	C ₈ O- α -Man	C ₈ O- β -Man
Covalent bond lengths (Å)				
O1-HO1	0.97	0.97	-	-
O2-HO2	0.97	0.98	0.97	0.98
O3-HO3	0.98	0.98	0.98	0.98
O4-HO4	0.98	0.97	0.98	0.98
O6-HO6	0.98	0.98	0.98	0.98
Hydrogen bond lengths (Å)				
O1...HO2	-	2.17	-	2.17
O2...HO3	2.19	2.18	2.18	2.16
Hydrogen bond angle (°)				
O2-HO2-O1	-	110.94	-	114
O3-HO3-O2	111.90	112.43	112	113

5.2 The thermodynamic properties

The thermodynamic properties of investigated compounds at the B3LYP/6-31G level of theory are given in Table 5.2. By comparing the electronic energies of both α - and β -anomers, it is clear that β -anomers are more stable than α -anomers. The differences in electronic energies between α -Man and β -D-Man are 0.75 kcal/mol, while between C₈O- α -Man and C₈O- β -Man are 1.38 kcal/mol. On the other hand, the

differences in electronic energies between α -Man and C₈O- α -Man are 197303.9 kcal/mol, while it is 197304.5kcal/mol between β -Man and C₈O- β -Man. These results show that sugars with straight chains (C8) could be more stable than sugars lacking one. As can be seen in Table 5.2, all of the electronic energy is exothermic. In addition, the dipole moment in β -anomers is weaker than α - anomers.

Table 5.2: The thermodynamic properties for α/β -Man and C ₈ O- α/β -Man at the B3LYP/6-31 G level of theory in the gas phase.				
Thermodynamic properties	α-Man	β-Man	C₈O-α-Man	C₈O-β-Man
$E_{(a.u.)}$	-686.9386	-686.9398	-1001.3671	-1001.3693
$\Delta H^0_{(a.u.)}$	-686.7292	-686.7304	-1000.9170	-1000.9190
$\Delta G^0_{(a.u.)}$	-686.7797	-686.7809	-1000.9961	-1000.9979
$\mu_{(Debye)}$	4.9	4.1	5.7	5.3

5.3 The electronic properties

Table 5.3 summarizes the electronic properties of these non-ionic surfactant, including the energy of the highest occupied molecular orbital $\epsilon_{(HOMO)}$, energy of the lowest unoccupied molecular orbital $\epsilon_{(LUMO)}$, ionization energy (I), electron affinity (A), chemical hardness (η), electronic chemical potential (μ), electrophilicity index (ω), and softness (S). The HOMO represents the ability to donate an electron, LUMO acts as an electron acceptor representing the ability to obtain an electron, The HOMO and LUMO energy are calculated using the B3LYP/6-31G method for investigated molecules, as shown in Figures 5.1–5.4. Both the highest occupied molecular orbital and the lowest unoccupied molecular orbital are the main orbitals taking part in chemical stability [228]. The electrophilicity index was defined as new descriptor to

quantify the global electrophilic nature of molecule within a relative scale [197]. The chemical hardness, electronic chemical potential, and softness are global reactivity descriptors [217, 218]. The stability of chemical species can be associated with its hardness. The soft molecules have a small energy band gap, but hard molecules have a larger one [182, 219].

According to our results, the energy band gap for β -Man and C₈O- β -Man are 0.4880 and 0.4908 eV, which are higher than those for α -Man and C₈O- α -Man, which are 0.4793 and 0.4789 eV, respectively. This is indicative of the fact that β -Man and C₈O- β -Man is a harder species compared to α -Man and C₈O- α -Man.

Table 5.3: Calculated the highest occupied molecular orbital energy $\mathcal{E}_{(HOMO)}$, and the lowest unoccupied molecular orbital energy $\mathcal{E}_{(LUMO)}$, ionization energy (I), electron affinity (A), chemical hardness (η), electronic chemical potential (μ), electrophilicity index (ω), and softness (S) of studied compounds at the B3LYP/6-31G level.

Electronic properties	α -Man	β -Man	C ₈ O- α -Man	C ₈ O- β -Man
Energy of LUMO	0.2036	0.2061	0.2064	0.2134
Energy of HOMO	-0.2756	-0.2818	-0.2724	-0.2774
Band gap($\Delta E_{(L-H)}$)	0.4739	0.4880	0.4789	0.4908
Ionization energy	0.2756	0.2818	0.2724	0.2774
Electron affinity	-0.2036	-0.2061	-0.2064	-0.2134
Chemical hardness	0.2396	0.2440	0.2394	0.2454
Electronic chemical potential	-0.3060	-0.0378	-0.0330	-0.0320
Electrophilicity index	0.0054	0.0059	0.0045	0.0042
Softness	4.1724	4.0980	4.1760	4.0748

Note: All units are (e.V.)

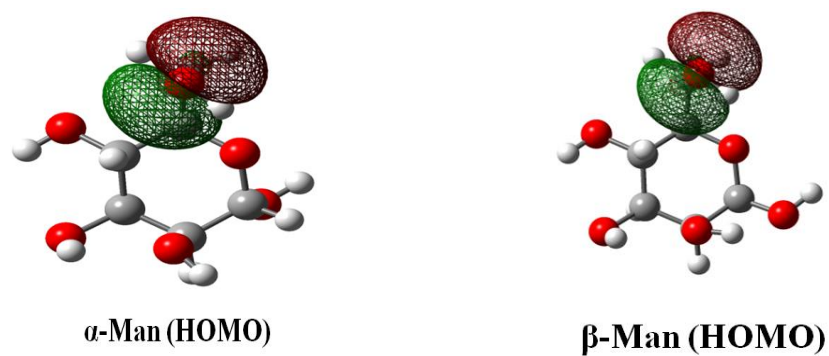


Figure 5.1: The NBO composition of the frontier orbitals (HOMO) for α/β -Man.

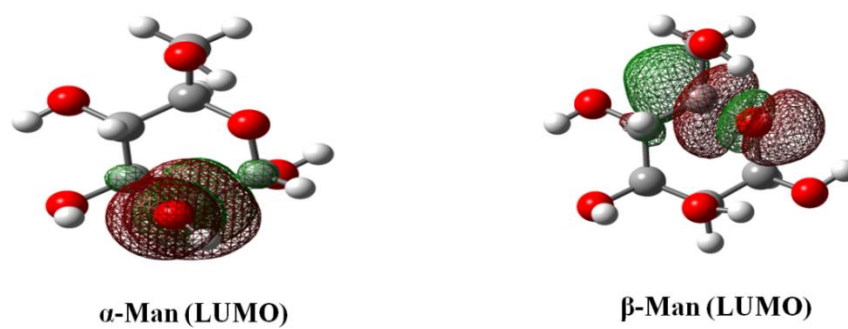
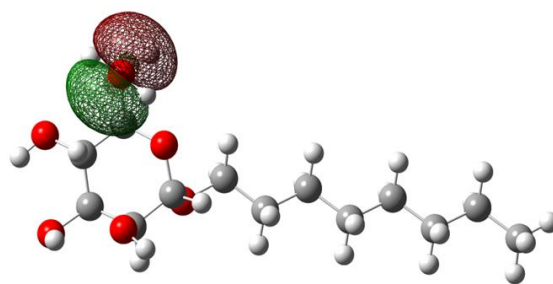
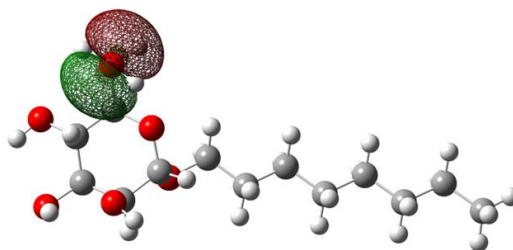


Figure 5.2: The NBO composition of the frontier orbitals (LUMO) for α/β -Man.

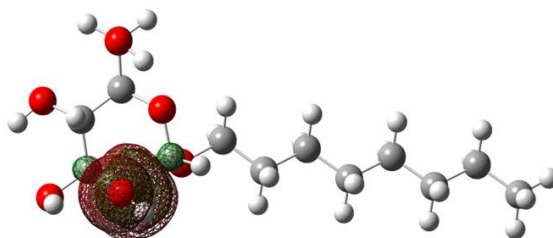


C₈O- α -Man (HOMO)

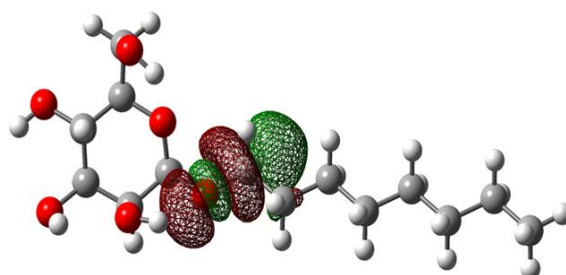


C₈O- β -Man (HOMO)

Figure 5.3: The NBO composition of the frontier orbitals (HOMO) for C₈O- α/β -Man.



C₈O- α -Man (LUMO)



C₈O- β -Man (LUMO)

Figure 5.4: The NBO composition of the frontier orbitals (LUMO) for C₈O- α/β -Man.

5.4 Atoms in molecules (AIM) analysis

The Atoms in molecules (AIM) [186] theory provides a very useful tool to analyze bond types via parameters, such as electron density $\rho(r)$, the Laplacian of the electron density, $\nabla^2\rho(r)$, and the ellipticity, ϵ , which are computed at the bond critical point (BCP) [221]. This theory is widely used as a theoretical tool to understand and analyze hydrogen bonds. Generally, for hydrogen bonds, the range of electron density and the Laplacian are 0.002-0.035 and 0.024-0.139 a.u., respectively [220]. The topological parameters and molecular graphs (indicating critical points and bond paths) of the investigated compounds are exhibited in Table 5.4.

The position of the bond critical point (Small red spheres) strongly depends on electronegativity. It is evident from the table that the value of $\rho(r)$ and $\nabla^2\rho(r)$ for these compounds in O1...HO2 and O2...HO3 positions are in the range of 0.0185-0.0186, 0.0174 - 0.0186, 0.0771- 0.0768 and 0.0744 - 0.0792 a.u., respectively. These values of electron densities at BCP imply the presence of hydrogen bonding interaction. For α -anomers, the molecular graphs represent one intra-molecular hydrogen bond, while for the β -anomers, the molecular graphs represent two intra-molecular hydrogen bonds (See Figures 5.5–5.6).

Two topological parameters at BCP are often applied to classify and characterize hydrogen bonds [186]. The Laplacian, $\nabla^2\rho(r)$, and the total energy density, $H(r)$, in all of the above hydrogen bonds are positive and negative, respectively. Therefore, these bonds are classified as medium hydrogen bonds and partially covalent-partially electrostatic (P_c - P_e) [222]. The electron density for α -D-Man and C₈O- α -Man in HO3...O2 position is between 0.0185-0.0186 a.u., while it is for β -Man and C₈O- β -D-Man in O2...HO3 position in the range of 0.0174 - 0.0177 a.u., and it is in O1...HO2

position in range of 0.0185-0.0186 a.u., respectively. The density change is due to the charge transfer from the proton donor (O-H) bond. Consequently, the electrons are delocalized in the bond. Ellipticity is a measure of the bond's stability, i.e., high ellipticity value indicates an unstable bond [204]. The instability order of hydrogen bond in α -anomers and β -anomers are:

$$\alpha\text{-Man} > \text{C}_8\text{O-}\alpha\text{-Man}$$

$$\beta\text{-Man (O2...HO3)} > \text{C}_8\text{O-}\beta\text{-Man (O2... HO3)}$$

$$\beta\text{-Man (O1...HO2)} > \text{C}_8\text{O-}\beta\text{-Man (HO2... O1)}$$

As a result of this, the hydrogen bond for β -Man and $\text{C}_8\text{O-}\beta$ -Man in O1...HO2 position is more stable than the ones in the O2... HO3 position. Furthermore, hydrogen bond in $\text{C}_8\text{O-}\alpha$ -Man is slightly more stable than α -Man. The stability of α - and β -anomers increases with increasing lengths of linear carbon chains.

Table 5.4: Topological parameters E (in a.u.), the electron densities $\rho(r)$, at O...H BCPs, their Laplacians $\nabla^2 \rho(r)$ and energetic parameters $V(r)$, $G(r)$, and $H(r)$ (in kcal/mol) in the α/β -Man and $\text{C}_8\text{O-}\alpha/\beta$ -Man at the B3LYP/6-31G.

Compound studied	HB-length	$\rho(r)$	$\nabla^2 \rho(r)$	$V(r)$	$G(r)$	$H(r)$	Ellipticity
α -Man	HO3...O2=2.19	0.0185	0.0744	-0.0173	0.0179	-0.0006	0.9412
β -Man	HO2...O1=2.17	0.0186	0.0768	-0.0174	0.0183	-0.0009	0.8390
	HO3...O2=2.18	0.0174	0.0758	-0.0163	0.0176	-0.0013	1.100
$\text{C}_8\text{O-}\alpha$ -Man	HO3...O2=2.18	0.0186	0.0792	-0.0173	0.0180	-0.0007	0.8838
$\text{C}_8\text{O-}\beta$ -Man	HO2...O1=2.17	0.0185	0.0771	-0.0173	0.0183	-0.0009	0.8093
	HO3...O2=2.16	0.0177	0.0765	-0.0165	0.0178	-0.0012	0.9182

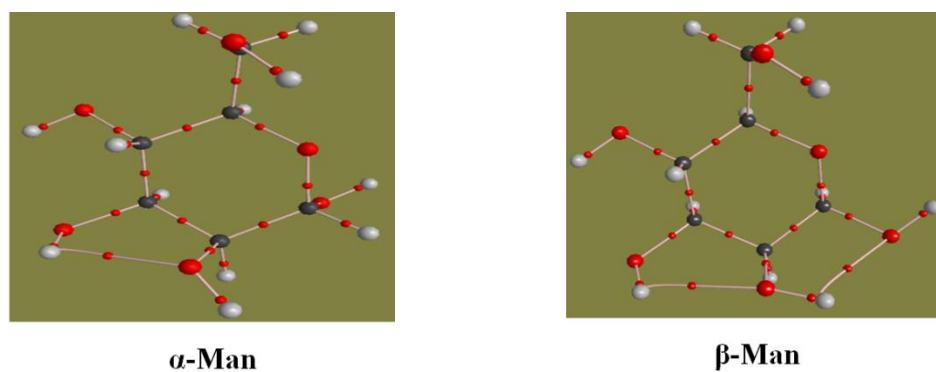
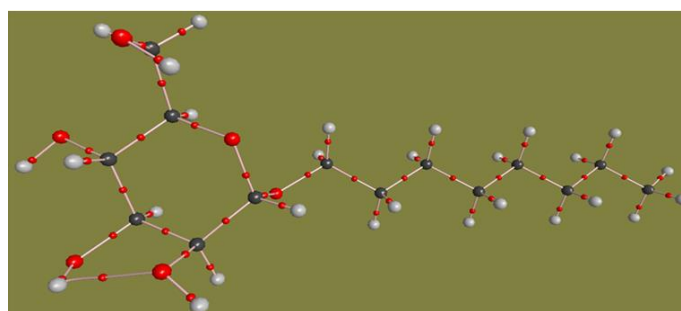
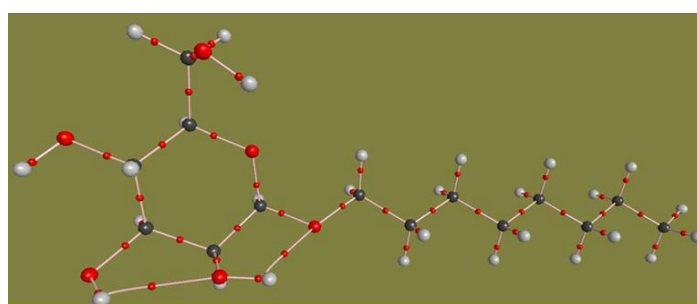


Figure 5.5: Molecular graph in the α/β -Man. Small red spheres and lines correspond to the bond critical points (BCP) and the bond paths, respectively.



C₈O- α -Man



C₈O- β -Man

Figure 5.6: Molecular graph in the C₈O- α/β -Man. Small red spheres and lines correspond to the bond critical points (BCP) and the bond paths, respectively.

5.5 Natural bond orbital (NBO) analysis

NBO analysis is a robust technique to investigate the effects of the stereoelectronic interactions on the reactivity and dynamic behaviors of chemical compounds. The larger the $E^{(2)}$ value are more intensive the interactions. The formation of hydrogen bonds in all of the investigated compounds implies that certain amounts of electronic charges are transferred from the lone pair to the anti-bonding orbital. As can be seen from our results in Table 5.5, electron charge is transferred from a lone pair n (O) atom in a donor fragment, to σ^* (O–H) anti-bonding orbital of an acceptor fragment. The stabilization energies $E^{(2)}$ in the α -Man and C₈O- α -Man in O2...HO3 position are 2.56 and 2.57, respectively. A comparison between the NBO analysis of these two compounds show that there is no significant difference of second-order perturbation energy. Moreover, the stabilization energies $E^{(2)}$ are 1.81 and 1.92 in O2...HO3 position, and are 2.21 and 2.28 kcal/mol in O1...HO2 position for β -Man and C₈O- β -Man, respectively. Therefore, the strength of hydrogen bond in C₈O- β -Man is greater than that in the β -Man. The hydrogen bond in O2...HO3 position is weaker than that of the O1...HO2 position. These data clearly indicate that α -anomers have one hydrogen bond, while β -anomers have two hydrogen bonds. As a result, the hydrogen bond in α -anomers is stronger than β -anomers.

Table 5.5: The second-order perturbation energies, $E^{(2)}$ (kcal/mol), corresponding to the most important charge transfer interaction (donor→acceptor) in the α/β -Man and C₈O- α/β -Man at the B3LYP/6-31G.

Compounds studied	Donor NBO(<i>i</i>)	Acceptor NBO(<i>j</i>)	$E^{(2)}$ (kcal/mol)	$\varepsilon_j - \varepsilon_i$
	<i>n</i> (O)	σ^* (O-H)	(O)→ σ^* (O-H)	
α -Man	LP(2)O3	BD*(2)HO3-O2	2.56	0.77
β -Man	LP(1)O3	BD*(1)HO3-O2	1.81	0.98
	LP(1)O2	BD*(1)HO2-O1	2.21	1.02
C ₈ O- α -Man	LP(2)O3	BD*(1)HO3-O2	2.57	0.77
	LP(1)O3	BD*(1)HO3-O2	1.92	0.98
C ₈ O- β -Man	LP(2)O2	BD*(1)HO2-O1	2.28	1.00

CHAPTER 6

INTERACTION BETWEEN CARBON NANO TUBES AND GLYCOLIPIDS

(Accepted Liq Cryst; 04 Oct 2014)

In this investigation (Chapter 6), we examined the usefulness of local reactivity descriptors in order to predict the reactivity of carbon atom sites on the external surface of (3, 0) zigzag SWNTs. Several other configurations of the SWNTs were explored including (7,0) zigzag and (5,5) armchair. However, small-diameter nanotubes are more popular due to their high curvature, leading to properties different from those of large-diameter SWNTs [160, 229]. Therefore, in this chapter we presented the interactions between (3,0) zigzag carbon nanotubes and n-octyl- β -D-glucopyranoside (C_8O - β -Glc) and the analysis in both gas and solution phases based on the density functional theory (DFT) methods. Our computational strategy was to obtain optimal structures at the B3LYP/6-31G level, and to use these structures for binding energy calculations at similar levels. Finally, the highest occupied molecular orbital lowest unoccupied molecular orbital and energy gaps of complexes were also determined.

6.1 Fukui calculations

In order to determine the regioselectivity of (3, 0) zigzag SWNTs, the following reactivity descriptors, $f^+(k)$, $s^+(k)$, $s^+(k)/s^-(k)$ and $f^2(k)$ were considered and summarized in Table 6.1. These descriptors are used to predict the most favored carbon atom for a nucleophilic attack. Similarly, for an electrophilic attack, we utilized $f^-(k)$, $s^-(k)$, $s^-(k)/s^+(k)$ and $f^2(k)$. It should be mentioned that $f^2(k)$ has the capability to evaluate both nucleophilic and electrophilic attacks. $f^2(k) > 0$ implies that the site favors a nucleophilic attack, while the site is susceptible to an electrophilic attack if $f^2(k) < 0$. Mulliken population analysis (MPA) is used to calculate these reactivity descriptors.

Figure 6.1(a), shows $f^+(k)$ and $f^-(k)$ derived from MPA for (3, 0) zigzag SWNTs exhibit exactly the same trend at B3LYP/6-31G functions. Moreover, Fukui functions and the corresponding local softness also display very similar trends. In addition, the carbon atoms with high electrophilicity (i.e., having high $f^+(k)$ and $s^+(k)$ values) also show high nucleophilicity (i.e., having high $f^-(k)$ and $s^-(k)$ values). Therefore, we have also plotted the $s^+(k)/s^-(k)$, $s^-(k)/s^+(k)$ and $f^2(k)$ functions versus the carbon position for electrophilic and nucleophilic attacks, in Figure 6.1(b), respectively. It is encouraging to note that $s^+(k)/s^-(k)$ and $f^2(k)$, which are derived from MPA at B3LYP/6-31G, displays a similar trend.

Table 6.1: The values of $f^+(k)$, $s^+(k)$, $\frac{s^+(k)}{s^-(k)}$, $\frac{s^-(k)}{s^+(k)}$, $f^-(k)$, $s^-(k)$ and $f^2(k)$ derived from MPA schemes at the B3LYP/6-31G level for various carbon atoms of (3,0) zigzag SWNT.							
Carbon atom*	$f^+(k)$	$s^+(k)$	$\frac{s^+(k)}{s^-(k)}$	$f^-(k)$	$s^-(k)$	$\frac{s^-(k)}{s^+(k)}$	$f^2(k)$
1	0.0200	0.5145	1.544	0.0145	0.3310	0.6433	0.0056
2	0.0255	0.6558	1.4593	0.0196	0.4494	0.6852	0.0059
3	0.0180	0.4630	1.0066	0.0201	0.4599	0.9934	-0.0021
4	0.0239	0.6137	1.1588	0.0231	0.5296	0.8630	0.0007
5	0.0277	0.7117	0.9246	0.0336	0.7698	1.0816	-0.0060
6	0.0076	0.1948	0.9636	0.0088	0.2021	1.0377	-0.0013

*The carbon atom label is given in Figures 3.2.

For a nucleophilic attack, the trends of $s^+(k)/s^-(k)$ and $f^2(k)$ for the selected carbon atoms are summarized in the following form:

$$C1 > C2 > C4 > C3 > C6 > C5 \quad \text{for } s^+(k)/s^-(k)$$

$$C2 > C1 > C4 > C3 > C6 > C5 \quad \text{for } f^2(k)$$

Based on the $s^+(k)/s^-(k)$ and $f^2(k)$ results, we found that C1, C2, C4 and C3 atoms are highly preferred for a nucleophilic attack, while the trend of $s^-(k)/s^+(k)$ is the opposite of $s^+(k)/s^-(k)$, and unlikely for an electrophilic attack. Figure 6.1(b) displays that the curve of $s^-(k)/s^+(k)$ is opposite to that of $f^2(k)$ in the population analysis using the same method. We predict that the highly preferred sites for an electrophilic attack are C5 and C6. To determine the adsorption behavior of $C_8O-\beta\text{-Glc}$ on the external surface of (3, 0) zigzag SWNTs, the electronic energy of (3, 0) zigzag carbon nanotubes and n-octyl- $\beta\text{-D-glucopyranoside}$ ($C_8O-\beta\text{-Glc}$) are separately calculated at the B3LYP/6-31G level of theory in gas phase and water solvents. The computational results are given in Table 6.2.

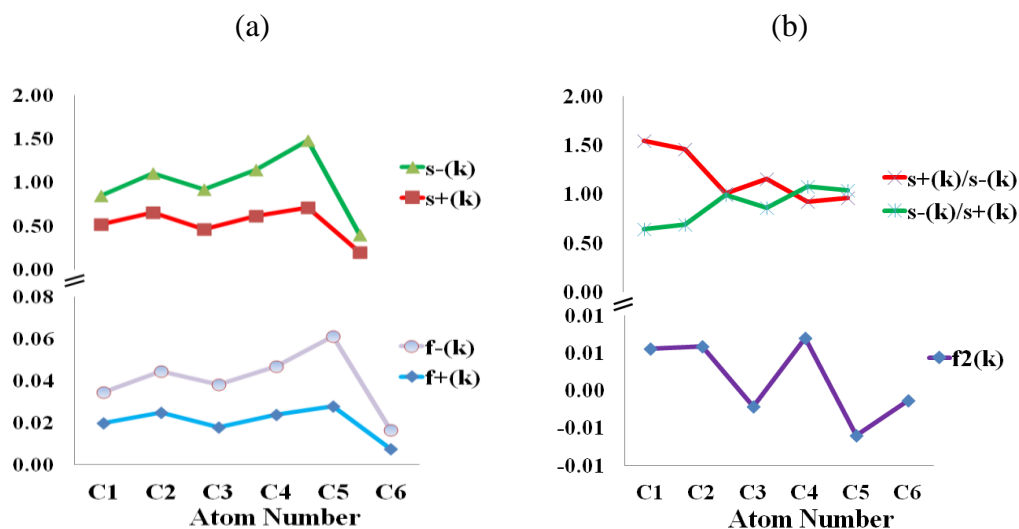


Figure 6.1: Variation of reactivity descriptors derived from MPA for different carbon atoms on the surface of (3,0) zigzag SWNTs computed at B3LYP/6-31G level, for (a) $f^+(k)$, $s^+(k)$, $f^-(k)$ and $s^-(k)$, and (b) for $s^+(k)/s^-(k)$, $s^-(k)/s^+(k)$, and $f^2(k)$.

6.2 Energy calculations

The binding energy of various configurations of surfactants relaxed on the CNT's surface are determined using the same method. Figures 6.2–6.3 show the

optimized structures of complexes (carbon nanotube-surfactant)—namely, B1H (CNT1–surfactant head group), B1T (CNT1–surfactant tail group), B2H (CNT2–surfactant head group) and B2T (CNT2–surfactant tail group) in the gas phase. Here, we used B to represent the (3, 0) SWNTs, while A represents the surfactant (C₈O-β-Glc). As seen in Table 6.3, the adsorption binding energy for complexes is exothermic.

Table 6.2: Calculated structural parameters of C₈O-β-Glc and (3, 0) zigzag SWNTs at the B3LYP/6-31 G level in gas and solution phases.

Studied compounds	Diameter (Å)	<i>E</i> (eV)		<i>μ</i> (D)	
		gas phase	PCM	gas phase	PCM
C ₈ O-β-Glc	-	-27247.17	-27247.61	4.01	4.23
(3,0) zigzag	2.41	-37378.52	-37379.13	0.03	0.01

From Table 6.3, ΔE_b shows that B1H complex (low concentration) demonstrates a favorable interaction. Furthermore, our computed results demonstrate that C5 and C6 atoms are predicted to highly prefer an electrophilic attack based on the values of Table 6.1. Therefore, one can conclude that an electrophilic attack is predicted to take place at the C6 site on the surface of (3,0) zigzag SWNTs. Briefly, an electrophilic attack happens when the oxygen atom of the OH group in sugar molecule (a nucleophile) are bound to the C6 carbon atom (an electrophile) (See Figure 6.2 arrow 1). Consequently, the hydrogen atom from the sugar OH (an electrophile) binds to the C3 (a nucleophile) position of the carbon nanotube (see Figure 6.2. arrow 2). These interaction mechanisms are identified as chemisorption, i.e. chemical reaction between a surface and an adsorbate. Chemisorption usually shows binding energies in the range of 1–10 eV. It is characterized by high enthalpy values (80–240 kJ/mol) [230, 231]. The interaction energies and enthalpy that are calculated for B1H complex were -2.67 eV and -245 kJ/mol, respectively.

Moreover, our data shows that chemisorption process happens in a B2H complex (high concentration) (Figure 6.3), as observed in the binding energy value in Table 6.3 (1.4 eV) and the enthalpy value in Table 6.4 (-123 kJ/mol). Although these values fit the criteria of a chemisorption process, we did not observe any binding between the carbon nanotube and the headgroup of the sugar [171]. This is because the binding energy value required for the B2H complex formation may not be enough to overcome the intermolecular hydrogen bonding between the two sugar head groups.

Table 6.3: Calculated binding energies of (3, 0) zigzag SWNTs in low concentration (one-surfactant) and high concentration (two-surfactants) in two configuration (head and tail) in gas and solution phases at the B3LYP/6-31G level.

Optimized complexes	gas phase		PCM		
	$E_{(complex)}$ (eV)	ΔE_b (eV)	$E_{(complex)}$ (eV)	ΔE_b (eV)	
Low concentration	B1H	-64628.37	-2.67	-64629.19	-2.45
	B1T	-64625.73	-0.04	-64626.77	-0.03
High concentration	B2H	-91874.26	-1.40	-91875.28	-0.92
	B2T	-91873.28	-0.43	-91874.81	-0.45

On the other hand, the calculations show that the adsorptions for the rest of the complexes are identified as physisorption. In recent years, binding energies have frequently been used to analyze the different physisorption and chemisorption processes of SWNTs [232, 233]. Table 6.4 is given Gibbs free energy and enthalpy complexes at the B3LYP/6-31G level.

For both orientations with low concentration of surfactants (B1H and B1T), the total Gibbs free energies (ΔG°) of the CNT-surfactant are calculated to be -192 and 32 kJ/mol respectively, while those for high concentration of surfactant (B2H and B2T), are -23 and 55 kJ/mol, respectively, in the gas phase.

The calculated Gibbs free energy shows that the complexes with head group of surfactant (B1H and B2H) are thermodynamically more favorable in the gas phase. In

addition, as the number of surfactants surrounding the carbon nanotubes increases, the binding energy exhibits sensitivity with respect to the increase in the concentration of the surfactant. In tail configurations from low concentration to high concentration (B1T to B2T), the values of binding energies increased from -0.04 eV to around -0.43 eV. Additionally, in the head group from low concentration to high concentration (B1H to B2H), a decrease from -2.67 eV to around -1.40 eV is detected to be interacting with carbon nanotubes. It can be clearly seen that the binding energy from B1T to B2T increases, but the binding energy from B1H to B2H decreases in the gas phase. As a result, in small carbon nanotube, increasing concentration of surfactant with tail configuration on the external surface of (3,0) SWNTs, could better disperse carbon nanotubes in a similar manner to other surfactants [234, 235].

Table 6.4: Calculated Gibbs free energy and enthalpy of complexes of (3,0) zigzag SWNTs at the B3LYP/6-31G level.

Complexes	ΔG° (kJ/mol)	ΔH° (kJ/mol)
B1H	-192	-245
B1T	32	2
B2H	-23	-123
B2T	55	-29

The results indicate that as the number of surfactant increases on the external surface of SWNTs, the CNT-head configuration became less stable compared to the CNT tail configuration. The dispersion of carbon nanotubes also increases with increasing tail configuration of surfactants on the external surface of carbon nanotubes.

Calculated data shows that the difference of the binding energy between the gas and the solution phases for the CNT-tail configuration is not high, and it is significantly higher for CNT-head configuration. These values in water, as a solvent for B1T and B2T complexes, are (-0.04 to -0.03) and (-0.43 to -0.45) eV, respectively, whereas

these values for B1H and B2H complexes are (-2.67 to -2.45) and (-1.40 to -0.92) eV, respectively. Therefore, the energy difference between the gas and the structure in an aqueous phase in tail groups is 0.23 and 0.46 kcal/mol, while those for head group are 5.07 and 11.06 kcal/mol, suggesting that a complex with tail group in water is more stable than in the gas phase. This trend could be explained by the strong interactions detected between head solvent and the weak interaction of tail-solvent. For a CNT-head complex, individual surfactants are more stable when PCM is used compared to the configuration of the complex, for which the head of the surfactant is not free to completely interact with the solvents. On the other hand, individual and in-complex configurations of the surfactant in CNT-tail are similarly stabilized by PCM. It seems that the head configuration in the surfactant has a greater tendency to interact with water, while the tail configuration in the surfactant interacts better with the surface of carbon nanotubes. Therefore, it can be proposed that the tail's configuration in the solution phase is more stable than in the gas phase, but the head configuration is less stable in the solution phase.

From the optimized structures, the HOMO-LUMO band gap is determined to be the differences between the HOMO and LUMO, and the electronic chemical potential (μ) as half of the energy of the HOMO and LUMO being a measure of the structural stability properties. Table 6.5 displays the quantum molecular descriptions of all the optimized structures of complexes. The results point out that the HOMO-LUMO energy gap of (3,0) is 0.0380 eV. Following the relaxation of surfactants onto SWNTs, the lowest band gap is obtained in B1H; (This value is 0.0431 eV). Therefore, there is a change in the conductivity due to the binding of the surfactant with head orientation. This finding confirms the stability of this complex in the gas phase.

Table 6.5: Calculated highest occupied molecular orbital (HOMO), lowest unoccupied molecular orbital (LUMO), energy gap for (3,0) zigzag SWNT with their complexes and chemical potential (μ) at the B3LYP/6-31G level.

Complexes	HOMO	LUMO	Energy gap (eV)	Chemical potential
B	-0.1988	-0.1608	0.0380	-0.1798
B1H	-0.1957	-0.1526	0.0431	-0.1741
B1T	-0.2008	-0.1628	0.0380	-0.1818
B2H	-0.2054	-0.1668	0.0386	-0.1861
B2T	-0.2025	-0.1645	0.0380	-0.1835

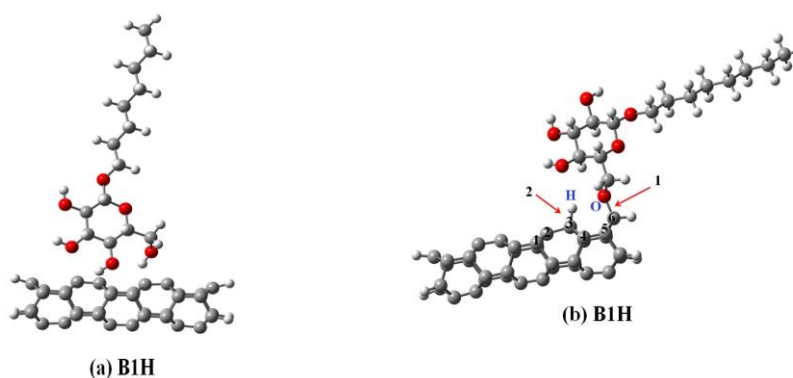


Figure 6.2: Various configurations of C_8O - β -Glc residing on the external surface of (3, 0) SWNTs at the B3LYP/6-31G level in the gas phase are depicted here before and after optimization. A configuration where CNT interact directly with the surfactant head group, at low concentration, B1H is shown in (a) before optimization and (b) after optimization, where the arrow indicate oxygen of the surfactant in B1H is bonded to the carbon of C6 of the carbon nanotube at low concentration.

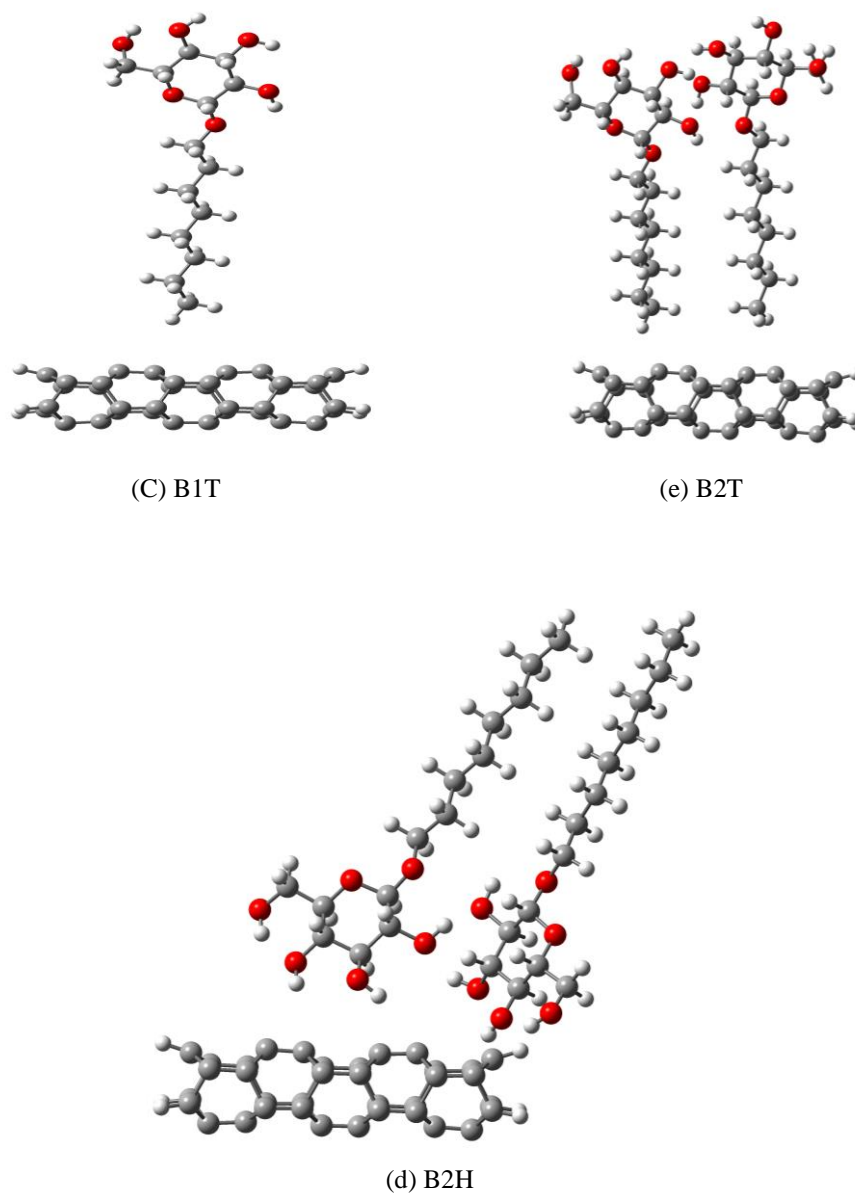


Figure 6.3: Various configurations of $C_8O\text{-}\beta\text{-Glc}$ residing on the external surface of (3, 0) SWNTs at the B3LYP/6-31G level in the gas phase is depicted here before and after optimization. A configuration where CNT interact directly with the surfactant head group (c) B1T configuration (CNT1–Surfactant tail group) after optimization at low concentration. The high concentration configurations after optimization are (d) B2H (CNT2–Surfactant head group) and (e) B2T (CNT2–Surfactant tail group).

CHAPTER 7

CONCLUSIONS

In this thesis, the first several methods such as density functional theory (DFT), atoms in molecules (AIM), and natural bond orbital (NBO) have been applied to understand and explore the behavior of glycolipids with different orientation OH in the head group in gas and solution phases with carbon nanotubes. Then, we have examined the realization of high accuracy terms of adsorption energies between glycolipid and carbon nanotubes (CNTs), and predicted the reactivity of different carbon atom sites of the SWNTs under study by the DFT-based local reactivity descriptor, Fukui function, local softness and dual reactivity.

In the first part of this work, the effects of epimerization at the C4 position of C₈O- β -Glc and C₈O- β -Gal were investigated using density functional theory. In C₈O- β -Glc, all the peripheral OH groups are equatorial, while in C₈O- β -Gal, OH₄ is axial. The O-H distances, bond lengths, and the electronic densities at the bond critical points (BCP) were used to compare the hydrogen bond's strength in the C₈O- β -Glc and C₈O- β -Gal. The results of a detailed population analysis of C₈O- β -Glc and C₈O- β -Gal by natural bond orbitals and the atoms in molecules methods can be concluded as follows: the higher energy in C₈O- β -Gal compared to C₈O- β -Glc indicates that the C₈O- β -Gal is more stable when forming an extra five-membered ring. The BCP calculation shows the presence of HB interaction, while further molecular graph representation shows that C₈O- β -Gal has two hydrogen bonds, and only one in C₈O- β -Glc. Hydrogen bond of type HO₆...O₄ in C₈O- β -Glc and C₈O- β -Gal shows partially covalent–partially electrostatic (Pc-Pe) nature, but hydrogen bond of type HO₄...O₃ exhibit van der Waals nature in C₈O- β -Gal. Hydrogen bond of type HO₆...O₄ in both C₈O- β -Glc and C₈O- β -Gal is classified as medium, while hydrogen bond type HO₄...O₃ in C₈O- β -Gal is regarded as weak. By comparison, it is apparent that hydrogen bond type HO₆...O₄ is much stronger than HO₆...O₄ in C₈O- β -Gal. The interactions in ($n2O3 \rightarrow \sigma^*(O4-HO4)$) and in

($n2O4 \rightarrow \sigma^*(O6-HO6)$) are most important for intra-molecular interaction that play a key role in the stability of studied compounds in this work. The lowest value (0.73 kcal/mol) for $C_8O-\beta$ -Glc in $n2O3 \rightarrow \sigma^*(O4-HO4)$, and the highest value (11.55 kcal/mol) for $C_8O-\beta$ -Gal in ($n2O4 \rightarrow \sigma^*(O6-HO6)$) are observed. In the final of this section work, IR frequencies the studied compounds have been recognized to fall into the short-wavelength-infrared region (1400-3000) nm. As a result of this, these materials absorb infrared frequency, which may be exploited as an infrared sensor material similar to that suggested for carbohydrate previously [225].

In second part of this research, the anomeric effects at the C1 position α/β -D-mannose with or without length (α -Man, β -Man, $C_8O-\alpha$ -Man and $C_8O-\beta$ -Man) were investigated using the density functional theory. In α -anomers of these compounds, the peripheral OH1 group in C1 is axial, while in β -anomers, OH1 is equatorial. The bond lengths, electronic properties, and the electronic density at the bond critical were used to compare the hydrogen bond strengths in these conformers. The higher energy in β -anomers compared to α -anomers indicate that anomers without chains are more unstable than the ones with chains. In addition, the β -Man and $C_8O-\beta$ -Man is more stable than α -Man and $C_8O-\alpha$ -Man. The computational results predicted that the length of chain in these kinds of glycolipids could stabilize the compounds in equatorial configuration due to the formation of an extra five-membered ring at the O1...HO2 position. Furthermore, β -anomers are hard, whereas α -anomers are soft. Therefore, β -anomers are regarded as a reactive species when compared to α -anomers. AIM analysis shows all hydrogen bond in this investigated compound in two positions; O2...HO3 and O1...HO2 are partially covalent-partially electrostatic (Pc-Pe) in nature. Moreover, the hydrogen bond in O2...HO3 position is weaker than in O1...HO2 position in β -anomers. By comparing α/β -anomers, it is apparent that intra-molecular hydrogen bond in α -anomers is stronger

than those in the β -anomers. The formation of two intra-molecular hydrogen bonds in the β -Man and C₈O- β -Man implies that certain electronic charges are transferred from the lone pair to the anti-bonding orbital. On the other hand, natural bond orbital analysis confirms that there is only one intra-molecular hydrogen bond in α -Man and C₈O- α -Man while for β -Man and C₈O- β -Man, they were two intra-hydrogen bonds. Finally, these results agree with preceding molecular dynamic (MD) study of n-octyl- α/β -D-mannopyranoside in an aqueous solution [171].

At the end of this investigation, carbon nanotubes are being utilized for highly-efficient drug and biomolecule deliveries, due to their large surface areas and unique optical and electrical properties. DFT-based local reactivity descriptors have the potential of predicting local (site) reactivity of chemical compounds. The local reactivity descriptors are calculated based on Mulliken population analysis (MPA) schemes. We have found that Fukui functions and the corresponding local softness display similar trends. It is predicted that the highly preferred sites for electrophilic attack are C5 and C6. From analyzing the data, when the number of surfactant residing on the surface of the CNTs increases, the interaction energy of CNT-head and tail configurations changes. When the surfactant number is increased, we observed a CNT-head system being reduced in energy. On the other hand, when more surfactants is added, a better binding was observed on the CNT-tail configurations, which means that $|\Delta E_b(\text{B1T})|$ is smaller compared to $|\Delta E_b(\text{B2T})|$, due to the hydrophobic effect (more surfactants) in the gas and solution phase. Moreover, complexes with CNT-head configuration, such as B1H and B2H, are identified as chemisorptions. CNT-tail configuration in PCM phase is more stable than the gas phase, but the head configuration is less stable in the solution phase.

Overall, the subject studied in this thesis confirms that a non-ionic surfactant is able to stabilize and disperse carbon nanotubes like other surfactants and polymers. The result from the investigations would facilitate the development of in drug delivery systems using glycolipids as non-ionic surfactants. (See Figure 7.1)

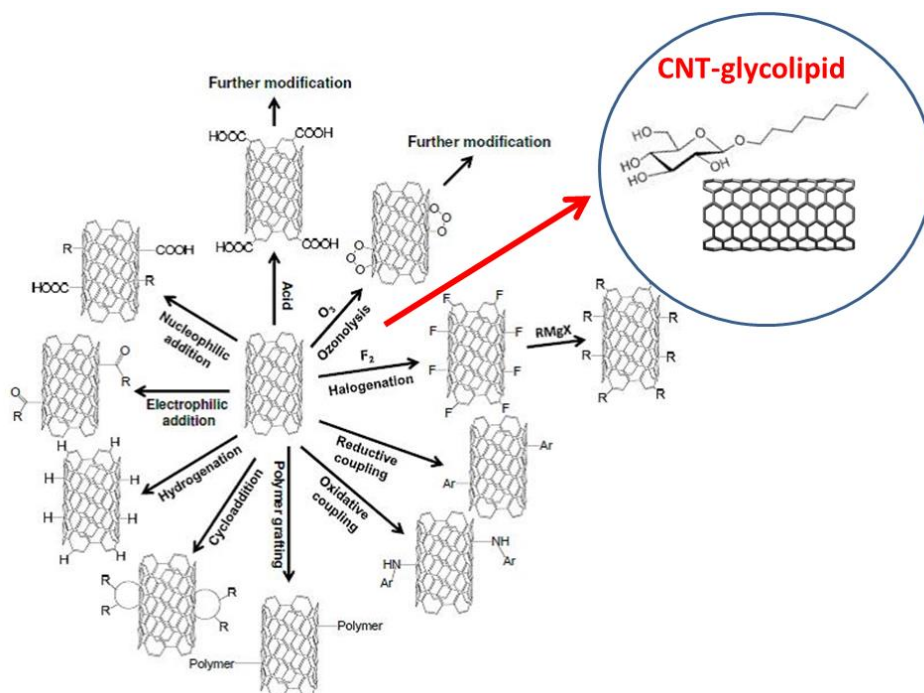


Figure 7.1: schematic representation of surface functionalization of CNTs with other molecules including glycolipids (a) shows new suggestion. (illustration adapted from [121]).

7.1 Future works

Some properties such as electronic energy between *n*-octyl- α/β -D-glucopyranoside with (7, 0) zigzag and (5, 0) armchair carbon nanotube are calculated for understanding chirality effect CNTs on interaction between them. Harmonic vibration frequencies, including both Infrared and Raman frequencies of *n*-octyl- α/β -D-glucopyranoside in the gas phase were investigated to study the potential energy distribution (PED) analysis.

Currently, several molecular dynamic simulations are being carried out to study the interaction between glycolipids (studied in thesis) and single-walled carbon nanotubes by using Gromacs. The aim of this future work is to investigate the mechanism of interaction of CNT-drug/biomolecule complexes with cell membrane.

We aim to investigate also solvent effect on the interaction between carbon nanotubs and glycolipids by PCM. Moreover, chirality effect carbon nanotubes will be investigated with CASTEP, Materials studio.

REFERENCES

1. Drexler KE, Minsky M. Engines of creation. London: Fourth Estate 1990.
2. Drexler KE. Nanosystems: molecular machinery, manufacturing, and computation. New York: John Wiley & Sons, Inc.; 1992.
3. Iijima S. Helical microtubules of graphitic carbon. *Nature*. 1991;354:56-58.
4. Thess A, Lee R, et al. Crystalline ropes of metallic carbon nanotubes. *Science-AAAS-Weekly Paper Edition*. 1996;273:483-487.
5. Munoz E, Maser W, et al. Single-walled carbon nanotubes produced by cw CO₂-laser ablation: study of parameters important for their formation. *Appl Phys A*. 2000;70:145-151.
6. Ebbesen T, Ajayan P. Large-scale synthesis of carbon nanotubes. *Nature*. 1992;358:220-222.
7. Ando Y, Iijima S. Preparation of carbon nanotubes by arc-discharge evaporation. *Jap J Appl Phys 2*. 1993;32:L107-L107.
8. Endo M, Takeuchi K, et al. Pyrolytic carbon nanotubes from vapor-grown carbon fibers. *Carbon*. 1995;33:873-881.
9. Terrones M, Grobert N, et al. Controlled production of aligned-nanotube bundles. *Nature*. 1997;388:52-55.
10. Ren Z, Huang Z, et al. Synthesis of large arrays of well-aligned carbon nanotubes on glass. *Science*. 1998;282:1105-1107.
11. Fan S, Chapline MG, et al. Self-oriented regular arrays of carbon nanotubes and their field emission properties. *Science*. 1999;283:512-514.
12. Iijima S, Ichihashi T. Single-shell carbon nanotubes of 1-nm diameter. *Nature*. 1993;363:603-605.
13. Swain MV. Structure and properties of ceramics. Berlin: Wiley-VCH; 1994.
14. Reich S, Thomsen C, et al. Carbon nanotubes: basic concepts and physical properties: New York:John Wiley & Sons; 2008.
15. Harris PJ, Harris PJF. Carbon nanotubes and related structures: new materials for the twenty-first century. Cambridge: University Press; 2001.
16. Ogata S, Shibutani Y. Ideal tensile strength and band gap of single-walled carbon nanotubes. *Phys Rev B*. 2003;68:165409.
17. Elliott JA, Sandler JK, et al. Collapse of single-wall carbon nanotubes is diameter dependent. *Phys Rev Lett*. 2004;92:095501.
18. Yu M-F, Files BS, et al. Tensile loading of ropes of single wall carbon nanotubes and their mechanical properties. *Phy Rev Lett*. 2000;84:5552.

19. Cui H-F, Vashist SK, et al. Interfacing carbon nanotubes with living mammalian cells and cytotoxicity issues. *Chem Res Toxicol*. 2010;23:1131-1147.
20. Vashist SK, Zheng D, et al. Delivery of drugs and biomolecules using carbon nanotubes. *Carbon*. 2011;49:4077-4097.
21. Winter AD, Jaye C, et al. Prestrain relaxation in non-covalently modified ethylene-vinyl acetate | PyChol | multiwall carbon nanotube nanocomposites. *APL Mater*. 2014;2:066105.
22. Saito R, Dresselhaus G, et al. Physical properties of carbon nanotubes. London: Imperial College Press; 1998.
23. Dillon A, Jones K, et al. Storage of hydrogen in single-walled carbon nanotubes. *Nature*. 1997;386:377-379.
24. Che G, Lakshmi BB, et al. Carbon nanotubule membranes for electrochemical energy storage and production. *Nature*. 1998;393:346-349.
25. Hirscher M, Becher M. Hydrogen storage in carbon nanotubes. *J nanosci Nanotechnol*. 2003;3:3-17.
26. Ajayan PM. Capillarity-induced filling of carbon nanotubes. *Nature*. 1993;361:333-334.
27. Tsang S, Chen Y, et al. A simple chemical method of opening and filling carbon nanotubes. *Nature*. 1994;372:159-162.
28. White CT, Todorov TN. Carbon nanotubes as long ballistic conductors. *Nature*. 1998;393:240-242.
29. Yakobson BI, Brabec C, et al. Nanomechanics of carbon tubes: instabilities beyond linear response. *Phys Rev Lett*. 1996;76:2511.
30. Choi W, Chung D, et al. Fully sealed, high-brightness carbon-nanotube field-emission display. *Appl Phys Lett*. 1999;75:3129-3131.
31. Saito Y. Carbon nanotube field emitter. *J Nanosci Nanotechnol*. 2003;3:39-50.
32. Wong SS, Joselevich E, et al. Covalently functionalized nanotubes as nanometre-sized probes in chemistry and biology. *Nature*. 1998;394:52-55.
33. Bianco A, Kostarelos K, et al. Biomedical applications of functionalised carbon nanotubes. *Chem Commun*. 2005:571-577.
34. Smart S, Cassady A, et al. The biocompatibility of carbon nanotubes. *Carbon*. 2006;44:1034-1047.
35. Bianco A, Kostarelos K, et al. Applications of carbon nanotubes in drug delivery. *Curr Opin Chem Biol*. 2005;9:674-679.
36. Oberdörster G, Oberdörster E, et al. Nanotoxicology: an emerging discipline evolving from studies of ultrafine particles. *Environ Health Persp*. 2005:823-839.
37. Donaldson K, Stone V, et al. Re: Induction of mesothelioma in p53[±]-mouse by intraperitoneal application of multi-wall carbon nanotube. *J Toxicol Sci*. 2008;33:386-388.

38. Lewinski N, Colvin V, et al. Cytotoxicity of nanoparticles. *Small*. 2008;4:26-49.
39. Reinitzer F. Beiträge zur kenntniss des cholesterins. *Monatshefte für Chemie/Chemical Monthly*. 1888;9:421-441.
40. Lehmann O. On flowing crystals. *Zeitschrift für Physikalische Chemie*. 1889;4:462.
41. Collings PJ, Hird M. *Introduction to liquid crystals: chemistry and physics*. Florida: CRC Press; 1997.
42. Wojtowicz PJ, Sheng P, et al. *Introduction to liquid crystals*. New York: Plenum Press; 1975.
43. Barnes H. *Detergents in rheometry industrial applications*. New York: John Wiley & Sons; 1980.
44. Somasundaran P, Mehta SC, et al. Nanotechnology and related safety issues for delivery of active ingredients in cosmetics. *Mrs Bulletin*. 2007;32:779-786.
45. Jan B. Influence of polar head groups on the gel to liquid-crystal transition in vesicular and lipid bilayer systems. *J Chem Soc Faraday T*. 1996;92:3163-3164.
46. Kim H-HY, Baianu IC. Novel liposome microencapsulation techniques for food applications. *Trends Food Sci Tech*. 1991;2:55-61.
47. Pilpel N, Rabbani M. Formation of liquid crystals in sunflower oil in water emulsions. *J Colloid Interf Sci*. 1987;119:550-558.
48. Kabalnov A, Tarara T, et al. Phospholipids as Emulsion Stabilizers: 2. Phase Behavior versus Emulsion Stability. *J Colloid Interf Sci*. 1996;184:227-235.
49. Kato T, Hirai Y, et al. Liquid-crystalline physical gels. *Chem Soc Rev*. 2007;36:1857-1867.
50. Barone V, Cossi M. Quantum calculation of molecular energies and energy gradients in solution by a conductor solvent model. *J Phys Chem A*. 1998;102:1995-2001.
51. Gray GW. *Thermotropic liquid crystals*. New York: John Wiley & Sons Inc; 1987.
52. Hamley IW. *Introduction to Soft Matter: polymer, colloids, amphiphiles and liquid crystals*. New York: John Wiley & Sons; 2000.
53. Jeffrey GA, Wingert LM. Carbohydrate liquid crystals. *Liq Cryst*. 1992;12:179-202.
54. Fairhurst CE, Fuller S, et al. Lyotropic surfactant liquid crystals. *Handbook of Liquid Crystals Set*. 1998:341-392.
55. Seddon J, Bartle E, et al. Inverse cubic liquid-crystalline phases of phospholipids and related lyotropic systems. *J Phys-Condens Mat*. 1990;2:SA285.
56. Hashim R, Sugimura A, et al. Nature-like synthetic alkyl branched-chain glycolipids: a review on chemical structure and self-assembly properties. *Liq Cryst*. 2012;39:1-17.
57. Vill V, Hashim R. Carbohydrate liquid crystals: structure–property relationship of thermotropic and lyotropic glycolipids. *Curr Opin Colloid Interf Sci*. 2002;7:395-409.

58. Holmberg K. *Novel Surfactants: Preparation Applications and Biodegradability, Revised and Expanded*. Florida: CRC Press; 2003.
59. Konidala P, He L, et al. Molecular dynamics characterization of n-octyl- β -d-glucopyranoside micelle structure in aqueous solution. *J Mol Graph Model*. 2006;25:77-86.
60. Hannun YA, Bell RM. Functions of sphingolipids and sphingolipid breakdown products in cellular regulation. *Science*. 1989;243:500-507.
61. Fendler JH. *Membrane mimetic chemistry: characterizations and applications of micelles, microemulsions, monolayers, bilayers, vesicles, host-guest systems, and polyions*. New York: Wiley 1982.
62. Lasic DD. *Liposomes: from physics to applications*. Amsterdam Elsevier 1993.
63. Zhang Z, Fukunaga K, et al. Synthesis of glycolipids: dialkyl N-[N-(4-lactonamidobutyl) succinamoyl] l-glutamates. *Carbohydr Res*. 1996;290:225-232.
64. Eskuchen R, Nitsche M. *Technology and production of alkyl polyglycosides*. Weinheim: Wiley-VCH 1997.
65. Hato M, Yamashita I, et al. Aqueous Phase Behavior of a 1-O-Phytanyl- β -d-xyloside/Water System. Glycolipid-Based Bicontinuous Cubic Phases of Crystallographic Space Groups Pn3m and Ia3d. *Langmuir*. 2004;20:11366-11373.
66. Nalwa HS. *Handbook of Nanostructured Biomaterials and Their Applications in Nanobiotechnology: Biomaterials*. 1: American Scientific Publishers; 2005.
67. Hunter R. *Foundations of Colloid Science* Clarendon. Michigan: Clarendon Press; 1987.
68. Evans DF, Wennerström H. *The colloidal domain: where physics, chemistry, biology, and technology meet*. Weinheim: Wiley-VCH; 1999.
69. Ben-Shaul A, Roux D. *Micelles, membranes, microemulsions, and monolayers*. New York: Springer-Verlag 1994.
70. Vill V, Vill V, et al. The stereochemistry of glycolipids. A key for understanding membrane functions? *Liq Cryst*. 2006;33:1351-1358.
71. Hill K, Rhode O. Sugar-based surfactants for consumer products and technical applications. *Fett-Lipid*. 1999;101:25-33.
72. Jackson M, Schmidt C, et al. Solubilization of phosphatidylcholine bilayers by octyl glucoside. *Biochem*. 1982;21:4576-4582.
73. Wang J, Balazs YS, et al. Solid-state REDOR NMR distance measurements at the ligand site of a bacterial chemotaxis membrane receptor. *Biochem*. 1997;36:1699-1703.
74. Harding MM, Anderberg PI, et al. 'Antifreeze' glycoproteins from polar fish. *Eur J Biochem*. 2003;270:1381-1392.
75. Varki A. Biological roles of oligosaccharides: all of the theories are correct. *Glycobiology*. 1993;3:97-130.

76. Robyt JF. Essentials of carbohydrate chemistry. Berlin: Springer Science & Business Media; 1998.
77. Alton G, Hasilik M, et al. Direct utilization of mannose for mammalian glycoprotein biosynthesis. *Glycobiology*. 1998;8:285-295.
78. Toyota S, Fukushi Y, et al. Anti-bacterial defense mechanism of the urinary bladder. Role of mannose in urine. *Jap J Urol*. 1989;80:1816-1823.
79. Niehues R, Hasilik M, et al. Carbohydrate-deficient glycoprotein syndrome type Ib. Phosphomannose isomerase deficiency and mannose therapy. *J Clin Invest*. 1998;101:1414.
80. Horton D. Advances in carbohydrate chemistry and biochemistry. Massachusetts: Academic Press; 2012.
81. Steiner T, Saenger W. Role of C-H...O hydrogen bonds in the coordination of water molecules. Analysis of neutron diffraction data. *J Am Chem Soc*. 1993;115:4540-4547.
82. Baker E, Hubbard R. Hydrogen bonding in globular proteins. *Prog Biophys Mol Bio*. 1984;44:97-179.
83. Hermansson M, von Heijne G. Inter-helical hydrogen bond formation during membrane protein integration into the ER membrane. *J Mol Bio*. 2003;334:803-809.
84. Arneson LS, Katz JF, et al. Hydrogen bond integrity between MHC class II molecules and bound peptide determines the intracellular fate of MHC class II molecules. *J Immunol*. 2001;167:6939-6946.
85. Nagy L, Milano F, et al. Protein/lipid interaction in the bacterial photosynthetic reaction center: phosphatidylcholine and phosphatidylglycerol modify the free energy levels of the quinones. *Biochem*. 2004;43:12913-12923.
86. Sakya P, Seddon J. Thermotropic and lyotropic phase behaviour of monoalkyl glycosides. *Liq Cryst*. 1997;23:409-424.
87. Israelachvili J. The science and applications of emulsions—an overview. *Colloid Surface A*. 1994;91:1-8.
88. Helm CA, Israelachvili JN, et al. Role of hydrophobic forces in bilayer adhesion and fusion. *Biochem*. 1992;31:1794-1805.
89. Bader RF. A quantum theory of molecular structure and its applications. *Chem Rev*. 1991;91:893-928.
90. Bader RF, Essen H. The characterization of atomic interactions. *J Chem Phys*. 1984;80:1943-1960.
91. Arnold WD, Oldfield E. The chemical nature of hydrogen bonding in proteins via NMR: J-couplings, chemical shifts, and AIM theory. *J Am Chem Soc*. 2000;122:12835-12841.
92. Espinosa E, Molins E, et al. Hydrogen bond strengths revealed by topological analyses of experimentally observed electron densities. *Chem Physics Lett*. 1998;285:170-173.

93. Grabowski SJ. A new measure of hydrogen bonding strength—ab initio and atoms in molecules studies. *Chem Phys Lett.* 2001;338:361-366.
94. Ikushima Y, Hatakeda K, et al. An in situ Raman spectroscopy study of subcritical and supercritical water: The peculiarity of hydrogen bonding near the critical point. *J Chem Phys.* 1998;108:5855-5860.
95. Young D. *Computational chemistry: a practical guide for applying techniques to real world problems.* New York: John Wiley & Sons; 2004.
96. Schrödinger E. An undulatory theory of the mechanics of atoms and molecules. *Phys Rev.* 1926;28:1049.
97. Atkins P, Friedman R. *Molecular quantum mechanics,* Oxford: Oxford University Press, ; 1997.
98. Leach AR. *Molecular modelling: principles and applications.* New Jersey: Prentice Hall; 2001.
99. Dewar MJS, Thiel W. Ground states of molecules. 38. The MNDO method. Approximations and parameters. *J Am Chem Soc.* 1977;99:4899-4907.
100. Thomas LH. *The calculation of atomic fields.* Cambridge: Univ Press; 1927.
101. Fermi E. A statistical method for the determination of some atomic properties and the application of this method to the theory of the periodic system of elements. *Z Phys.* 1928;48:73-79.
102. Teller E. On the stability of molecules in the Thomas-Fermi theory. *Rev Mod Phys.* 1962;34:627.
103. Jones RO, Gunnarsson O. The density functional formalism, its applications and prospects. *Rev Modern Phys.* 1989;61:689.
104. Koch W, Holthausen MC. *A chemist's guide to density functional theory.* Weinheim: Wiley-VCH; 2000.
105. Parr RG. Density functional theory. *Annu Rev Phys Chem.* 1983;34:631-656.
106. Ziegler T. Approximate density functional theory as a practical tool in molecular energetics and dynamics. *Chem Rev.* 1991;91:651-667.
107. Parr RG, Yang W. *Density-functional theory of atoms and molecules.* Oxford: University Press; 1989.
108. Dreizler RM, Gross EK. *Density functional theory of relativistic systems. Density Functional Theory.* Berlin: Springer; 1990. p. 245-271.
109. Kohn W, Sham LJ. Self-consistent equations including exchange and correlation effects. *Phys Rev.* 1965;140:A1133.
110. Hohenberg P, Kohn W. Inhomogeneous electron gas. *Phy Rev.* 1964;136:B864.
111. Levy M. Electron densities in search of Hamiltonians. *Phys Rev A.* 1982;26:1200.

112. Auerbach A. Interacting electrons and quantum magnetism. New York: Springer; 1994.
113. Jensen F. Introduction to computational chemistry. New York: John Wiley & Sons; 2007.
114. Matta CF, Hernández-Trujillo J, et al. Hydrogen–hydrogen bonding: a stabilizing interaction in molecules and crystals. *Chem-A Eur J*. 2003;9:1940-1951.
115. Weinhold F, Landis CR. Natural bond orbitals and extensions of localized bonding concepts. *Chem Educ Res Pract*. 2001;2:91-104.
116. Glendening ED, Landis CR, et al. Natural bond orbital methods. *Comput Mol Sci*. 2012;2:1-42.
117. Weinhold F, Landis CR. Valency and bonding: a natural bond orbital donor-acceptor perspective. Cambridge University Press; 2005.
118. Wang H. Dispersing carbon nanotubes using surfactants. *Curr Opin Colloid Interf Sci*. 2009;14:364-371.
119. Vaisman L, Wagner HD, et al. The role of surfactants in dispersion of carbon nanotubes. *Adv Colloid Interface Sci*. 2006;128:37-46.
120. Sitko R, Zawisza B, et al. Modification of carbon nanotubes for preconcentration, separation and determination of trace-metal ions. *TrAC Trends Analyt Chem*. 2012;37:22-31.
121. Wu H-C, Chang X, et al. Chemistry of carbon nanotubes in biomedical applications. *J Mater Chem*. 2010;20:1036-1052.
122. Rosen MJ, Kunjappu JT. Surfactants and interfacial phenomena. New York: John Wiley & Sons; 2012.
123. Yurekli K, Mitchell CA, et al. Small-angle neutron scattering from surfactant-assisted aqueous dispersions of carbon nanotubes. *J Am Chem Soc*. 2004;126:9902-9903.
124. Shvartzman-Cohen R, Levi-Kalisman Y, et al. Generic approach for dispersing single-walled carbon nanotubes: the strength of a weak interaction. *Langmuir*. 2004;20:6085-6088.
125. Hertel T, Hagen A, et al. Spectroscopy of single-and double-wall carbon nanotubes in different environments. *Nano lett*. 2005;5:511-514.
126. Jiang L, Gao L, et al. Production of aqueous colloidal dispersions of carbon nanotubes. *J Colloid Int Sci*. 2003;260:89-94.
127. Vaisman L, Marom G, et al. Dispersions of surface-modified carbon nanotubes in water-soluble and water-insoluble polymers. *Adv Func Mater*. 2006;16:357-363.
128. Chatterjee T, Yurekli K, et al. Single-walled carbon nanotube dispersions in poly(ethylene oxide). *Adv Func Mater*. 2005;15:1832-1838.
129. O'connell MJ, Bachilo SM, et al. Band gap fluorescence from individual single-walled carbon nanotubes. *Science*. 2002;297:593-596.
130. Steinmetz J, Glerup M, et al. Production of pure nanotube fibers using a modified wet-spinning method. *Carbon*. 2005;43:2397-2400.

131. Islam M, Rojas E, et al. High weight fraction surfactant solubilization of single-wall carbon nanotubes in water. *Nano Lett.* 2003;3:269-273.
132. Camponeschi E, Florkowski B, et al. Uniform directional alignment of single-walled carbon nanotubes in viscous polymer flow. *Langmuir.* 2006;22:1858-1862.
133. Matarredona O, Rhoads H, et al. Dispersion of single-walled carbon nanotubes in aqueous solutions of the anionic surfactant NaDDBS. *J Phys Chem B.* 2003;107:13357-13367.
134. Li Z, Liu Z, et al. Synthesis of single-crystal gold nanosheets of large size in ionic liquids. *J Phys Chem B.* 2005;109:14445-14448.
135. Chen RJ, Zhang Y, et al. Noncovalent sidewall functionalization of single-walled carbon nanotubes for protein immobilization. *J Am Chem Soc.* 2001;123:3838-3839.
136. Chen J, Liu H, et al. Noncovalent engineering of carbon nanotube surfaces by rigid, functional conjugated polymers. *J Am Chem Soc.* 2002;124:9034-9035.
137. Shim M, Shi Kam NW, et al. Functionalization of carbon nanotubes for biocompatibility and biomolecular recognition. *Nano Lett.* 2002;2:285-288.
138. Dyke CA, Tour JM. Unbundled and highly functionalized carbon nanotubes from aqueous reactions. *Nano Lett.* 2003;3:1215-1218.
139. Dyke CA, Tour JM. Overcoming the insolubility of carbon nanotubes through high degrees of sidewall functionalization. *Chem-A Eur J.* 2004;10:812-817.
140. Barraza HJ, Pompeo F, et al. SWNT-filled thermoplastic and elastomeric composites prepared by miniemulsion polymerization. *Nano Lett.* 2002;2:797-802.
141. Zhang X, Zhang J, et al. Surfactant-directed polypyrrole/CNT nanocables: Synthesis, characterization, and enhanced electrical properties. *ChemPhysChem.* 2004;5:998-1002.
142. Jin H-J, Choi HJ, et al. Carbon nanotube-adsorbed polystyrene and poly (methyl methacrylate) microspheres. *Chem Mater.* 2005;17:4034-4037.
143. Poulin P, Vigolo B, et al. Films and fibers of oriented single wall nanotubes. *Carbon.* 2002;40:1741-1749.
144. Fugami K, Sano M. Role of polymers in fabrication of carbon nanotube fibers using flow-induced condensation method. *New Diam Front C Tech.* 2005;15:53-58.
145. Strano MS, Moore VC, et al. The role of surfactant adsorption during ultrasonication in the dispersion of single-walled carbon nanotubes. *J Nanosci Nanotechnol.* 2003;3:1-2.
146. Moore VC, Strano MS, et al. Individually suspended single-walled carbon nanotubes in various surfactants. *Nano Lett.* 2003;3:1379-1382.
147. O'Connell MJ, Boul P, et al. Reversible water-solubilization of single-walled carbon nanotubes by polymer wrapping. *Chem Phys Lett.* 2001;342:265-271.
148. Kim B, Lee Y-H, et al. Enhanced colloidal properties of single-wall carbon nanotubes in α -terpineol and Texanol. *Colloid Surface A.* 2006;273:161-164.

149. Monthieux M, Smith B, et al. Sensitivity of single-wall carbon nanotubes to chemical processing: an electron microscopy investigation. *Carbon*. 2001;39:1251-1272.
150. Gong X, Liu J, et al. Surfactant-assisted processing of carbon nanotube/polymer composites. *Chem Mater*. 2000;12:1049-1052.
151. Cui S, Canet R, et al. Characterization of multiwall carbon nanotubes and influence of surfactant in the nanocomposite processing. *Carbon*. 2003;41:797-809.
152. Velasco-Santos C, Martinez-Hernandez A, et al. Dynamical–mechanical and thermal analysis of carbon nanotube–methyl-ethyl methacrylate nanocomposites. *J Phys D: Appl Phys*. 2003;36:1423.
153. Ke PC, Qiao R. Carbon nanomaterials in biological systems. *J Phys-Condens Mat*. 2007;19:373101.
154. Zheng M, Jagota A, et al. DNA-assisted dispersion and separation of carbon nanotubes. *Nat Mater*. 2003;2:338-342.
155. Georgakilas V, Tagmatarchis N, et al. Amino acid functionalisation of water soluble carbon nanotubes. *Chem Commun*. 2002:3050-3051.
156. Huang W, Taylor S, et al. Attaching proteins to carbon nanotubes via diimide-activated amidation. *Nano Lett*. 2002;2:311-314.
157. Wu Y, Hudson JS, et al. Coating single-walled carbon nanotubes with phospholipids. *J Phys Chem B*. 2006;110:2475-2478.
158. Bachilo SM, Strano MS, et al. Structure-assigned optical spectra of single-walled carbon nanotubes. *Science*. 2002;298:2361-2366.
159. Shirvani BB, Beheshtian J, et al. DFT study of $\text{NH}_3(\text{H}_2\text{O})_n$, $n=0,1,2,3$ complex adsorption on the (8,0) single-walled carbon nanotube. *Comput Mater Sci*. 2010;48:655-657.
160. Wang W, Bai X, et al. Low temperature growth of single-walled carbon nanotubes: Small diameters with narrow distribution. *Chem Phys Lett*. 2006;419:81-85.
161. Wallace EJ, Sansom MS. Carbon nanotube self-assembly with lipids and detergent: a molecular dynamics study. *Nanotechnology*. 2009;20:045101.
162. Schuster P, Zundel G, et al. Hydrogen bond; recent developments in theory and experiments. *Hydrogen bond; recent developments in theory and experiments*. Michigan: North-Holland 1976.
163. Gilli G, Gilli P. The nature of the hydrogen bond: outline of a comprehensive hydrogen bond theory: Oxford University Press; 2009.
164. Grabowski SJ. Hydrogen bonding: new insights. Netherlands: Springer; 2006.
165. Emsley J. Very strong hydrogen bonding. *Chem Soc Rev*. 1980;9:91-124.
166. Claesson PM, Kjellin M, et al. Short-range interactions between non-ionic surfactant layers. *Phys Chem Chem Phys*. 2006;8:5501-5514.

167. Larson J, McMahon T. Gas-phase bihalide and pseudobihalide ions. An ion cyclotron resonance determination of hydrogen bond energies in XHY-species (X, Y= F, Cl, Br, CN). *Inorg Chem.* 1984;23:2029-2033.
168. Fringant C, Tvaroska I, et al. Hydration of α -maltose and amylose: molecular modelling and thermodynamics study. *Carbohyd Res.* 1995;278:27-41.
169. French AD, Brady JW. Computer modeling of carbohydrate molecules. California: Am Chem Soc; 1990.
170. Brady J, Schmidt R. The role of hydrogen bonding in carbohydrates: molecular dynamics simulations of maltose in aqueous solution. *J Phys Chem A.* 1993;97:958-966.
171. Chong TT, Heidelberg T, et al. Computer modelling and simulation of thermotropic and lyotropic alkyl glycoside bilayers. *Liq Cryst.* 2007;34:267-281.
172. Ionescu AR, Bérces A, et al. Conformational pathways of saturated six-membered rings. A static and dynamical density functional study. *J Phys Chem A.* 2005;109:8096-8105.
173. Barnett CB, Naidoo KJ. Stereoelectronic and solvation effects determine hydroxymethyl conformational preferences in monosaccharides. *J Phys Chem B.* 2008;112:15450-15459.
174. Grabowski SJ. Ab initio calculations on conventional and unconventional hydrogen bonds study of the hydrogen bond strength. *J Phys Chem A.* 2001;105:10739-10746.
175. Gilli P, Bertolasi V, et al. Covalent nature of the strong homonuclear hydrogen bond. Study of the OH---O system by crystal structure correlation methods. *J Am Chem Soc.* 1994;116:909-915.
176. Cook AG, Wardell JL, et al. Non-symmetric liquid crystal dimer containing a carbohydrate-based moiety. *Carbohyd Res.* 2012;360:78-83.
177. Cook AG, Martinez-Felipe A, et al. New insights into the transitional behaviour of methyl-6-O-(n-dodecanoyl)- α -D-glucopyranoside using variable temperature FTIR spectroscopy and X-ray diffraction. *Liq Cryst.* 2013;40:1817-1827.
178. Hehre W, Lathan W, et al. Gaussian 70. Quantum Chemistry Program Exchange, Program. 1970.
179. Miertuš S, Scrocco E, et al. Electrostatic interaction of a solute with a continuum. A direct utilization of AB initio molecular potentials for the prevision of solvent effects. *Chem Phys.* 1981;55:117-129.
180. Tomasi J, Mennucci B, et al. Quantum mechanical continuum solvation models. *Chem Rev.* 2005;105:2999-3094.
181. Cossi M, Rega N, et al. Energies, structures, and electronic properties of molecules in solution with the C-PCM solvation model. *J Comput Chem.* 2003;24:669-681.
182. Pearson RG. Absolute electronegativity and hardness: application to inorganic chemistry. *Inorg Chem.* 1988;27:734-740.
183. Becke A, Matta CF, et al. The quantum theory of atoms in molecules: from solid state to DNA and drug design. New York: John Wiley & Sons; 2007.

184. Bader RF, Beddall P. Virial field relationship for molecular charge distributions and the spatial partitioning of molecular properties. *J Chem Phys.* 1972;56:3320-3329.
185. Bader RF. A bond path: a universal indicator of bonded interactions. *J Phys Chem A.* 1998;102:7314-7323.
186. Bader RF. *Atoms in molecules*: Wiley Online Library; 1990.
187. Reed AE, Curtiss LA, et al. Intermolecular interactions from a natural bond orbital, donor-acceptor viewpoint. *Chem Rev.* 1988;88:899-926.
188. Saha S, Dinadayalane TC, et al. Surface reactivity for chlorination on chlorinated (5, 5) armchair SWCNT: a computational approach. *J Phys Chem C.* 2012;116:22399-22410.
189. Bania KK, Deka RC. Experimental and theoretical evidence for encapsulation and tethering of 1, 10-phenanthroline complexes of Fe, Cu, and Zn in Zeolite-Y. *J Phys Chem C.* 2012;116:14295-14310.
190. Saikia N, Deka RC. Theoretical study on pyrazinamide adsorption onto covalently functionalized (5, 5) metallic single-walled carbon nanotube. *Chem Phys Lett.* 2010;500:65-70.
191. Bagaria P, Saha S, et al. A comprehensive decomposition analysis of stabilization energy (CDASE) and its application in locating the rate-determining step of multi-step reactions. *Phys Chem Chem Phys.* 2009;11:8306-8315.
192. Saha S, Dinadayalane TC, et al. Open and capped (5, 5) armchair SWCNTs: a comparative study of DFT-based reactivity descriptors. *Chem Phys Lett.* 2012;541:85-91.
193. Parr RG, Yang W. Density functional approach to the frontier-electron theory of chemical reactivity. *J Am Chem Soc.* 1984;106:4049-4050.
194. Yang W, Mortier WJ. The use of global and local molecular parameters for the analysis of the gas-phase basicity of amines. *J Am Chem Soc.* 1986;108:5708-5711.
195. Roy D, Parthasarathi R, et al. Careful scrutiny of the philicity concept. *J Phys Chem A.* 2006;110:1084-1093.
196. Morell C, Grand A, et al. New dual descriptor for chemical reactivity. *J Phys Chem A.* 2005;109:205-212.
197. Chattaraj PK, Giri S. Electrophilicity index within a conceptual DFT framework. *Annu Rep Pro Sec C Phys Chem.* 2009;105:13-39.
198. Becke AD. Density-functional thermochemistry. III. The role of exact exchange. *J Chem Phys.* 1993;98:5648-5652.
199. Lee C, Yang W, et al. Development of the colle-salvetti correlation-energy formula into a functional of the electron density. *Phys Rev B.* 1988;37:785.
200. Ditchfield R, Hehre WJ, et al. Self-consistent molecular-orbital methods. IX. An extended Gaussian-type basis for molecular-orbital studies of organic molecules. *J Chem Phys.* 1971;54:724-728.
201. Francl MM, Pietro WJ, et al. Self-consistent molecular orbital methods. XXIII. A polarization-type basis set for second-row elements. *J Chem Phys.* 1982;77:3654-3665.

202. Frisch MJ, Trucks GW, et al. Gaussian 09, Revision A. 02, . Wallingford, CT. 2009.
203. Dennington RD, Keith TA, et al. GaussView 5.0. 8. Gaussian Inc. 2008.
204. Popelier P, Aicken F, et al. Atoms in molecules. Chem Model- Appl Theor. 2000;1:143-198.
205. Reed AE, Weinstock RB, et al. Natural population analysis. J Chem Phys. 1985;83:735-746.
206. Mulliken R. Electronic population analysis on LCAO–MO molecular wave functions. II. Overlap populations, bond orders, and covalent bond energies. J Chem Phys. 1955;23:1841-1846.
207. Espinosa E, Souhassou M, et al. Topological analysis of the electron density in hydrogen bonds. Acta Crystallogr B. 1999;55:563-572.
208. Weinhold F. Nature of H-bonding in clusters, liquids, and enzymes: an ab initio, natural bond orbital perspective. J Mol Struct. 1997;398:181-197.
209. Saenger W, Jeffrey G. Hydrogen bonding in biological structures. Berlin: Springer-Verlag 1991.
210. Pimentel GC, McClellan AL. The hydrogen bond: Freeman; 1960.
211. Momany FA, Appell M, et al. B3LYP/6-311++G** geometry-optimization study of pentahydrates of α - and β -d-glucopyranose. Carbohyd Res. 2005;340:1638-1655.
212. Appell M, Willett JL, et al. DFT study of α - and β -d-mannopyranose at the B3LYP/6-311++G** level. Carbohyd Res. 2005;340:459-468.
213. Momany FA, Appell M, et al. DFT study of α - and β -d-galactopyranose at the B3LYP/6-311++G** level of theory. Carbohyd Res. 2006;341:525-537.
214. Moss G, Smith P, et al. Glossary of class names of organic compounds and reactivity intermediates based on structure (IUPAC Recommendations 1995). Pure Appl Chem. 1995;67:1307-1375.
215. Silvestrelli PL, Parrinello M. Water molecule dipole in the gas and in the liquid phase. Phys Rev Lett. 1999;82:3308.
216. Ortiz EdV, López MB. Density functional theory (DFT) applied to the study of the reactivity of platinum surface modified by nickel nanoparticles. Mec Comp. 2007;26:1692.
217. Pearson R. Chemical hardness–Applications from molecules to solids Weinheim: Wiley-VCH; 1997.
218. Parr RG, Zhou Z. Absolute hardness: unifying concept for identifying shells and subshells in nuclei, atoms, molecules, and metallic clusters. Acc Chem Res. 1993;26:256-258.
219. Pearson RG. Recent advances in the concept of hard and soft acids and bases. J Chem Edu. 1987;64:561.
220. Popelier P, Bader R. The existence of an intramolecular C-H-O hydrogen bond in creatine and carbamoyl sarcosine. Chem Phys Lett. 1992;189:542-548.

221. Popelier P. Characterization of a dihydrogen bond on the basis of the electron density. *J Phys Chem A*. 1998;102:1873-1878.
222. Nazari F, Doroodi Z. The substitution effect on heavy versions of cyclobutadiene. *Int J Quantum Chem*. 2010;110:1514-1528.
223. Popelier PL, Hall P. *Atoms in molecules: an introduction*. London: Prentice Hall 2000.
224. Henderson R. Wavelength considerations. *Institut für Umform-und Hochleistungs* Archived from the original on. 2007:10-28.
225. Amerov AK, Chen J, et al. Molar absorptivities of glucose and other biological molecules in aqueous solutions over the first overtone and combination regions of the near-infrared spectrum. *Appl Spect*. 2004;58:1195-1204.
226. Appell M, Strati G, et al. B3LYP/6-311++G** study of α - and β -d-glucopyranose and 1,5-anhydro-d-glucitol: 4C1 and 1C4 chairs, 3,OB and B3,O boats, and skew-boat conformations. *Carbohydr Res*. 2004;339:537-551.
227. Schnupf U, Willett JL, et al. DFT study of α - and β -d-allopyranose at the B3LYP/6-311++G** level of theory. *Carbohydr Res*. 2007;342:196-216.
228. Sebastian S, Sundaraganesan N. The spectroscopic (FT-IR, FT-IR gas phase, FT-Raman and UV) and NBO analysis of 4-Hydroxypiperidine by density functional method. *Spectrochem Acta A*. 2010;75:941-952.
229. Tan Y, Resasco DE. Dispersion of single-walled carbon nanotubes of narrow diameter distribution. *J Phys Chem B*. 2005;109:14454-14460.
230. Lüth H. *Surfaces and interfaces of solids*. Berlin: Springer; 1993.
231. Oura K, Lifshits V, et al. *Surface science: An introduction (Advanced texts in physics)*. Berlin: Springer; 2003.
232. Dinadayalane T, Kaczmarek A, et al. Chemisorption of hydrogen atoms on the sidewalls of armchair single-walled carbon nanotubes. *J Phys Chem C*. 2007;111:7376-7383.
233. Lu X, Chen Z, et al. Are stone-wales defect sites always more reactive than perfect sites in the sidewalls of single-wall carbon nanotubes? *J Am Chem Soc*. 2005;127:20-21.
234. Liu J, Rinzler AG, et al. Fullerene pipes. *Science*. 1998;280:1253-1256.
235. Richard C, Balavoine F, et al. Supramolecular self-assembly of lipid derivatives on carbon nanotubes. *Science*. 2003;300:775-778.

APPENDIX (A)

Gaussian 09

A.1 Setting up and Running a typical Gaussian Job

This part briefly discusses the setting up and the running Gaussian calculations with Gauss View. To build the desired molecule, the first step produces a Gaussian input file. The bond lengths, bond angles, and dihedral angles for the molecule will be drawn by Gauss View. Once this is completed, Gaussian 09 program will be opened and will choose the (.gjf) input file. Then, in the "Existing file job edit" panel which includes different part, the path of input file will be written in the %Section part. Next, in the Root section, method, the basis set, and job type is presented. Although, the high method and basis set gives accurate calculation, it requires an extended period of time to complete. We are aware of the fact that the charge and spin fields specify the molecule's charge and spin multiplicity, so, the values for these fields, based on the molecular structure, will be selected by GV. If it needs modification, it will be performed at this stage. After finishing the job, in the bottom output file (.out), the "normal termination of Gaussian" must be checked.

A.2 Preparation of the input file in Gaussian 09 in Windows and Linux environment

"Input file for beta-mannose"

```
%chk=D:\g09\temp\Scratch\A\manose1.chk
%nprocshared=4
%mem=500MB
# b3lyp/6-31g fopt freq
```

Title Card Required

```
0 1
C          5.24222138    -2.93231900    2.30906316
C          3.92378941    -2.43664144    2.92817954
C          4.91974894    -3.71317178    1.03313544
C          4.16539161    -2.78071373    0.08385636
O          3.23412860    -1.58413841    1.99486500
C          2.88618545    -2.28970798    0.78987884
O          5.92798328    -3.77842563    3.23710352
H          5.86419258    -2.09260736    2.06729103
H          3.30199498    -3.27592402    3.16669008
C          4.23551569    -1.64179641    4.20981695
O          6.12992508    -4.16580550    0.41739141
```

H	4.30686994	-4.55580173	1.27167774
H	3.90715080	-3.30829043	-0.81002145
O	4.99022634	-1.65913810	-0.24739955
H	2.27046775	-3.12929094	1.03518664
O	2.17351488	-1.41098371	-0.08435469
C	0.98078000	-0.95504440	0.56139315
C	0.21274119	-0.01885615	-0.38899474
C	-1.07573847	0.47212763	0.29713178
C	-1.83853193	1.40120358	-0.66459036
C	-3.13339688	1.89502417	0.00812731
C	-3.89079471	2.81786254	-0.96582968
C	-5.19024749	3.30848942	-0.30319989
C	-5.94713186	4.22866358	-1.27980340
O	5.06233928	-0.52160532	3.88470186
H	6.12677983	-3.28428836	4.03719882
H	4.74887407	-2.27468377	4.90427068
H	3.32338153	-1.29687047	4.64891569
H	5.92008873	-4.65100498	-0.38526083
H	1.23605876	-0.42455498	1.45390962
H	0.36740133	-1.79569255	0.80984185
H	-0.04226773	-0.54905275	-1.28276548
H	0.82876695	0.82021058	-0.63453502
H	-0.82413104	1.00647178	1.18999133
H	-1.69043680	-0.36738858	0.54696118
H	-2.08628069	0.86383256	-1.55634009
H	-1.22195363	2.23951054	-0.91219365
H	-2.89148563	2.43467209	0.89914781
H	-3.74935121	1.05603038	0.25451481
H	-4.12630404	2.27471800	-1.85725124
H	-3.27777570	3.65979905	-1.21258103
H	-4.95244304	3.85330514	0.58677275
H	-5.80505714	2.46943077	-0.05344128
H	-6.18450921	3.68798018	-2.17206868
H	-5.33206679	5.06785527	-1.52450988
H	-6.85102188	4.57013519	-0.82002654
H	5.87981335	-0.83158364	3.48728677
H	4.51160008	-1.07064289	-0.83704996

APPENDIX (B)

AIM SOFTWARE

"Input file for beta-mannose"

```
%chk=D:\g09\temp\Scratch\A\manoselaim.chk  
%nprocshared=4  
%mem=500MB  
# b3lyp/6-31g out=wfn
```

Title Card Required

```
0 1  
C -4.59091400 0.23364900 0.07833100  
C -3.62926800 1.21755900 -0.58439000  
C -4.32093700 -1.20354700 -0.37410700  
C -2.86226800 -1.60197600 -0.15929600  
O -2.24759800 0.79756700 -0.28327400  
C -1.90074700 -0.54580400 -0.71143900  
O -5.93023500 0.62173700 -0.31893800  
H -4.46466300 0.30601900 1.16453900  
H -3.79381400 1.21829500 -1.67228900  
C -3.73186200 2.63562600 -0.03491100  
O -5.20934900 -2.11087500 0.33237400  
H -4.58678200 -1.29256800 -1.43287800  
H -2.64918000 -2.56023000 -0.65143200  
O -2.70097800 -1.73987700 1.27715100  
H -1.88999900 -0.56931800 -1.81466900  
O -0.62466500 -0.86145900 -0.17955300  
C 0.49980100 -0.03933700 -0.65334700  
C 1.77418000 -0.62008500 -0.05627800  
C 3.02930200 0.16745900 -0.47709000  
C 4.32767900 -0.41402800 0.11142400  
C 5.58668600 0.37136300 -0.29782000  
C 6.88705300 -0.21359600 0.28208100  
C 8.14679300 0.57381600 -0.12300900  
C 9.44079900 -0.01895900 0.45707600  
O -3.38007500 2.67236200 1.37134200  
H -6.55186900 -0.06033400 0.01077700  
H -4.76303000 2.98224900 -0.10813600  
H -3.07976400 3.29875500 -0.61980400  
H -4.79821200 -2.29232700 1.20720200  
H 0.33818100 0.99690700 -0.34029100  
H 0.52043300 -0.07414500 -1.75255800  
H 1.86675700 -1.66904800 -0.36679900  
H 1.68296900 -0.61923000 1.03799400  
H 2.92689900 1.21687900 -0.16197200  
H 3.10508200 0.18019400 -1.57510700  
H 4.43276000 -1.46198200 -0.20813300  
H 4.25167400 -0.43277500 1.20919000  
H 5.48298700 1.41808500 0.02709100
```

H	5.65844700	0.39597500	-1.39614500
H	6.99344000	-1.25941400	-0.04534900
H	6.81563100	-0.24155100	1.38038100
H	8.04097500	1.61809000	0.20628500
H	8.21620900	0.60379200	-1.22050900
H	9.58880000	-1.05149600	0.11629000
H	9.41130400	-0.03227000	1.55390900
H	10.31887500	0.56253100	0.15322500
H	-2.52245600	2.20722300	1.47307400
H	-1.74623300	-1.67677400	1.48995100

D:\g09\temp\Scratch\A\manose1aim.wfn

APPENDIX (C)

NBO ANALYSIS

"Output file for beta-mannose"

Second Order Perturbation Theory Analysis of Fock Matrix in NBO Basis

Threshold for printing: 0.50 kcal/mol

Donor NBO (i)	Acceptor NBO (j)	E(2)	E(j)-E(i)	F(i,j)	kcal/mol	a.u.	a.u.
=====							
within unit 1							
1. BD (1)C 1 - C 2	/ 90. RY*(2)C 3	0.53	1.57	0.026			
1. BD (1)C 1 - C 2	/ 97. RY*(1)O 5	0.67	1.82	0.031			
1. BD (1)C 1 - C 2	/106. RY*(2)O 7	0.67	1.92	0.032			
1. BD (1)C 1 - C 2	/111. RY*(1)C 10	1.39	1.37	0.039			
1. BD (1)C 1 - C 2	/190. BD*(1)C 1 - C 3	0.67	0.99	0.023			
1. BD (1)C 1 - C 2	/192. BD*(1)C 1 - H 8	0.74	1.09	0.025			
1. BD (1)C 1 - C 2	/194. BD*(1)C 2 - H 9	0.61	1.06	0.023			
1. BD (1)C 1 - C 2	/195. BD*(1)C 2 - C 10	0.98	1.00	0.028			
1. BD (1)C 1 - C 2	/197. BD*(1)C 3 - O 11	2.67	0.87	0.043			
1. BD (1)C 1 - C 2	/205. BD*(1)O 7 - H 26	1.71	1.05	0.038			
1. BD (1)C 1 - C 2	/208. BD*(1)C 10 - H 28	1.22	1.07	0.032			
2. BD (1)C 1 - C 3	/ 86. RY*(2)C 2	0.97	1.61	0.035			
2. BD (1)C 1 - C 3	/ 94. RY*(2)C 4	1.31	1.57	0.041			
2. BD (1)C 1 - C 3	/105. RY*(1)O 7	0.54	1.69	0.027			
2. BD (1)C 1 - C 3	/115. RY*(1)O 11	0.78	1.68	0.032			
2. BD (1)C 1 - C 3	/189. BD*(1)C 1 - C 2	1.03	0.99	0.029			
2. BD (1)C 1 - C 3	/192. BD*(1)C 1 - H 8	0.65	1.08	0.024			
2. BD (1)C 1 - C 3	/195. BD*(1)C 2 - C 10	2.09	0.99	0.041			
2. BD (1)C 1 - C 3	/196. BD*(1)C 3 - C 4	0.84	0.98	0.026			
2. BD (1)C 1 - C 3	/198. BD*(1)C 3 - H 12	0.77	1.07	0.026			
2. BD (1)C 1 - C 3	/200. BD*(1)C 4 - H 13	1.64	1.06	0.037			
3. BD (1)C 1 - O 7	/193. BD*(1)C 2 - O 5	2.35	1.01	0.044			
3. BD (1)C 1 - O 7	/196. BD*(1)C 3 - C 4	1.72	1.14	0.040			
4. BD (1)C 1 - H 8	/ 85. RY*(1)C 2	0.81	1.30	0.029			
4. BD (1)C 1 - H 8	/ 90. RY*(2)C 3	0.64	1.45	0.027			
4. BD (1)C 1 - H 8	/105. RY*(1)O 7	0.60	1.57	0.028			
4. BD (1)C 1 - H 8	/189. BD*(1)C 1 - C 2	0.55	0.87	0.020			
4. BD (1)C 1 - H 8	/194. BD*(1)C 2 - H 9	2.79	0.93	0.046			
4. BD (1)C 1 - H 8	/197. BD*(1)C 3 - O 11	0.84	0.74	0.022			
4. BD (1)C 1 - H 8	/198. BD*(1)C 3 - H 12	2.50	0.95	0.043			
5. BD (1)C 2 - O 5	/101. RY*(1)C 6	1.42	1.57	0.042			
5. BD (1)C 2 - O 5	/112. RY*(2)C 10	0.54	1.51	0.026			
5. BD (1)C 2 - O 5	/191. BD*(1)C 1 - O 7	2.03	1.03	0.041			
5. BD (1)C 2 - O 5	/204. BD*(1)C 6 - O 16	2.05	1.04	0.041			
5. BD (1)C 2 - O 5	/207. BD*(1)C 10 - H 27	1.24	1.25	0.035			
6. BD (1)C 2 - H 9	/ 82. RY*(2)C 1	0.88	1.51	0.033			
6. BD (1)C 2 - H 9	/191. BD*(1)C 1 - O 7	0.51	0.77	0.018			
6. BD (1)C 2 - H 9	/192. BD*(1)C 1 - H 8	2.38	0.98	0.043			
6. BD (1)C 2 - H 9	/206. BD*(1)C 10 - O 25	3.74	0.78	0.048			

7. BD (1)C 2 - C 10	/ 82. RY*(2)C 1	0.78	1.61	0.032
7. BD (1)C 2 - C 10	/ 83. RY*(3)C 1	0.51	1.40	0.024
7. BD (1)C 2 - C 10	/ 98. RY*(2)O 5	1.14	1.82	0.041
7. BD (1)C 2 - C 10	/189. BD*(1)C 1 - C 2	1.22	0.99	0.031
7. BD (1)C 2 - C 10	/190. BD*(1)C 1 - C 3	1.99	0.99	0.040
7. BD (1)C 2 - C 10	/194. BD*(1)C 2 - H 9	0.83	1.05	0.027
7. BD (1)C 2 - C 10	/202. BD*(1)O 5 - C 6	2.48	0.85	0.041
7. BD (1)C 2 - C 10	/207. BD*(1)C 10 - H 27	0.64	1.10	0.024
8. BD (1)C 3 - C 4	/ 82. RY*(2)C 1	1.42	1.62	0.043
8. BD (1)C 3 - C 4	/102. RY*(2)C 6	0.53	1.36	0.024
8. BD (1)C 3 - C 4	/190. BD*(1)C 1 - C 3	0.73	1.00	0.024
8. BD (1)C 3 - C 4	/191. BD*(1)C 1 - O 7	2.32	0.89	0.040
8. BD (1)C 3 - C 4	/198. BD*(1)C 3 - H 12	0.77	1.08	0.026
8. BD (1)C 3 - C 4	/199. BD*(1)C 4 - C 6	0.75	0.98	0.024
8. BD (1)C 3 - C 4	/200. BD*(1)C 4 - H 13	0.86	1.08	0.027
8. BD (1)C 3 - C 4	/204. BD*(1)C 6 - O 16	2.13	0.89	0.039
8. BD (1)C 3 - C 4	/210. BD*(1)O 14 - H 48	1.68	1.05	0.038
9. BD (1)C 3 - O 11	/189. BD*(1)C 1 - C 2	1.63	1.16	0.039
9. BD (1)C 3 - O 11	/199. BD*(1)C 4 - C 6	1.56	1.13	0.038
10. BD (1)C 3 - H 12	/ 81. RY*(1)C 1	0.78	1.33	0.029
10. BD (1)C 3 - H 12	/116. RY*(2)O 11	0.54	1.70	0.027
10. BD (1)C 3 - H 12	/191. BD*(1)C 1 - O 7	0.92	0.77	0.024
10. BD (1)C 3 - H 12	/192. BD*(1)C 1 - H 8	2.52	0.98	0.044
10. BD (1)C 3 - H 12	/201. BD*(1)C 4 - O 14	3.82	0.74	0.048
10. BD (1)C 3 - H 12	/209. BD*(1)O 11 - H 29	2.22	0.93	0.041
11. BD (1)C 4 - C 6	/ 90. RY*(2)C 3	0.54	1.60	0.026
11. BD (1)C 4 - C 6	/ 91. RY*(3)C 3	0.55	1.37	0.025
11. BD (1)C 4 - C 6	/ 97. RY*(1)O 5	0.82	1.85	0.035
11. BD (1)C 4 - C 6	/127. RY*(2)O 16	0.75	1.88	0.034
11. BD (1)C 4 - C 6	/196. BD*(1)C 3 - C 4	0.86	1.01	0.026
11. BD (1)C 4 - C 6	/197. BD*(1)C 3 - O 11	2.66	0.89	0.044
11. BD (1)C 4 - C 6	/200. BD*(1)C 4 - H 13	0.64	1.09	0.024
11. BD (1)C 4 - C 6	/203. BD*(1)C 6 - H 15	0.61	1.06	0.023
11. BD (1)C 4 - C 6	/211. BD*(1)O 16 - C 17	3.00	0.87	0.046
12. BD (1)C 4 - H 13	/103. RY*(3)C 6	0.56	1.49	0.026
12. BD (1)C 4 - H 13	/190. BD*(1)C 1 - C 3	3.05	0.89	0.047
12. BD (1)C 4 - H 13	/196. BD*(1)C 3 - C 4	0.57	0.88	0.020
12. BD (1)C 4 - H 13	/202. BD*(1)O 5 - C 6	4.66	0.75	0.053
13. BD (1)C 4 - O 14	/198. BD*(1)C 3 - H 12	1.41	1.25	0.038
13. BD (1)C 4 - O 14	/203. BD*(1)C 6 - H 15	1.16	1.21	0.034
14. BD (1)O 5 - C 6	/ 85. RY*(1)C 2	1.05	1.61	0.037
14. BD (1)O 5 - C 6	/ 93. RY*(1)C 4	0.53	1.56	0.026
14. BD (1)O 5 - C 6	/195. BD*(1)C 2 - C 10	1.01	1.18	0.031
14. BD (1)O 5 - C 6	/200. BD*(1)C 4 - H 13	1.06	1.25	0.033
15. BD (1)C 6 - H 15	/ 94. RY*(2)C 4	0.67	1.50	0.028
15. BD (1)C 6 - H 15	/ 97. RY*(1)O 5	0.54	1.75	0.028
15. BD (1)C 6 - H 15	/126. RY*(1)O 16	0.52	1.73	0.027
15. BD (1)C 6 - H 15	/201. BD*(1)C 4 - O 14	3.87	0.78	0.049
16. BD (1)C 6 - O 16	/ 95. RY*(3)C 4	0.52	1.54	0.025
16. BD (1)C 6 - O 16	/135. RY*(2)C 18	0.51	1.55	0.025
16. BD (1)C 6 - O 16	/193. BD*(1)C 2 - O 5	1.40	1.07	0.035
16. BD (1)C 6 - O 16	/196. BD*(1)C 3 - C 4	1.56	1.21	0.039
16. BD (1)C 6 - O 16	/212. BD*(1)C 17 - C 18	0.85	1.23	0.029
17. BD (1)O 7 - H 26	/ 81. RY*(1)C 1	1.04	1.51	0.035
17. BD (1)O 7 - H 26	/189. BD*(1)C 1 - C 2	2.58	1.06	0.047
18. BD (1)C 10 - O 25	/194. BD*(1)C 2 - H 9	1.41	1.20	0.037
19. BD (1)C 10 - H 27	/163. RY*(2)O 25	0.53	1.64	0.026
19. BD (1)C 10 - H 27	/193. BD*(1)C 2 - O 5	4.39	0.72	0.050
19. BD (1)C 10 - H 27	/236. BD*(1)O 25 - H 47	2.39	0.93	0.042
20. BD (1)C 10 - H 28	/162. RY*(1)O 25	0.60	1.57	0.028
20. BD (1)C 10 - H 28	/189. BD*(1)C 1 - C 2	3.46	0.87	0.049
20. BD (1)C 10 - H 28	/193. BD*(1)C 2 - O 5	0.51	0.73	0.017
21. BD (1)O 11 - H 29	/ 89. RY*(1)C 3	2.04	1.45	0.049

21. BD (1) O 11 - H 29	/198. BD*(1) C 3 - H 12	1.94	1.15	0.042
22. BD (1) O 14 - H 48	/93. RY*(1) C 4	0.93	1.48	0.033
22. BD (1) O 14 - H 48	/196. BD*(1) C 3 - C 4	2.01	1.08	0.042
23. BD (1) O 16 - C 17	/102. RY*(2) C 6	0.77	1.50	0.030
23. BD (1) O 16 - C 17	/199. BD*(1) C 4 - C 6	1.52	1.12	0.037
23. BD (1) O 16 - C 17	/215. BD*(1) C 18 - C 19	1.76	1.15	0.040
24. BD (1) C 17 - C 18	/139. RY*(2) C 19	0.64	1.36	0.026
24. BD (1) C 17 - C 18	/140. RY*(3) C 19	0.51	1.40	0.024
24. BD (1) C 17 - C 18	/204. BD*(1) C 6 - O 16	2.12	0.87	0.039
24. BD (1) C 17 - C 18	/213. BD*(1) C 17 - H 30	0.63	1.06	0.023
24. BD (1) C 17 - C 18	/214. BD*(1) C 17 - H 31	0.62	1.04	0.023
24. BD (1) C 17 - C 18	/215. BD*(1) C 18 - C 19	0.67	0.99	0.023
24. BD (1) C 17 - C 18	/216. BD*(1) C 18 - H 32	0.64	1.06	0.023
24. BD (1) C 17 - C 18	/217. BD*(1) C 18 - H 33	0.64	1.06	0.023
24. BD (1) C 17 - C 18	/218. BD*(1) C 19 - C 20	1.96	1.00	0.040
25. BD (1) C 17 - H 30	/126. RY*(1) O 16	0.54	1.70	0.027
25. BD (1) C 17 - H 30	/134. RY*(1) C 18	0.85	1.36	0.030
25. BD (1) C 17 - H 30	/216. BD*(1) C 18 - H 32	2.59	0.96	0.045
26. BD (1) C 17 - H 31	/134. RY*(1) C 18	0.80	1.36	0.030
26. BD (1) C 17 - H 31	/217. BD*(1) C 18 - H 33	2.58	0.97	0.045
27. BD (1) C 18 - C 19	/144. RY*(3) C 20	0.61	1.36	0.026
27. BD (1) C 18 - C 19	/211. BD*(1) O 16 - C 17	2.85	0.81	0.043
27. BD (1) C 18 - C 19	/212. BD*(1) C 17 - C 18	0.52	0.97	0.020
27. BD (1) C 18 - C 19	/216. BD*(1) C 18 - H 32	0.67	1.03	0.024
27. BD (1) C 18 - C 19	/217. BD*(1) C 18 - H 33	0.68	1.03	0.024
27. BD (1) C 18 - C 19	/218. BD*(1) C 19 - C 20	0.68	0.97	0.023
27. BD (1) C 18 - C 19	/219. BD*(1) C 19 - H 34	0.56	1.02	0.021
27. BD (1) C 18 - C 19	/220. BD*(1) C 19 - H 35	0.56	1.02	0.021
27. BD (1) C 18 - C 19	/221. BD*(1) C 20 - C 21	1.91	0.98	0.039
28. BD (1) C 18 - H 32	/138. RY*(1) C 19	0.66	1.35	0.027
28. BD (1) C 18 - H 32	/211. BD*(1) O 16 - C 17	0.60	0.71	0.018
28. BD (1) C 18 - H 32	/213. BD*(1) C 17 - H 30	2.72	0.94	0.045
28. BD (1) C 18 - H 32	/219. BD*(1) C 19 - H 34	2.64	0.93	0.044
29. BD (1) C 18 - H 33	/138. RY*(1) C 19	0.68	1.35	0.027
29. BD (1) C 18 - H 33	/211. BD*(1) O 16 - C 17	0.63	0.71	0.019
29. BD (1) C 18 - H 33	/214. BD*(1) C 17 - H 31	2.84	0.91	0.045
29. BD (1) C 18 - H 33	/220. BD*(1) C 19 - H 35	2.67	0.93	0.044
30. BD (1) C 19 - C 20	/136. RY*(3) C 18	0.81	1.30	0.029
30. BD (1) C 19 - C 20	/148. RY*(3) C 21	0.58	1.37	0.025
30. BD (1) C 19 - C 20	/212. BD*(1) C 17 - C 18	1.97	0.96	0.039
30. BD (1) C 19 - C 20	/215. BD*(1) C 18 - C 19	0.80	0.96	0.025
30. BD (1) C 19 - C 20	/219. BD*(1) C 19 - H 34	0.68	1.02	0.024
30. BD (1) C 19 - C 20	/220. BD*(1) C 19 - H 35	0.68	1.02	0.024
30. BD (1) C 19 - C 20	/221. BD*(1) C 20 - C 21	0.70	0.97	0.023
30. BD (1) C 19 - C 20	/222. BD*(1) C 20 - H 36	0.60	1.02	0.022
30. BD (1) C 19 - C 20	/223. BD*(1) C 20 - H 37	0.60	1.02	0.022
30. BD (1) C 19 - C 20	/224. BD*(1) C 21 - C 22	1.90	0.97	0.038
31. BD (1) C 19 - H 34	/134. RY*(1) C 18	0.64	1.33	0.026
31. BD (1) C 19 - H 34	/142. RY*(1) C 20	0.71	1.34	0.028
31. BD (1) C 19 - H 34	/216. BD*(1) C 18 - H 32	2.66	0.93	0.044
31. BD (1) C 19 - H 34	/222. BD*(1) C 20 - H 36	2.63	0.93	0.044
32. BD (1) C 19 - H 35	/134. RY*(1) C 18	0.73	1.33	0.028
32. BD (1) C 19 - H 35	/142. RY*(1) C 20	0.73	1.34	0.028
32. BD (1) C 19 - H 35	/217. BD*(1) C 18 - H 33	2.64	0.93	0.044
32. BD (1) C 19 - H 35	/223. BD*(1) C 20 - H 37	2.63	0.93	0.044
33. BD (1) C 20 - C 21	/140. RY*(3) C 19	0.72	1.36	0.028
33. BD (1) C 20 - C 21	/152. RY*(3) C 22	0.68	1.39	0.028
33. BD (1) C 20 - C 21	/215. BD*(1) C 18 - C 19	1.97	0.95	0.039
33. BD (1) C 20 - C 21	/218. BD*(1) C 19 - C 20	0.72	0.96	0.024
33. BD (1) C 20 - C 21	/222. BD*(1) C 20 - H 36	0.65	1.02	0.023
33. BD (1) C 20 - C 21	/223. BD*(1) C 20 - H 37	0.66	1.02	0.023
33. BD (1) C 20 - C 21	/224. BD*(1) C 21 - C 22	0.73	0.97	0.024
33. BD (1) C 20 - C 21	/225. BD*(1) C 21 - H 38	0.62	1.02	0.022

33. BD (1) C 20 - C 21	/226. BD*(1) C 21 - H 39	0.62	1.02	0.022
33. BD (1) C 20 - C 21	/227. BD*(1) C 22 - C 23	1.92	0.97	0.038
34. BD (1) C 20 - H 36	/138. RY*(1) C 19	0.66	1.34	0.027
34. BD (1) C 20 - H 36	/146. RY*(1) C 21	0.68	1.34	0.027
34. BD (1) C 20 - H 36	/219. BD*(1) C 19 - H 34	2.70	0.92	0.044
34. BD (1) C 20 - H 36	/225. BD*(1) C 21 - H 38	2.66	0.92	0.044
35. BD (1) C 20 - H 37	/138. RY*(1) C 19	0.64	1.34	0.026
35. BD (1) C 20 - H 37	/146. RY*(1) C 21	0.70	1.34	0.027
35. BD (1) C 20 - H 37	/220. BD*(1) C 19 - H 35	2.69	0.92	0.044
35. BD (1) C 20 - H 37	/226. BD*(1) C 21 - H 39	2.67	0.92	0.044
36. BD (1) C 21 - C 22	/144. RY*(3) C 20	0.63	1.35	0.026
36. BD (1) C 21 - C 22	/155. RY*(2) C 23	0.79	1.34	0.029
36. BD (1) C 21 - C 22	/218. BD*(1) C 19 - C 20	2.00	0.96	0.039
36. BD (1) C 21 - C 22	/221. BD*(1) C 20 - C 21	0.74	0.96	0.024
36. BD (1) C 21 - C 22	/225. BD*(1) C 21 - H 38	0.65	1.02	0.023
36. BD (1) C 21 - C 22	/226. BD*(1) C 21 - H 39	0.65	1.02	0.023
36. BD (1) C 21 - C 22	/227. BD*(1) C 22 - C 23	0.69	0.96	0.023
36. BD (1) C 21 - C 22	/228. BD*(1) C 22 - H 40	0.61	1.02	0.022
36. BD (1) C 21 - C 22	/229. BD*(1) C 22 - H 41	0.61	1.02	0.022
36. BD (1) C 21 - C 22	/230. BD*(1) C 23 - C 24	1.94	0.96	0.039
37. BD (1) C 21 - H 38	/142. RY*(1) C 20	0.67	1.33	0.027
37. BD (1) C 21 - H 38	/150. RY*(1) C 22	0.67	1.33	0.027
37. BD (1) C 21 - H 38	/222. BD*(1) C 20 - H 36	2.70	0.92	0.045
37. BD (1) C 21 - H 38	/228. BD*(1) C 22 - H 40	2.68	0.92	0.044
38. BD (1) C 21 - H 39	/142. RY*(1) C 20	0.66	1.33	0.027
38. BD (1) C 21 - H 39	/150. RY*(1) C 22	0.68	1.33	0.027
38. BD (1) C 21 - H 39	/223. BD*(1) C 20 - H 37	2.69	0.92	0.044
38. BD (1) C 21 - H 39	/229. BD*(1) C 22 - H 41	2.68	0.92	0.044
39. BD (1) C 22 - C 23	/148. RY*(3) C 21	0.66	1.36	0.027
39. BD (1) C 22 - C 23	/158. RY*(1) C 24	0.90	1.31	0.031
39. BD (1) C 22 - C 23	/221. BD*(1) C 20 - C 21	1.97	0.96	0.039
39. BD (1) C 22 - C 23	/224. BD*(1) C 21 - C 22	0.74	0.96	0.024
39. BD (1) C 22 - C 23	/228. BD*(1) C 22 - H 40	0.63	1.02	0.023
39. BD (1) C 22 - C 23	/229. BD*(1) C 22 - H 41	0.63	1.02	0.023
39. BD (1) C 22 - C 23	/230. BD*(1) C 23 - C 24	0.60	0.96	0.021
39. BD (1) C 22 - C 23	/231. BD*(1) C 23 - H 42	0.59	1.02	0.022
39. BD (1) C 22 - C 23	/232. BD*(1) C 23 - H 43	0.58	1.02	0.022
39. BD (1) C 22 - C 23	/235. BD*(1) C 24 - H 46	1.48	1.03	0.035
40. BD (1) C 22 - H 40	/146. RY*(1) C 21	0.66	1.33	0.027
40. BD (1) C 22 - H 40	/154. RY*(1) C 23	0.61	1.28	0.025
40. BD (1) C 22 - H 40	/225. BD*(1) C 21 - H 38	2.70	0.92	0.045
40. BD (1) C 22 - H 40	/231. BD*(1) C 23 - H 42	2.64	0.93	0.044
41. BD (1) C 22 - H 41	/146. RY*(1) C 21	0.65	1.33	0.026
41. BD (1) C 22 - H 41	/154. RY*(1) C 23	0.61	1.28	0.025
41. BD (1) C 22 - H 41	/226. BD*(1) C 21 - H 39	2.70	0.92	0.045
41. BD (1) C 22 - H 41	/232. BD*(1) C 23 - H 43	2.65	0.93	0.044
42. BD (1) C 23 - C 24	/152. RY*(3) C 22	0.54	1.38	0.024
42. BD (1) C 23 - C 24	/224. BD*(1) C 21 - C 22	2.10	0.97	0.040
42. BD (1) C 23 - C 24	/227. BD*(1) C 22 - C 23	0.72	0.96	0.024
42. BD (1) C 23 - C 24	/231. BD*(1) C 23 - H 42	0.60	1.03	0.022
42. BD (1) C 23 - C 24	/232. BD*(1) C 23 - H 43	0.60	1.03	0.022
42. BD (1) C 23 - C 24	/233. BD*(1) C 24 - H 44	0.57	1.03	0.022
42. BD (1) C 23 - C 24	/234. BD*(1) C 24 - H 45	0.57	1.03	0.022
42. BD (1) C 23 - C 24	/235. BD*(1) C 24 - H 46	0.63	1.03	0.023
43. BD (1) C 23 - H 42	/150. RY*(1) C 22	0.60	1.32	0.025
43. BD (1) C 23 - H 42	/159. RY*(2) C 24	0.50	1.13	0.021
43. BD (1) C 23 - H 42	/228. BD*(1) C 22 - H 40	2.75	0.92	0.045
43. BD (1) C 23 - H 42	/233. BD*(1) C 24 - H 44	2.74	0.93	0.045
44. BD (1) C 23 - H 43	/150. RY*(1) C 22	0.59	1.32	0.025
44. BD (1) C 23 - H 43	/159. RY*(2) C 24	0.51	1.13	0.021
44. BD (1) C 23 - H 43	/229. BD*(1) C 22 - H 41	2.75	0.92	0.045
44. BD (1) C 23 - H 43	/234. BD*(1) C 24 - H 45	2.74	0.93	0.045
45. BD (1) C 24 - H 44	/154. RY*(1) C 23	0.53	1.29	0.023

45. BD (1) C 24 - H 44	/231. BD*(1) C 23 - H 42	2.60	0.93	0.044
46. BD (1) C 24 - H 45	/154. RY*(1) C 23	0.52	1.29	0.023
46. BD (1) C 24 - H 45	/232. BD*(1) C 23 - H 43	2.60	0.93	0.044
47. BD (1) C 24 - H 46	/227. BD*(1) C 22 - C 23	3.10	0.87	0.046
48. BD (1) O 25 - H 47	/111. RY*(1) C 10	1.60	1.43	0.043
48. BD (1) O 25 - H 47	/207. BD*(1) C 10 - H 27	2.01	1.17	0.043
49. CR (1) C 1	/ 87. RY*(3) C 2	1.11	10.85	0.098
49. CR (1) C 1	/ 91. RY*(3) C 3	1.78	10.82	0.124
49. CR (1) C 1	/109. RY*(1) H 8	0.68	10.77	0.077
49. CR (1) C 1	/191. BD*(1) C 1 - O 7	1.26	10.35	0.103
50. CR (1) C 2	/ 82. RY*(2) C 1	0.55	11.11	0.070
50. CR (1) C 2	/ 83. RY*(3) C 1	1.04	10.90	0.095
50. CR (1) C 2	/110. RY*(1) H 9	0.57	10.75	0.070
50. CR (1) C 2	/112. RY*(2) C 10	0.64	10.85	0.075
50. CR (1) C 2	/113. RY*(3) C 10	0.59	10.81	0.072
50. CR (1) C 2	/193. BD*(1) C 2 - O5	1.25	10.34	0.102
50. CR (1) C 2	/202. BD*(1) O 5 - C 6	0.61	10.35	0.072
51. CR (1) C 3	/ 81. RY*(1) C 1	0.79	10.93	0.083
51. CR (1) C 3	/ 84. RY*(4) C 1	0.72	11.39	0.081
51. CR (1) C 3	/ 95. RY*(3) C 4	1.34	10.81	0.107
51. CR (1) C 3	/119. RY*(1) H 12	0.59	10.74	0.071
51. CR (1) C 3	/197. BD*(1) C 3 - O 11	1.20	10.35	0.100
52. CR (1) C 4	/ 89. RY*(1) C 3	0.64	10.87	0.075
52. CR (1) C 4	/ 91. RY*(3) C 3	0.73	10.84	0.079
52. CR (1) C 4	/104. RY*(4) C 6	1.23	11.22	0.105
52. CR (1) C 4	/120. RY*(1) H 13	0.58	10.73	0.070
52. CR (1) C 4	/201. BD*(1) C 4 - O 14	1.17	10.35	0.099
53. CR (1) O 5	/ 85. RY*(1) C 2	1.67	19.75	0.162
53. CR (1) O 5	/101. RY*(1) C 6	1.90	19.75	0.173
54. CR (1) C 6	/ 93. RY*(1) C 4	0.89	10.95	0.088
54. CR (1) C 6	/ 94. RY*(2) C 4	0.81	11.14	0.085
54. CR (1) C 6	/125. RY*(1) H 15	0.55	10.81	0.069
54. CR (1) C 6	/193. BD*(1) C 2 - O 5	0.70	10.41	0.077
54. CR (1) C 6	/199. BD*(1) C 4 - C 6	0.69	10.53	0.077
54. CR (1) C 6	/202. BD*(1) O 5 - C 6	0.75	10.42	0.080
54. CR (1) C 6	/211. BD*(1) O 16 - C 17	0.79	10.41	0.082
55. CR (1) O 7	/ 81. RY*(1) C 1	1.44	19.75	0.151
56. CR (1) C 10	/ 86. RY*(2) C 2	0.52	11.10	0.068
56. CR (1) C 10	/ 87. RY*(3) C 2	0.56	10.85	0.069
56. CR (1) C 10	/ 88. RY*(4) C 2	0.76	11.37	0.083
56. CR (1) C 10	/167. RY*(1) H 27	0.70	10.75	0.078
56. CR (1) C 10	/168. RY*(1) H 28	0.54	10.74	0.068
56. CR (1) C 10	/206. BD*(1) C 10 - O 25	1.21	10.36	0.100
57. CR (1) O 11	/ 89. RY*(1) C 3	1.84	19.69	0.170
58. CR (1) O 14	/ 93. RY*(1) C 4	1.46	19.71	0.152
58. CR (1) O 14	/ 95. RY*(3) C 4	0.67	19.65	0.103
59. CR (1) O 16	/102. RY*(2) C 6	2.22	19.69	0.187
59. CR (1) O 16	/130. RY*(1) C 17	1.33	19.76	0.145
60. CR (1) C 17	/135. RY*(2) C 18	0.84	10.82	0.085
60. CR (1) C 17	/137. RY*(4) C 18	0.52	11.45	0.069
60. CR (1) C 17	/170. RY*(1) H 30	0.64	10.77	0.074
60. CR (1) C 17	/171. RY*(1) H 31	0.55	10.77	0.069
60. CR (1) C 17	/204. BD*(1) C 6 - O 16	0.69	10.38	0.076
60. CR (1) C 17	/211. BD*(1) O 16 - C 17	1.38	10.34	0.107
61. CR (1) C 18	/132. RY*(3) C 17	0.61	10.71	0.072
61. CR (1) C 18	/133. RY*(4) C 17	0.53	11.26	0.069
61. CR (1) C 18	/139. RY*(2) C 19	0.76	10.79	0.081
61. CR (1) C 18	/172. RY*(1) H 32	0.56	10.71	0.069
61. CR (1) C 18	/173. RY*(1) H 33	0.56	10.71	0.069
62. CR (1) C 19	/135. RY*(2) C 18	1.13	10.75	0.098
62. CR (1) C 19	/143. RY*(2) C 20	0.90	10.81	0.088
62. CR (1) C 19	/174. RY*(1) H 34	0.53	10.72	0.067
62. CR (1) C 19	/175. RY*(1) H 35	0.52	10.72	0.067

63. CR (1) C 20	/139. RY*(2) C 19	0.98	10.78	0.092
63. CR (1) C 20	/147. RY*(2) C 21	0.88	10.80	0.087
63. CR (1) C 20	/176. RY*(1) H 36	0.52	10.72	0.067
63. CR (1) C 20	/177. RY*(1) H 37	0.52	10.72	0.067
64. CR (1) C 21	/143. RY*(2) C 20	0.95	10.79	0.091
64. CR (1) C 21	/151. RY*(2) C 22	0.92	10.79	0.089
64. CR (1) C 21	/153. RY*(4) C 22	0.54	11.30	0.070
64. CR (1) C 21	/178. RY*(1) H 38	0.52	10.72	0.066
64. CR (1) C 21	/179. RY*(1) H 39	0.51	10.72	0.066
65. CR (1) C 22	/147. RY*(2) C 21	0.96	10.79	0.091
65. CR (1) C 22	/156. RY*(3) C 23	0.91	10.69	0.088
65. CR (1) C 22	/180. RY*(1) H 40	0.52	10.72	0.066
65. CR (1) C 22	/181. RY*(1) H 41	0.52	10.72	0.066
66. CR (1) C 23	/151. RY*(2) C 22	0.95	10.79	0.090
66. CR (1) C 23	/160. RY*(3) C 24	1.25	10.79	0.104
66. CR (1) C 23	/182. RY*(1) H 42	0.52	10.71	0.067
66. CR (1) C 23	/183. RY*(1) H 43	0.52	10.71	0.066
67. CR (1) C 24	/155. RY*(2) C 23	1.08	10.80	0.096
67. CR (1) C 24	/184. RY*(1) H 44	0.57	10.70	0.070
67. CR (1) C 24	/185. RY*(1) H 45	0.57	10.70	0.070
67. CR (1) C 24	/186. RY*(1) H 46	0.57	10.69	0.070
68. CR (1) O 25	/111. RY*(1) C 10	1.13	19.68	0.133
69. LP (1) O 5	/85. RY*(1) C 2	2.10	1.38	0.049
69. LP (1) O 5	/101. RY*(1) C 6	2.52	1.38	0.053
69. LP (1) O 5	/189. BD*(1) C 1 - C 2	1.06	0.95	0.028
69. LP (1) O 5	/194. BD*(1) C 2 - H 9	0.73	1.01	0.024
69. LP (1) O 5	/195. BD*(1) C 2 - C 10	0.92	0.96	0.027
69. LP (1) O 5	/199. BD*(1) C 4 - C 6	1.75	0.92	0.036
69. LP (1) O 5	/204. BD*(1) C 6 - O 16	3.69	0.84	0.050
69. LP (1) O 5	/236. BD*(1) O 25 - H 47	1.21	1.01	0.031
70. LP (2) O 5	/189. BD*(1) C 1 - C 2	4.17	0.67	0.047
70. LP (2) O 5	/191. BD*(1) C 1 - O 7	1.03	0.55	0.022
70. LP (2) O 5	/194. BD*(1) C 2 - H 9	4.88	0.74	0.054
70. LP (2) O 5	/199. BD*(1) C 4 - C 6	4.64	0.64	0.049
70. LP (2) O 5	/203. BD*(1) C 6 - H 15	5.59	0.71	0.057
70. LP (2) O 5	/236. BD*(1) O 25 - H 47	0.52	0.73	0.018
71. LP (1) O 7	/81. RY*(1) C 1	2.16	1.39	0.049
71. LP (1) O 7	/84. RY*(4) C 1	0.64	1.85	0.031
71. LP (1) O 7	/189. BD*(1) C 1 - C 2	1.07	0.94	0.029
71. LP (1) O 7	/190. BD*(1) C 1 - C 3	0.94	0.94	0.027
71. LP (1) O 7	/192. BD*(1) C 1 - H 8	1.29	1.04	0.033
71. LP (1) O 7	/193. BD*(1) C 2 - O 5	0.67	0.80	0.021
72. LP (2) O 7	/190. BD*(1) C 1 - C 3	5.45	0.65	0.053
72. LP (2) O 7	/192. BD*(1) C 1 - H 8	5.22	0.74	0.056
72. LP (2) O 7	/196. BD*(1) C 3 - C 4	0.85	0.64	0.021
73. LP (1) O 11	/89. RY*(1) C 3	2.86	1.32	0.055
73. LP (1) O 11	/190. BD*(1) C 1 - C 3	0.98	0.94	0.027
73. LP (1) O 11	/196. BD*(1) C 3 - C 4	1.71	0.93	0.036
73. LP (1) O 11	/198. BD*(1) C 3 - H 12	1.25	1.02	0.032
74. LP (2) O 11	/189. BD*(1) C 1 - C 2	1.17	0.66	0.025
74. LP (2) O 11	/190. BD*(1) C 1 - C 3	5.93	0.66	0.056
74. LP (2) O 11	/196. BD*(1) C 3 - C 4	3.97	0.65	0.045
74. LP (2) O 11	/199. BD*(1) C 4 - C 6	0.59	0.63	0.017
74. LP (2) O 11	/205. BD*(1) O 7 - H 26	0.91	0.72	0.023
75. LP (1) O 14	/93. RY*(1) C 4	1.77	1.32	0.043
75. LP (1) O 14	/196. BD*(1) C 3 - C 4	1.19	0.92	0.030
75. LP (1) O 14	/198. BD*(1) C 3 - H 12	0.52	1.01	0.020
75. LP (1) O 14	/199. BD*(1) C 4 - C 6	0.89	0.90	0.025
75. LP (1) O 14	/200. BD*(1) C 4 - H 13	1.60	1.00	0.036
75. LP (1) O 14	/209. BD*(1) O 11 - H 29	1.92	0.98	0.039
76. LP (2) O 14	/199. BD*(1) C 4 - C 6	5.18	0.67	0.053
76. LP (2) O 14	/200. BD*(1) C 4 - H 13	4.61	0.77	0.053
76. LP (2) O 14	/209. BD*(1) O 11 - H 29	0.84	0.74	0.022

77. LP (1) O 16	/101. RY*(1) C 6	0.59	1.37	0.026
77. LP (1) O 16	/102. RY*(2) C 6	2.69	1.30	0.053
77. LP (1) O 16	/130. RY*(1) C 17	1.39	1.38	0.039
77. LP (1) O 16	/196. BD*(1) C 3 - C 4	0.57	0.93	0.021
77. LP (1) O 16	/199. BD*(1) C 4 - C 6	1.13	0.92	0.029
77. LP (1) O 16	/202. BD*(1) O 5 - C 6	0.64	0.80	0.020
77. LP (1) O 16	/203. BD*(1) C 6 - H 15	1.96	0.98	0.039
77. LP (1) O 16	/210. BD*(1) O 14 - H 48	2.28	1.00	0.043
77. LP (1) O 16	/212. BD*(1) C 17 - C 18	0.89	0.96	0.026
77. LP (1) O 16	/214. BD*(1) C 17 - H 31	1.21	1.00	0.031
77. LP (1) O 16	/215. BD*(1) C 18 - C 19	0.55	0.95	0.021
78. LP (2) O 16	/202. BD*(1) O 5 - C 6	14.09	0.54	0.078
78. LP (2) O 16	/203. BD*(1) C 6 - H 15	4.42	0.72	0.051
78. LP (2) O 16	/213. BD*(1) C 17 - H 30	4.71	0.75	0.054
78. LP (2) O 16	/214. BD*(1) C 17 - H 31	3.49	0.73	0.046
79. LP (1) O 25	/111. RY*(1) C 10	1.63	1.31	0.041
79. LP (1) O 25	/195. BD*(1) C 2 - C 10	1.32	0.94	0.032
79. LP (1) O 25	/207. BD*(1) C 10 - H 27	1.23	1.04	0.032
79. LP (1) O 25	/208. BD*(1) C 10 - H 28	1.06	1.01	0.029
80. LP (2) O 25	/194. BD*(1) C 2 - H 9	0.56	0.70	0.018
80. LP (2) O 25	/195. BD*(1) C 2 - C 10	5.14	0.64	0.051
80. LP (2) O 25	/208. BD*(1) C 10 - H 28	5.64	0.72	0.057

APPENDIX (D)

PH.D PUBLICATIONS

D.1 Journal Articles

1. Zahrabatoul Mosapour Koteh, Reza Behjatmanesh-Ardakanib, Rauzah Hashim, Vijayan Manickam Achari, Hydrogen bonds in galactopyranoside and glucopyranoside: a density functional theory study .J Mol Model ,2013;19(2),589-599. (Impact factor=1.8)
2. Zahrabatoul Mosapour Koteh, Reza Behjatmanesh-Ardakani, Rauzah Hashim, AIM and NBO analyses on hydrogen bonds formation in sugar-based surfactants(α/β - D-mannose and n-octyl- α/β -D-mannopyranoside): a density functional theory study. Liq Cryst,2014; 41(6):784-792). (Impact factor=2.3)
3. Zahrabatoul Mosapour Koteh, Reza Behjatmanesh-Ardakani, Rauzah Hashim, The Interaction between Sugar-based Surfactant with zigzag Single-walled Carbon Nanotubes: Insight from a Computational Study.(accepted Liq. Cryst, on 4 Oct 2014). (Impact factor= 2.3)

D.2 Manuscripts in preparation

1. Interaction between n-octyl- β -D-glucopyranoside and (7, 0)zigzag and (5, 5)armchair single-walled carbon nanotubes: a DFT study.
2. A DFT study on the vibrational spectrum of glycolipid sugar-based surfactant; n-octyl- β -D-glucopyranoside.
3. Interaction between n-octyl- β -D-glucopyranoside and single-walled carbon nanotubes: a MD simulation study.

APPENDIX (E)

ATTANDANCE TO CONFERENCE/ SEMINAR/ WORKSHOP

4. **Title:** A DFT study on the vibrational spectrum of glycolipid sugar-based surfactant; n-octyl- β -D-glucopyranoside.

❖ **Date:** 10th Jun-05th July 2013

Program: Advanced Molecular Simulation Methods in the Physical Sciences.

Venue: Kavli Institute of Theoretical Physics China (KITPC), Beijing, China

Role: Participant in the Training /Poster presentation

- ❖ **Title:** Interaction between n-octyl- β -D-glucopyranoside and (7,0) and (5,5) single walled carbon nanotubes: a DFT study

Date: 19th-22nd Nov 2013

Conferences: 3rd International Conference on the Advancement of Materials and Nanotechnology (ICAMN).

Venue: Penang, Malaysia

Role: Oral presenter

- ❖ **Title:** Hydrogen bonds in Galactopyranoside and Glucopyranoside: a density functional theory study

Date: 15th-17th Oct 2012

Conference: 17th Malaysian Chemical Congress (17MCC), Symposium on Physical and Computational Chemistry

Venue: KL, Malaysia

Role: Oral presenter

❖ **Title:** Hydrogen bonds formation in α/β -D-mannose and n-octyl- α/β -D-mannopyranoside using AIM and NBO analyses

Date: 11th-12th Feb 2014

Symposium: 5th UM-NUS-CU Trilateral mini symposium and scientific meeting.

Venue: University of Malaya, Malaysia

Role: Poster presenter

RESEARCH GRANT

Grant: High Impact Research

Project Name: Fundamental Science of Self-Assembly (FSSA).

Project Number: UM.C/625/1/HIR/MOHE/05